Methanol electro-oxidation catalyzed by platinum deposited on various substrates using Electrochemical Atomic Layer Deposition (ECALD)

by

Eldah Kemoamogetse Louw

Submitted in partial fulfilment of the requirements for the degree

MAGISTER TECHNOLOGIAE: CHEMISTRY

in the

Department of Chemistry

FACULTY OF SCIENCE

TSHWANE UNIVERSITY OF TECHNOLOGY

Supervisor: Dr L M Cele

Co–supervisor: Dr R M Modibedi

2013

Declaration

“I hereby declare that the dissertation submitted for the degree M Tech Chemistry at Tshwane University of Technology is my original work and has not previously been submitted to any other institute of higher education. I further declare that all sources cited or quoted are indicated and acknowledged by means of a comprehensive list of references.”

Eldah Kemoamogetse Louw

Dedication

This study is dedicated to my family and friends for their love and support.

Acknowledgements

I would like to express my sincere gratitude and appreciation to my supervisor Dr Cele and co-supervisor Dr Modibedi for their positive attitude and guidance, Tshwane University of Technology, the CSIR for allowing me to do my research in their laboratory and the NRF for financial assistance and a special thanks to the Energy Material girls for keeping me sane.

Abstract

Electrochemical atomic layer deposition technique was chosen in this study for the deposition of platinum nanostructures onto various substrates such as carbon paper, nickel foam and titanium mesh. Electrochemical evaluation and morphological studies were carried out on the electrodeposited Pt. Cyclic voltammograms of the electrodeposited platinum nanostructures showed features characteristic of polycrystalline platinum electrodes. The substrates were also modified with a layer of carbon black in 40 % Nafion. The Pt/C/Ni foam electrode with its higher real surface area proved to be the better substrate compared to others electrodes in terms of performance in hydrogen oxidation, methanol oxidation activity, CO tolerance in acidic electrolytes. Scanning electron microscopy images showed good quality deposits that uniformly covered the substrates and energy dispersive x-ray spectroscopy confirmed the presence of Pt in all electrodes. According to the Atomic Force Microscopy histogram analysis, the particle size was found to range from 24-99.2 nm. Inductively coupled plasma optical emission spectroscopy indicated an increase in weight with every repetition of Pt loading. The Pt/Ni foam electrode had a higher Pt loading due the higher surface area of Ni foam as compared to that of carbon paper and Ti mesh. This work has demonstrated the ease and flexibility of this technique for preparing nanostructures on various substrates.

CONTENTS PAGES

LIST OF FIGURES

LIST OF TABLES

CHAPTER 1

INTRODUCTION

Background and Motivation

Countries across the globe count on coal, oil and natural gas to supply most of their energy needs, but reliance on fossil fuels presents a big problem. Fossil fuels are a finite resource of energy. Eventually, the world will run out of fossil fuels, or it will become too expensive to retrieve those that remain. Fossil fuels also produce greenhouse gases that contribute to global warming (Pletcher, 2009). Fuel cell technology is one of the proposed renewable energy systems that may replace fossil fuels; but first scientists will have to sort out a few major issues such as:

- Cost per kilowatt.
- The production costs of the proton exchange membrane (PEM).
- Water and air management.
- Temperature management.
- Durability, service life, and special requirements for some cell types.
- Limited carbon monoxide tolerance of some cathodes.
- Provision of a fuel delivery system.
- Hydrogen generation, storage and delivery infrastructure.
- Other Considerations (Larmine, 2003).

A fuel cell (FC) is an electrochemical cell that converts chemical energy from fuel into electrical energy. Electricity is generated from the reaction between a fuel supply and an oxidizing agent. The reactants flow into the cell, and the reaction products flow out of it, while the electrolyte remains within it. The energy produced

is continuous as long as the flow of the reactants and oxidants is maintained (Grove, 1839). Among the various types of fuel cells, direct methanol fuel cells (DMFCs) have highly advantageous features such as a low-operating temperature, sustained operation at high-current density, low weight, compactness, potential for low-cost and volume, long stack life, fast start-ups as well as suitability for discontinuous operation (Bard & Faulkner, 2001). These features have made DMFCs among the most promising and attractive candidates for a variety of power applications including portable and stationary power supplies (Gotterfeld and Zawodzinski, 1997).

The membrane electrode assembly (MEA) is referred to as the heart of the DMFC and is usually made up of a proton exchange membrane electrolyte sandwiched between two catalyst-coated gas diffusion layers (GDLs). The electrolyte is generally a proton exchange polymer membrane (Kordesch and Simadar, 1996). Platinum and/or similar noble metals are usually used as the catalysts for DMFC. Platinum-based catalysts have proved to be the best materials for alcohol oxidation. So far, DMFCs are not economical enough for commercial applications. The cost of platinum - $1665 per troy ounce - is primarily a concern (Johnson Matthey, 2012) . This led to the consideration that reducing the platinum loading whilst increasing its efficiency could make the cell more affordable.

Various deposition techniques continue to be investigated to reduce platinum loading and increase its utilization. These techniques include modified thin films, sputter deposition, dual ion-beam assisted deposition, electroless deposition and electrochemical deposition. A range of catalyst support materials such as, carbon black (Dickinson *et al.*, 2002), carbon nanotubes (Bagkar *et al.*, 2009), nanofibres

(Iannielo *et al.*, 1994) and graphene (Rajalakshmi & Dhathathreyan, 2007), are used with the intention of lowering the Pt loading on the electrode due to their high surface area and conductivity. Table 1.1 summarizes the advantages and disadvantages of the above-mentioned techniques (Wee, Lee and Kim, 2007).

Table 1.1: Summary of the advantages and disadvantages of Pt deposition methods (Wee *et al.,* 2007)

Preparation methods	**Advantages**	**Disadvantages**
Modified thin film	Relatively higher Pt utilization	Relatively high Pt-loadings
Electrodeposition	Relatively higher Pt utilization	Relatively higher Pt loadings
Sputter deposition	Lowest Pt loadings	Relatively lower Pt utilization
Dual ion-beam assisted deposition	Relatively lower Pt loadings and higher Pt utilization	Complex processes and/or steps involved
Electroless deposition	Effective for Pt/Ru binary anode electrocatalyst	Higher fabrication cost
Nano-carbons as catalyst support material	Relatively lower Pt loadings and higher Pt utilization	Strongly dependent on Pt loading methods; high price of synthesis of nano-carbons

Few of these techniques can simultaneously reduce Pt loading and increase its efficiency. The few that could attain this goal are either complicated or not cost effective.

The deposition technique proposed for this project, Electrochemical Atomic Layer Deposition (ECALD), has several attractive features such as simplicity of operation, ease of control of the deposition and low cost of fabrication. ECALD involves alternating electrodeposition of atomic layers of elements onto a substrate, employing under-potential deposition (UPD), in which one element deposits onto another element at a voltage lower than that necessary to deposit the element onto itself (Kim *et al.,* 2006). The ECALD technique offers a homogeneous dispersion of Pt nanoparticles on the substrate thus increasing the

functionality while reducing the amount of platinum used (Vukmirovic *et al*., 2011). This, in combination with a highly conductive substrate, will help to contribute towards the decrease in the cost of fuel cells.

1.2 Problem Statement

The cost of the platinum catalyst is prohibitive for the commercialization of proton-exchange membrane fuel cells (PEMFCs). This is partly because existing deposition techniques, such as modified thin films, sputter deposition, dual ion-beam assisted deposition and electroless deposition are either unable to simultaneously reduce Pt loading and increase its efficiency or are too complicated to operate and not cost effective.

1.3 Objectives

The main objective of this study is to explore the practicality of using ECALD in synthesizing catalytically active Pt nanostructures and depositing these on various substrate materials.

1.3.1 Specific objectives

The specific objectives for this project are to:

- Deposit Pt on various substrates by ECALD.
- Characterise the structural and morphological properties of the prepared Pt nanostructures.
- Characterise electrochemical properties of the prepared Pt nanostructures.

1.4. Hypothesis

ECALD has the ability to reduce the amount Pt on the electrode and increase its utilization in the electro-oxidation of methanol in acidic electrolyte.

1.5 Dissertation layout

Chapter 1 is an introduction to this work. This includes theoretical background on PEM fuel cells and motivation for ECALD application. **Chapter 2** discusses the progress made by researchers to solve or to minimise problems encountered with DMFCs problems. A brief introduction into fuel cell technology is given at the beginning of the section.

Chapter 3 is dedicated to describing the experimental approach, the synthesis and characterization of the nanostructured Pt electrocatalysts. An overview of the methodology is given so that readers can get an idea of what was done to accomplish the goal of the study. This is followed by a more thorough account of the experiment. The data collected from Chapter 3 is discussed in **Chapter 4.** The conclusions and recommendations of this study are given in **Chapter 5**. This is followed by the appendix which includes the references cited and a list of presentations that emerged from the project.

CHAPTER 2

LITERATURE SURVEY

2.1 History of fuel cells

Hydrogen is the most commonly used fuel in these cells, but hydrocarbons such as natural gas and alcohols like methanol are used as well. Fuel cells differ from batteries in that they require a constant source of fuel and oxygen to run, but can produce electricity continuously for as long as these inputs are supplied (Pletcher, 2009).

Welsh Physicist William Grove developed the first crude fuel cells in 1839 (Grove, 1839). The first commercial use of fuel cells was in NASA space programs to generate power for probes, satellites and space capsules. Since then, fuel cells have been used in many other applications (Arico, Baglio, & Antonucci, 2009). Fuel cells are used for primary and backup power for commercial, industrial and residential buildings and in remote areas (Weiner, 1998). They can be used to power vehicles, such as golf carts, cars, buses, forklifts, airplanes, boats, motorcycles and submarines (Kawats, 1998).

2.2 Working principles of fuels and types of fuel cells

A fuel cell consists of an anode (negative side), a cathode (positive side) and an electrolyte that allows charges to move between the two sides of the fuel cell. Electrons are drawn from the anode to the cathode through an external circuit, producing direct current electricity. Individual fuel cells produce very small amounts of electricity, about 0.7 V, so cells are stacked, or placed in series or parallel circuits, to increase the voltage and current output to meet an application's power generation requirements. In addition to electricity, fuel cells produce water,

heat and, depending on the fuel source, very small amounts of nitrogen dioxide and other emissions. The energy efficiency of a fuel cell is generally from 40-60 %, or up to 85 % efficient if waste heat is captured for use (Barbir, 2005; Kolbe, 2008).

There are several different types of fuel cells, each using a different chemistry. Table 2.1 presents different types of fuel cells according to their temperatures and electrolyte. Fuel cells are used in stationary power generation, portable electronics and transportation. The main types of fuel cells are described below.

2.2.1 Solid oxide fuel cell (SOFC)

These fuel cells are best suited for large-scale stationary power generators that could provide electricity for factories or towns. This type of fuel cell operates at very high temperatures (between 700 and 1000°C). This high temperature makes reliability a problem because parts of the fuel cell can break down after cycling on and off repeatedly. However, SOFCs are very stable when in continuous use. In fact, the SOFC has demonstrated the longest operating life of any fuel cell under certain operating conditions. The high temperature also has an advantage: the steam produced by the fuel cell can be channelled into turbines to generate more electricity. This process is called cogeneration of heat and power (CHP) and it improves the overall efficiency of the system (Barbir, 2005).

2.2.2 Alkaline fuel cell (AFC)

Long used by NASA on space missions, Alkaline Fuel Cells (AFC) can achieve power generating efficiencies of up to 70%. They were used on the Apollo spacecraft to provide both electricity and drinking water. Their operating temperature is 150 to 200° C. They use an aqueous solution of alkaline potassium

hydroxide soaked in a matrix as the electrolyte. This is advantageous because the cathode reaction is faster in the alkaline electrolyte, which means higher performance. Until recently, they were too costly for commercial applications, but several companies are examining ways to reduce costs and improve operating flexibility. They typically have a cell output ranging from 300 W to 5 kW (Larmine, 2003).

2.2.3 Molten-carbonate fuel cell (MCFC)

Molten Carbonate Fuel Cells (MCFC) use a liquid solution of lithium, sodium and/or potassium carbonates, soaked in a matrix for an electrolyte. They promise high fuel-to-electricity efficiencies, about 60 % normally or 85 % with co-generation, and operate at about 650° C. The high operating temperature is needed to achieve sufficient conductivity of the electrolyte. Because of this high temperature, noble metal catalysts are not required for the cell's electrochemical oxidation and reduction processes. To date, MCFCs have been operated on hydrogen, carbon monoxide, natural gas, propane, landfill gas, marine diesel, and simulated coal gasification products. MCFCs of 10 kW to 2 MW have been tested on a variety of fuels and are primarily targeted to electric utility applications. Carbonate fuel cells for stationary applications have been successfully demonstrated in Japan and Italy. The high operating temperature serves as a big advantage because this implies higher efficiency and the flexibility to use more types of fuels and inexpensive catalysts as the reactions involving the breaking of carbon bonds in larger hydrocarbon fuels occur much faster as the temperature is increased. A disadvantage to this, however, is that high temperatures enhance corrosion and the breakdown of cell components (Barbir, 2005).

2.2.4 Phosphoric-acid fuel cell (PAFC)

Phosphoric Acid Fuel Cells (PAFC) are the most mature fuel cell technology and are commercially available today. More than 200 fuel cell systems have been installed all over the world in hospitals, nursing homes, hotels, office buildings, schools, utility power plants, an airport terminal, landfills and waste water treatment plants. PAFCs generate electricity at more than 40 % efficiency and nearly 85 % of the steam this fuel cell produces is used for co-generation. This compares to about 35 % of the utility power grid in the United States. Operating temperatures are in the range of 150 - 200 °C. At lower temperatures, phosphoric acid is a poor ionic conductor, and carbon monoxide (CO) poisoning of the Platinum (Pt) electro-catalyst in the anode becomes severe. The electrolyte is liquid phosphoric acid soaked in a matrix. One of the main advantages of this type of fuel cell, besides the nearly 85 % generation efficiency, is that it can use impure hydrogen as fuel. Disadvantages of PAFCs include its use of expensive platinum as a catalyst, low current and power generation compared to other types of fuel cells, and its generally large size and weight (Pletcher, 2009).

2.2.5 Proton exchange membrane fuel cell (PEMFC)

Proton Exchange Membrane (PEM) fuel cells (also called the solid polymer electrolyte, the polymer electrolyte or hydrogen fuel cell) operate at the lowest temperature range (< 200 °C), have high power density, can vary their output quickly to meet shifts in power demand, and are suited for applications, such as in automobiles, where a quick start-up is required. The proton exchange membrane is a thin plastic sheet that allows hydrogen ions to pass through it. The membrane is sandwiched between active catalyst (mostly platinum) layers. The electrolyte used is a solid organic polymer, poly-perflourosulfonic acid. The solid electrolyte is

an advantage because it reduces corrosion and management problems. Hydrogen is fed to the anode side of the fuel cell where the catalyst encourages the hydrogen atoms to release electrons and become hydrogen ions (protons). The electrons travel in the form of an electric current that can be utilized before it returns to the cathode side of the fuel cell where oxygen has been fed. At the same time, the protons diffuse through the membrane (electrolyte) to the cathode, where the hydrogen atom is recombined and reacted with oxygen to produce water, thus completing the overall process. This type of fuel cell is, however, sensitive to fuel impurities. Cell outputs generally range from 50 to 250 kW (Kawats, 1998).

Table 2.1: Summary of the properties of the different types of fuel cells (U.S Department of Energy, 2011)

Fuel cell name	Electrolyte	Qualified power (W)	Working temperature (°C)	Efficiency (cell)	Efficiency (system)	Status
Alkaline fuel cell	Aqueous alkaline solution	10 – 100 kW	< 80	60–70 %	62 %	Commercial / Research
Direct carbon fuel cell	Several different		700-850	80 %	70 %	Commercial / Research
Direct formic acid fuel cell (DFAFC)	Polymer membrane (ionomer)	< 50 W	< 40			Commercial / Research
Direct methanol fuel cell	Polymer membrane (ionomer)	100 mW – 1 kW	90–120	20–30 %	10–20 %	Commercial / Research
Direct-ethanol fuel cell	Polymer membrane (ionomer)	< 140 mW/cm²	90–120			Research
Molten carbonate fuel cell	Molten alkaline carbonate	100 MW	600-650	55 %	47 %	Commercial / Research
Phosphoric acid fuel cell	Molten phosphoric acid (H_3PO_4)	< 10 MW	150-200	55 %	40 % Co-Gen: 90 %	Commercial / Research
Proton exchange membrane fuel cell	Polymer membrane (ionomer)	100 W – 500 kW	50–120 (Nafion) 125–220 (PBI)	50–70 %	30–50 %	Commercial / Research
Solid oxide fuel cell	O^{2-}-conducting ceramic oxide	<100 MW	850-1100	60–65 %	55–60 %	Commercial / Research

2.3 Direct-methanol fuel cell (DMFC)

Direct Methanol Fuel Cells (DMFCs) are similar to the PEM cells in that they both use a polymer membrane as the electrolyte. However, in the DMFC, the anode catalyst itself draws the hydrogen from the liquid methanol, eliminating the need for a fuel reformer. Efficiencies of about 40 % are expected with this type of fuel

cell, which would typically operate at a temperature between 50 -100 °C. This is a relatively low range, making this fuel cell attractive for tiny to mid-sized applications, to power cellular phones and laptops, or portable power sources for soldiers in the field. Higher efficiencies are achieved at higher temperatures (Pletcher, 2009).

Methanol is used because of its high power density, safety, low cost, ease of handling and distribution, and high electrochemical activity. In a DMFC, the methanol / water solution is fed into the anode as fuel. This allows for a substantial system design simplification relative to reformat-based fuel cells and a higher energy density than that presently available with hydrogen-based systems. However, at present, DMFCs require much higher platinum loadings than either hydrogen or reformate-based systems (Larmine, 2003). DMFCs have several well-established problems related to their performance optimization. These problems are responsible for the short lifetime and low cell performance and can be summarized as follows: (a) low alcohol electro-oxidation kinetics, (b) alcohol crossover, and (c) electrode poisoning. The progress made to solve or minimize these problems is discussed in the following sections.

Just like in a PEM fuel cell, the DMFC has two catalytic electrodes where the methanol oxidation (anode) and the oxygen reduction (cathode) occur. These electrodes are separated by a membrane, which conducts protons from anode to cathode, while diffusion of other compounds is blocked. The combination of anode/membrane/cathode is called membrane electrode assembly (MEA) (Hamnett, 2003). Each electrode is made of a gas diffusion layer and a catalytic layer (Figure 2.2). The state-of-the-art membrane, Nafion from DuPont, is the

popular choice. In order for this device to operate, an aqueous methanol solution is fed at the anode side. The solution diffuses through the diffusion layer to the catalytic layer where methanol oxidation (MOR) takes place to produce mainly carbon dioxide, protons and electrons (Bockris & Srinivasan, 1969).

$$CH_3OH + H_2O \rightarrow CO_2 + 6H^+ + 6e^- \quad [E_a=0.02V \text{ vs. SHE}] \qquad (2.1)$$

Protons generated at the anode pass through the proton exchange membrane to the cathode catalytic layer and combine with the electrons and the oxidant air or oxygen simultaneously reducing to water and heat. This reaction is known as the oxygen reduction reaction (ORR):

$$3/2O_2 + 6H^+ + 6e^- \rightarrow 3H_2O \quad [E_c =1.23V \text{ vs. SHE}] \qquad (2.2)$$

Reactions (2.1) and (2.2) are combined to give the overall reaction (2.3):

$$CH_3OH + 3/2O_2 \rightarrow CO_2 + 2H_2O \quad [E_{cell} =1.21V \text{ vs. SHE}] \qquad (2.3)$$

The free energy (ΔG) of overall reactions at 25 °C and one atm is 686 $kJ.mol^{-1}$ for CH_3OH. The structure of the cell is described in Figure 2.1. (Bockris & Srinivasan, 1969). The DMFCs (or PEMFCs) fundamental components (Hamnett, 2003) are discussed in more detail in the following sections:

2.3.1 Membrane

The proton exchange membrane (PEM) is a specially treated material that only conducts positively charged ions. The three main properties a fuel cell membrane must exhibit are protonic conductivity, a barrier to mixing of fuel and reactant gases, and chemical and mechanical stability within the fuel cell environment (Paddison, 2003).

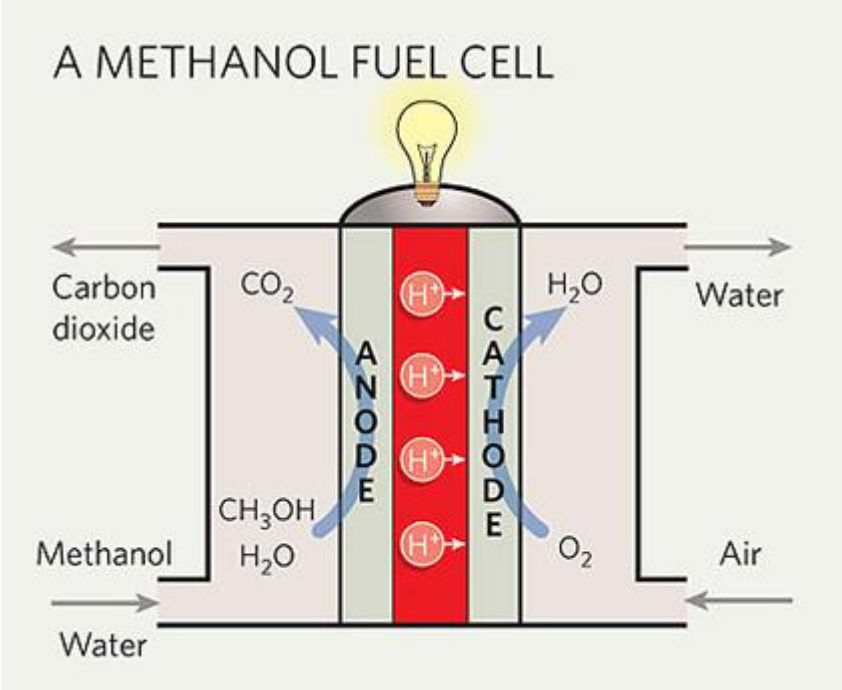

Figure 2.1: Schematic of diagram DMFC Principles (Barbir, 2005)

Typically, the membranes for PEMFCs are made of perfluorocarbon-sulfonic acid ionomer (PSA). This is essentially a copolymer of tetrafluorethylene (TFE) and various perfluorosulfonate monomers (Paddison, 2003). The popular Nafion was created by the addition of sulfonic acid groups into the bulk polymer matrix of Teflon. These sites have strong ionic properties and act as proton exchange sites.

2.3.2 Gas Diffusion Electrode (GDEs)

The electrode of a fuel cell is a thin layer of catalyst embedded between the ionomer membrane and a porous, electrically conducting substrate. It is also the layer where the electrochemical reactions take place. Typical electrodes for DMFC applications are made of a gas diffusion layer (GDL) and a catalyst layer (CL) consisting of finely dispersed platinum (Hamnett, 2003).

2.3.2.1 Gas Diffusion Layer (GDL)

The GDL typically has a dual-layer structure with a macro porous substrate layer (SL) and a thinner coated micro porous layer (MPL). The SL plays an important role in DMFCs performance and has several functions. A well-qualified SL must have the following:

- Must be sufficiently porous to allow permeability to gases, liquids and products.
- Must be electrically and thermally conductive.
- Must be sufficiently rigid to support the MEA.
- Must be chemically stable.
- Must have low cost.
- Must be hydrophobic in order to avoid the flooding in their bulk (Hammer & Norskov, 2000).

Most of the above-mentioned properties are met by fibrous carbon paper or woven carbon cloth (Barbir, 2005; Abson, 2006). Other materials such as Ti mesh (Shoa *et al*., 2006), stainless steel (Arico, Baglio, & Antonucci, 2009), Ni mesh and Ni foam (Bidault*, et al*., 2009) have been explored since they also meet most of the above requirements.

In this work, Ti mesh and Ni foam were selected as substrates for electrochemical atomic layer deposition of Pt to decrease the problems experienced in fuel cells with the carbon support such as corrosion and Pt dissolution (Rahin & Hassan, 2009; Piela *et al.* 2004). They both also have the added advantage of being flexible thus enabling versatile cell designs.

The addition of an MPL onto the surface of the SL has proven to be an effective way of improving the GDL's water/gas-management. The layer consists of carbon or graphite particles mixed with a hydrophobic agent, such as Polytetrafluoroethylene (PTFE) or in this case Nafion, which serves as a binder. The following is a brief summary of the pore size and thickness range of both the MPL and SL.

MPL pore size range: 100-500 nm

MPL thickness range: 5-50 µm

SL pore size range: 10-30 µm

SL thickness range: 100-300 µm

(Zhang, Wang, & Zhang, 2008)

The primary purpose of the MPL is water management and reactant redistribution. It can provide effective wicking of liquid water from the cathode CL into the SL and then effective transportation of gases in the opposite direction. It also contributes significantly to the reduction of electrical contact resistance between the SL and CL (Zhang, Wang, & Zhang, 2008).

2.3.2.2 Catalyst Layer (CL)

The MEA is typically a five layer composite structure that includes an anode GDL, an anode CL, the membrane, the cathode CL and the cathode GDL. Two different MEA structures have been developed according to the CL location. Applying the catalyst onto the GDL, leads to a basic two-layer structure called a catalyst coated GDL (CGDL), while catalyst directly applied to the membrane results in a three layer structure called a catalyst coated membrane (CCM). The final five-layered MEA is then formed by sandwiching the membrane between two CGDLs or a

CCM between the GDLs (Mehta & Copper, 2003). The two MEA compositions are represented in Figure 2.2.

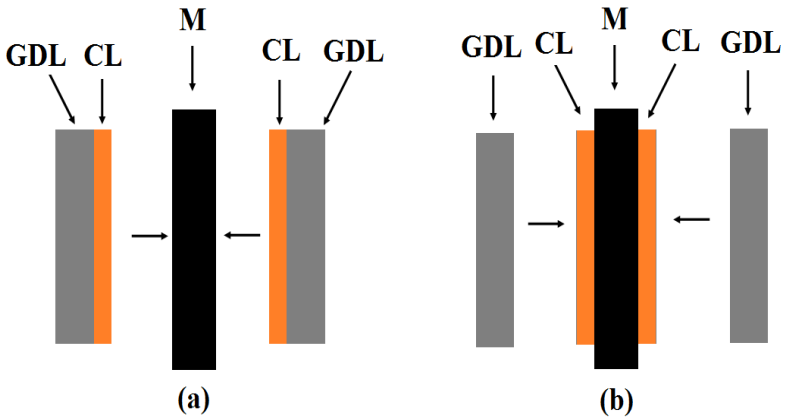

Figure 2.2: Illustration of the two MEA compositions (a) CGDL and (b) CCM (Hammer & Norskov, 2000)

All the electrochemical reactions take place on the CL, making it the key component of the GDE. The protons produced from the reaction have to travel through the electrolyte and electrically conductive solids, including the catalyst itself. Therefore, CL particles should be in close contact with each other, the electrolyte and the neighbouring GDLs (Zhang, Wang, & Zhang, 2008).

The catalyst layer needs to be designed so that it generates high reaction rates, whilst using a minimum amount of catalysts to reach the required levels of power output. The reaction zone can be amplified by either roughening the surface or by reducing the catalyst particle size or incorporating the ionomer in the catalyst layer. Platinum is the most extensively used metal in the anode and cathode electrodes because of its high catalytic activity for both oxidation and reduction reactions. However, the high cost of Pt is prohibitive for commercial applications of DMFCs and research efforts are currently directed towards minimizing platinum

utilization by improving the MEA preparation techniques (Rajalakshmi & Dhathathreyan, 2007).

In order to achieve uniform, highly dispersed and low Pt loadings, fuel cell catalysts are usually supported on carbon supports with a high surface area. Some of the common supporting materials are carbon blacks with a high degree of graphitic character: Vulcan XC-72R, Vulcan XC-72, Black Pearls BP 2000, Ketjen Carbon Black, etc. (Bagkar *et al.,* 2009).

2.3.3 Bipolar plates

Some of the properties bipolar plates must exhibit are:

- They connect cells electrically in series; therefore they must be electrically conductive.
- They must be impermeable to gases as they separate gases in adjacent layers.
- They must provide structural support.
- They must be thermally conductive as they conduct heat from the active cells to the cooling cells.

So far, two families of materials have been used for PEMFCs in the construction of the bipolar plates, namely graphite-composite and metals (Hamnett, 2003).

2.4 Catalyst synthesis processes

The main factors preventing DMFCs from widespread applications are high cost and undesirable degradation of Pt-based electrocatalysts. The state-of-the-art Pt catalysts supported on carbon (Pt/C) are routinely prepared through impregnation-reduction, (Fedkiv & Her, 1989), the microemulsion method (Boutonnet *et al*., 1982) and the co-precipitation method (Bagkar, 2009). For the impregnation

method, Pt and transition metal precursors are first adsorbed on a carbon support and subsequently the mixture is dried and reduced with a hydrogen stream at a temperature range of 200-700 ˚C in a tubular furnace. The high temperature of the hydrogen drives the reaction to completion. The disadvantage is that the high temperature decreases the active surface area because of the aggregation of the nanoparticles (Fedkiv & Her, 1989).

Pt-alloy catalysts have been mainly synthesized by incorporation of second or third metals on the pre-formed Pt/C in colloidal sol (Delmon, 1979), sol-gel (Zou, Robinson, & Gonzalez, 1992), hydroxide/hydrous oxide (Chem *et al.*, 2005), and via carbonyl complexes (Dickinson *et al.,* 2002). Recently, mono-dispersed Pt/Ni/Fe ternary nanoparticles have been synthesized from a molecular encapsulation via the aid of capping agents (Luo, *et al.*, 2006). This method has been successfully demonstrated to render binary and ternary compositions (Zhong *et al*., 2010). In all the cases mentioned above, the preparation involves tedious wet chemistry steps, including filtering, pH control, washing, and drying. The ability to control particle size, composition, as well as to achieve alloying between Pt and transitional metals remains elusive with these methods (Mehta & Copper, 2003).

2.5 Thin film deposition catalyst layers

A current trend in electrode preparation is to reduce the catalyst layer thickness to improve the mass transfer efficiency at the interface, such as the efficient movement of the protons, electrons and dissolved reactants in the reaction zone. In addition, a thinner electrode will be beneficial to reduce catalyst loading and increase mass power density. The deposition technique is an effective way to achieve a thinner electrode through depositing a nanoscale catalyst film onto the

substrate (Wee, Lee, & Kim, 2007). Deposition methods include aerosol assisted deposition (AAD), electrodeposition, electrochemical atomic layer deposition (ECALD), physical or thermal deposition (e.g. sputter deposition) as well as ion beam deposition. These techniques are discussed briefly below.

2.5.1 Aerosol assisted deposition (AAD) method

Properties of the nanoparticles differ from those of the bulk since quantum size effects dominate their characteristics. The synthesis of well-controlled shapes and sizes of colloidal particles is critical for various applications. The catalytic activity of Pt electrodes, as an example, depends on the size of the nanoparticles (Mayrhofer *et al.,* 2005). The AAD method, as distinct from wet chemistry techniques, allows the direct deposition of active species on the substrate without any further treatment. This eliminates the steps of impregnation, washing, drying, calcination, and reduction. Most drawbacks of classical synthesis of catalysts due to the use of liquid solvents are avoided: redistribution of active sites during drying, surface poisoning during impregnation and migration or agglomeration of particles during sintering in the steps of preparation involving high temperatures. Moreover, the structure and features of the substrate, in particular its porosity and its specific area, remain unaltered by the AAD process. Deposition methods such as metal organic chemical vapour deposition in a fluidized bed and physical vapour deposition methods such as sputtering and e-beam evaporation, are known to produce nanoparticles at low substrate temperature range, however, they require the use of high vacuum and expensive vacuum equipment in order to control the particle or film purity (Hierso, Feuner, & Kalck, 2000). However, there are only a few reports of synthesis of platinum nanoparticles using this method (Xue *et al.,* 2006).

2.5.2 Sputter deposition

Sputter deposition is the deposition of particles vaporized from a surface (sputter-target) by the physical sputtering process. Physical sputtering is a non-thermal vaporization process where surface atoms are physically ejected by momentum transfer from an energetic bombarding particle that is usually a gaseous ion accelerated from plasma or an "ion gun." This physical vapour deposition process is often called sputtering.

Sputter deposition can be performed in a vacuum or low-pressure gas (<5 mTorr) where the sputtered particles do not suffer gas-phase collisions in the space between the target and the substrate. It can also be done in a higher gas pressure (5-15 mTorr) where energetic particles that are sputtered or reflected from the sputtering target are "thermalized" by gas-phase collisions before they reach the substrate (Hirano, Kim, & Srinivasan, 1997).

The most common sputtering sources are the planar magnetrons where the plasma is magnetically confined close to the target surface and ions are accelerated from the plasma to the target surface. In the unbalanced magnetron configuration, the magnetic field is configured to allow electrons to escape and form plasma away from the target. The high sputtering rates attainable in magnetron sputtering allows reactive deposition of compound films as long as the sputtering target is not allowed to react with the reactive gas to form a low-sputtering rate compound (target poisoning) (Mukerjee, Srinivasan, & Appleby, 1993; (Hirano, Kim, & Srinivasan, 1997).

2.5.3 Ion beam deposition

Ion plating uses concurrent or periodic energetic particle bombardment of the depositing film to modify and control the composition and properties of the deposited film and to improve surface coverage and adhesion. The depositing material may be vaporized by evaporation, sputtering, arc erosion or other vaporization source. It can be obtained also from the decomposition of a chemical vapour precursor species.

The energetic particles used for bombardment are usually ions of an inert or reactive gas or ions of the depositing material (film ions). Ion plating can be done in a plasma environment where ions for bombardment are extracted from the plasma, or it can be done in a vacuum environment where ions for bombardment are formed in a separate ion gun. The latter ion-plating configuration is often called ion beam assisted deposition (Gulla, Saha, & Mukerjee, 2005).

2.5.4 Electrodeposition

Electrodeposition is a plating process in which metal ions in a solution are moved by an electric field to coat an electrode. The process uses electrical current to reduce cations of a desired material from a solution and coat a conductive object with a thin layer of the material, such as a metal. This technique is primarily used for depositing a layer of material to obtain a desired surface that otherwise lacks a certain property. Another application of electroplating is to build up thickness on miniature parts (Bagkar *et al*., 2009).

This process is similar to a galvanic cell in reverse. The part to be plated is the cathode of the circuit. In one technique, the anode is made of the metal to be plated on the part. Both components are immersed in a solution called an

electrolyte containing one or more dissolved metal salts as well as other ions that permit the flow of electricity. A power source provides a direct current to the anode, oxidizing the metal atoms that comprise it and allowing them to dissolve in the solution. At the cathode, the dissolved metal ions in the electrolyte solution are reduced at the interface between the solution and the cathode, such that they "plate out" onto the cathode. The rate at which the anode is dissolved is equal to the rate at which the cathode is plated, with reference to the current flowing through the circuit. In this manner, the anode continuously replenishes the ions in the electrolyte bath (Taylor, Anderson, & Vilambi, 1992).

The ECALD technique, discussed below, can be described as the marriage of the simplistic, cost effective electrodeposition method and the controlled efficiency of sputter deposition, AAD or ion beam deposition.

2.5.4.1 Electrochemical atomic layer deposition (ECALD)

Electrochemical atomic layer deposition (ECALD) has been studied for many years to produce high quality thin films (Stickney, 2002). Atomic layer deposition (ALD) is a methodology used initially to improve epitaxy in the growth of thin films by molecular beam epitaxy or chemical vapour deposition. The principle of ALD is to use surface-limited reactions to form each atomic layer of a deposit. If no more than an atomic layer is ever deposited, the growth will be two-dimensional (2-D), layer-by-layer. Surface-limited reactions are developed for the deposition of each component element, and a cycle is formed with them. With each cycle, a compound monolayer is formed, and the deposit thickness is controlled by the number of cycles (Brankovic, Wang, & Adzic, 2005).

Most surface-limited reactions are referred to as underpotential deposition (UPD) (Stickney, 2002; Kolbe *et al*., 1974). The UPD phenomenon can be explained as follows: In the deposition of one element on a second, frequently the first element will form an atomic layer at a potential prior to that needed to deposit the element on itself. One way of looking at UPD is that a surface compound, or alloy, is formed, and the shift in potential results from the free energy of formation of the surface compound.

Electrochemical ALD is the combination of UPD and ALD. Atomic layers of component elements are deposited at underpotentials in a cycle, to directly form a compound. It is layer-by-layer growth, avoiding three-dimensional (3-D) nucleation, and offering increased degrees of freedom, atomic level control, and promoting of epitaxy (Stickney, 2002). It allows compound electrodeposition to be broken down into a series of individual controllable steps, resulting in an opportunity to learn more about the mechanisms, and join a series of new control points for electrodeposition. In this process, each reactant has its own solution and deposition potential, and there are generally rinse solutions as well.

Each solution can be separately optimized, so that the pH, electrolyte, and additives or complexing agents are tailored to fit the precursor. Finally, electrochemical ALD involves growth in a condensed phase with potential control instead of thermal. This increases the variable space for producing materials and the diversity of conditions under which compounds can be formed (Kim *et al.*, 2006).

ECALD has been used in the past to form compound semiconductors on gold such as II-VI compounds, e.g. CdS, CdSe (Lister & Stickney, 1996) and InTe

(Venkatasamy *et al*., 2007), IV-VI, e.g. PbSe (Vaidyanathan, Stickney, & Happek, 2004; Vaidyanathan *et al*., 2006) and PbTe (Vaidyanathan, Stickney, & Happek, 2004), and III-V e.g. GaAs (Villegas & Stickney, 1992). In the growth of compounds, the UPD of the elements making up a compound can be alternated to grow compound nanofilms. As noted above, UPD of a metal on itself cannot be performed, by definition, so the strict application of UPD in a simple cycle will not result in the growth of nanofilms of pure metal. Adzic *et al.* (2007) proposed that the UPD adlayer is oxidized by the more noble metal cations, which are simultaneously reduced and deposited on the gold substrate, and this can be expressed as:

$$M^0_{UPD} + (m/z)\, P^{z+} \rightarrow M^{m+} + (m/z)\, P^0, \qquad (2.4)$$

where M^0_{UPD} represents a UPD metal adatom on the electrode surface S and P^{z+} is a noble metal cation with positive charge z+ and valence z. However, in case of Pt (IV) replacement, a submonolayer of Pt is formed because of the stoichiometry:

$$2Cu^0 \text{ UPD} + Pt^{4+} \rightarrow 2Cu^{2+} + Pt^0. \qquad (2.6)$$

Their report suggested that the growth of mono-atomically high, nanoclusters randomly distributed on the Au (111) surface could be formed by the spontaneous redox replacement of a previously prepared Cu UPD layer by Pt (IV) solute. Figure 2.3 shows the illustration of Pt surface-limited redox replacement reaction (SLR^3) with a Cu sacrificial UPD layer (Adzic, *et al*.,2007).

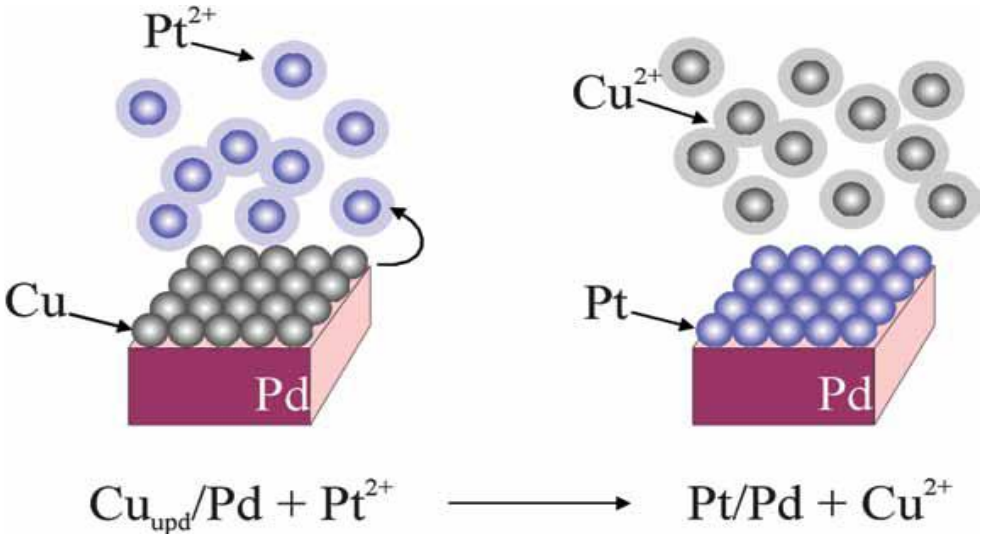

Figure 2.3: Illustration of Pt surface-limited redox reactions (Adzic, *et al*., 2007)

Regardless of the random distribution of these nanoparticles, the results of Brankovic *et al.* (2001) suggested that it might be possible to form ideal single-crystalline nanofilms of Pt by repeating this SLR^3 in a layer-by-layer methodology. In fact, Stickney *et al.* (2006) has attempted to grow Pt nanofilms by repeated application of the SLR^3. Stickney and his colleagues used iodine atomic layer as a surfactant to promote layer-by-layer growth and the formation of well-ordered deposits. It appeared that the first atomic layer of the deposited Pt resulted in a surface alloy, while depositions of the second Pt atomic layer lead to the formation of a well-ordered Pt adlayer.

The Pt atomic layer deposition approach has several unique features that make these electrocatalysts very attractive for practical applications. It is primarily because of their potential for resolving the problems of high Pt content and low efficiency in conventional Pt electrocatalysts fabrications (Mukerjee, Srinivasan, & Appleby,1993). This is done by synthesizing electrocatalysts with submonolayer amounts of Pt on Ru nanoparticles for hydrogen and/or methanol oxidation (Brankovic, Wang, & Adzic, 2005). The ones with a monolayer of Pt on Pd

nanoparticles are for the oxygen reduction reaction (Zhang, *et al*., 2005a; Zhang *et al*., 2005b). Long-term tests on fuel cells showed that these catalysts showed good stability, and they therefore have the potential to overcome the obstacles mentioned in Chapter 1. This could assist in producing a more marketable fuel cell power source. These catalysts also are likely to be of value to a broad range of other catalytic processes. Some of their features include:

- **High Pt utilization**

  The Pt atoms can be completely utilized, since most of the substrate's surface will be uniformly covered with them (Brankovic, Wang, & Adzic, 2005)

- **Enhanced (or decreased) activity**

  Activity can be enhanced (or decreased) by the configuration of substrate-induced strain, tensile or compressive, in combination with the ligand effect. Strain-induced d-band centre shifts apparently are a major factor determining the catalysts' activity (Hammer & Norskov, 2000). Furthermore, electronic (ligand) effects reflecting the electronic coupling between the overlayer and its supporting substrate play an additional role in determining the catalysts' activity.

- **Enhanced stability**

  Decreased oxidation of the Pt adlayer, resulting from the interaction with the substrate, can enhance the stability of the catalyst. A strong Pt surface segregation, as in a Pt/Ru system, can keep a Pt monolayer/submonolayer at the support surfaces; for this system, both the Ru and Pt atoms are necessary to ensure high activity. This is easily achieved with a Pt submonolayer on Ru (Pt/Ru_{20}) catalyst (Saski *et al.,* 2004).

- **Direct activity correlations**.

  A more direct correlation between the platinum atoms' catalytic activity and their physical properties is attained with this technique. This is because all Pt atoms involved in the reaction can be sampled by the measuring technique. For conventional catalysts, the opposite is true since the measured physical property is determined mostly by bulk Pt atoms that do not interact with the reactants (Adzic *et al.,* 2007).

2.6 Experimental Techniques for Characterization of Electrocatalysts

Electrochemical energy conversion for technical applications relies largely on the high catalytic reactivity of electrocatalysts (Hammer & Norskov 2000). Characterisation methods play an important role in the selection of appropriate electrocatalyst materials for direct methanol fuel cell application. A large number of experimental techniques have been explored for the atomic characterisation of electrocatalyst nanostructures and significant progress has been made in understanding their unique structures and properties. The capabilities of diffraction, microscopy and several spectroscopic techniques in realizing the physical properties and atomic structures of these catalysts are reviewed in this section.

2.6.1 Microscopy

It is important to know the degree of aggregation, particle size, and morphology of the particles deposited or adsorbed onto a substrate. There are various types of microscopies that can be used to obtain the above- mentioned properties.

2.6.1.1 Electron Microscopy

An electron microscope is a type of microscope that uses an electron beam to illuminate a specimen and produce a magnified image. An electron microscope (EM) has greater resolving power than a light optical microscope and can reveal the structure of smaller objects because electrons have wavelengths about 100,000 times shorter than visible light photons. They can achieve better than 50 pm resolution and magnifications of up to about a million times whereas ordinary, non-confocal light microscopes are limited by diffraction to about 200 nm resolution and useful magnifications below two thousand times (Skoog, Holler, & Crouch, 2007).The electron microscope uses electrostatic and electromagnetic lenses to control the electron beam and focus it to form an image. These electron optical lenses are analogous to the glass lenses of a light optical microscope (Skoog, Holler, & Crouch, 2007). Electron microscopes are used to investigate the ultrastructure of a wide range of biological and inorganic specimens including microorganisms, cells, large molecules, biopsy samples, metals, and crystals. Industrially, the electron microscope is often used for quality control and failure analysis. Modern electron microscopes produce electron micrographs, using specialised digital cameras (Pauwels *et al*, 2001).

- **Transmission electron microscopy (TEM)**

Transmission electron microscopy (TEM), in which the electrons pass through the sample, generally requires the nanoparticles to be dispersed onto an electron-transparent substrate, such as a thin carbon-coated microgrid. TEM is particularly useful because of the high contrast between the metal atoms (especially heavy metals) and any passivating organic molecules or polymers.

- **High-resolution TEM (HRTEM, HREM)**

High-resolution TEM offers resolution down to the Angstrom level and enables information to be obtained on the structure (atomic packing) rather than just HAADF or “Z-contrast” imaging technique to reveal the internal structure of the nanoparticle. This is based on the different electron scattering powers of different elements, so that chemical information can be obtained in tandem with structural information (Voyles *et al.,* 2006).

This method is particularly useful for studying bimetallic nanoparticles (e.g., Pd-Pt and Pt-Au) where the constituent elements have similar lattice spacings, but they have quite different atomic numbers. Cazayous (2006) and colleagues used energy-filtered TEM to map out the elements in core-shell segregated nanoalloys, such as Cu core Ag shells.

- **Scanning electron microscopy (SEM)**

Scanning electron microscopy (SEM) is similar to TEM but its images are due to secondary electrons emitted by the sample surface following excitation by the primary electron beam. Although SEM images have lower resolution than TEM, SEM is better for imaging bulk samples and has a greater depth of view, giving rise to better 3D images of the sample (Bradley, 1994).

2.6.1.2 Scanning Probe Microscopy

Scanning probe microscopies constitute a group of techniques, including, for example, atomic force microscopy and scanning tunnelling microscopy (STM), in which a surface is imaged at high (sometimes atomic) resolution by rastering an atomically sharp tip across the surface. Measurement of the strength of the

interaction is used to map out the topography, electronic/magnetic structure, or chemistry of the surface (Bradley, 1994; Samor, 2004).

- **Atomic Force Microscopy (AFM).**

A fine tip is brought into close contact with the sample and senses the small repulsive force between the probe tip and the surface. The tip is rastered over the sample to measure the surface topography (Briggs & Seth, 1990).

- **Scanning Tunnelling Microscopy (STM)**

A fine tip is again brought extremely close to the surface, and a voltage is applied between the tip and the sample. The tip is conductive until a tunneling current flows. This flowing current is very sensitive to the distance between the tip and the surface. In the constant current mode, the STM tip is rastered across the surface and moved up or down to keep the current flow constant, thereby generating real-space, atomic resolution topographic images of the sample. In constant height mode, the tunneling current is measured with the tip maintained at a constant height, which can provide information on electronic structure as well as topography. Scanning tunneling spectroscopy is an off-shoot of STM, which measures the local electronic structure (which depends on the atomic species and its environment) of a surface atom. Current vs. voltage (I-V) curves (which are characteristic of the electronic structure at a specific location on the surface) are obtained by measuring the tunneling current as a function of the bias voltage (Briggs & Seth, 1990).

2.6.2 Spectroscopy

Spectroscopy is the study of the interaction between matter and radiated energy. Historically, spectroscopy originated through the study of visible light dispersed

according to its wavelength. Later the concept was expanded greatly to comprise any interaction with radioactive energy as a function of its wavelength or frequency. Spectroscopic data are often represented by a spectrum, a plot of the response of interest as a function of wavelength or frequency (Skoog, Holler, & West, 1996).

2.6.2.1 X-ray Spectroscopy

High-energy X-ray radiation is particularly useful for studying metallic nanoparticles because the binding energies of the atomic core electrons are very sensitive/ responsive to the atomic number of the element, generally allowing metals which are adjacent in the periodic table to be distinguished (Skoog, Holler, & Crouch, 2007).

- **X-ray Diffraction (XRD)**

X-ray and electron diffraction can be performed on single nanoparticles or arrays of nanoparticles. XRD has been particularly widely used to study surface-supported nanoparticles, affording information on structure, crystallinity, lattice spacing, particle size, and qualitative chemical composition information (Renouprez *et al*., 1996).

Electron diffraction, on the other hand, has been more widely used for molecular beams of clusters. Although interpretation of the electron diffraction results is complex, information on the geometry, average size, and temperature of the nanoparticles may be obtained (Maier-Borst *et al.*, 1999).

-
-

- **X-ray Absorption Spectroscopy (XAS)**

XAS is very useful for probing the internal structures of metal nanoparticles and species adsorbed on them (Bradley, 1994; Russell & Rose, 2004). Its use has increased due to the availability of synchrotron radiation facilities around the world. Each element's X-ray absorption spectrum is unique and enables information to be obtained about the elements present in the nanoparticle and the local atomic environment and geometry, electron density, oxidation state, electronic configuration, site symmetry, coordination number, and interatomic distances. A recent review of the application of XAS to Pt-containing nanoalloys (with particular emphasis on electrocatalysts for fuel cell applications) has been presented by Russell and Rose (2004).

- **Extended X-ray Absorption Fine Structure (EXAFS)**

A monochromatic X-ray beam is directed at the sample. The photon energy of the X-rays is gradually increased so that it traverses one of the absorption edges of the elements contained within the sample. Below the absorption edge the photons cannot excite the electrons of the relevant atomic level, and thus, absorption is low. However, when the photon energy is just sufficient to excite the electrons, a large increase in absorption occurs, which is known as the absorption edge. The resulting photoelectrons have low kinetic energies and can be backscattered by the atoms surrounding the emitting atom. The backscattering of the photoelectron affects whether the X-ray photon is absorbed in the first place. Hence, the probability of X-ray absorption depends on the photon energy. The net result is a series of oscillations on the high photon energy side of the absorption edge. These oscillations can be used to determine the atomic number, distance, and coordination number of the atoms surrounding the element whose absorption edge

is being examined. The necessity to scan the photon energy requires the use of synchrotron radiation in EXAFS experiments (Bard & Faulkner, 2001).

- **Near-edge X-ray Absorption Fine Structure (NEX-AFS)**

It is generally applied to study chemisorbed molecules on surfaces. Information concerning the orientation of the molecule can be inferred from the polarization dependence. NEXAFS is sensitive to bond angles, whereas EXAFS is sensitive to the interatomic distances. NEXAFS spectra are frequently dominated by intramolecular resonances of ð or ó symmetry. The energy, intensity, and polarization dependence of these resonances can be used to determine the orientation and intramolecular bond lengths of the molecule on the surface (Briggs & Seth, 1990).

- **X-ray Absorption Near-Edge Structure (XANES)**

It uses radiation up to 40 eV from the X-ray absorption edge and can provide information about the vacant orbitals, electronic configuration, and site symmetry of the absorbing atom. The absolute position of the edge contains information about the oxidation state of the absorbing atom. In the near edge region, multiple scattering events dominate. Theoretical multiple scattering calculations are compared with experimental XANES spectra in order to determine the geometrical arrangement of the atoms surrounding the absorbing atom (Briggs & Seth, 1990).

- **X-ray Photoelectron Spectroscopy (XPS)**

XPS is based on the photoelectric effect, whereby absorption of light by an atom, molecule, or solid/surface results in the ejection of electrons, provided that the photon energy is sufficient to overcome the binding energy of the electron. For XPS, Al KR (1486.6 eV) or Mg KR (1253.6 eV) photons are generally used

(Menezes & Knickelbein, 1991). Both valence and core electrons can be ejected by X-ray radiation. The core electron binding energies are characteristic of each element, and the peak areas can be used to determine the composition. As the peak shape and binding energy are sensitive to the oxidation and chemical state of the emitting atom, XPS can also provide chemical bonding information (Nonose, Sone, & Kaya, 1991; Hoshino *et al*., 1995; Koyasu *et al.,* 2002). The XPS technique is surface specific due to the short range of the ejected photoelectrons.

- **Energy-Disperse X-ray Spectroscopy (EDX, EDS)**

This analytical technique is often used in conjunction with SEM or TEM. An electron beam (typically 10-20 keV) strikes the surface of a conducting sample, causing X-rays to be emitted, whose energies depend on the material under examination. The X-rays are generated in a region about 2 m in depth. By scanning the electron beam across the material, an image of each element in the sample can be obtained. EDX is a high-resolution variant of electron microprobe analysis or X-ray microanalysis whereby information can be obtained on the chemical composition of individual nanoparticles (Arico, Baglio, & Antonucci, 2009).

2.6.2.2 Infrared (IR) Spectroscopy

IR (including Fourier transform IR (FT-IR)) spectroscopy is widely used to study the vibrational spectra of small molecules adsorbed on metallic clusters. For example, by making comparisons with pure metal clusters or surfaces, IR spectroscopy of small molecules (e.g., CO) adsorbed on bimetallic nanoparticles can be used as a probe of the surface composition and structure (Bradley, 1994; Toshima & Yonezawa, 1998).

2.6.2.3 Photoelectron Spectroscopy

Electronic and dynamical properties of metal clusters can be investigated with photoelectron spectroscopy by using lower energy radiation (from IR to UV) (Bragg *et al*., 2005).

2.6.2.4 Surface-Enhanced Raman Spectroscopy

The Raman scattering intensity of molecules is greatly enhanced (by as much as 5 orders of magnitude) when they are absorbed on certain metals (Bradley, 1994). The effect (which again probes the vibrational structure) has been used to study the binding of adsorbates on metallic nanoparticles and the cluster formation process (Bradley, 1994).

2.6.2.5 Nuclear Magnetic Resonance (NMR*)*

NMR spectroscopy probes the local magnetic environment of a nucleus with non-zero magnetic moment in terms of its chemical shift (which depends on the amount of diamagnetic and paramagnetic shielding or deshielding) and line splitting due to magnetic coupling to the nuclear spins of neighbouring atoms. In the case of quadrupolar nuclei (with nuclear spin I > 1/2) the line shape and number of peaks can also give information on the symmetry of the atomic environment. Regarding mono- and bimetallic nanoparticles, NMR spectroscopy has been performed on metallic nuclei (e.g., ^{63} Cu, ^{103} Rh, ^{195} Pt, and ^{197} Au), where the chemical shift is dominated by the Knight shift, arising from the conduction electrons, thereby giving a measure of the metallic nature of the particle (Bradley, 1994).

Cluster paramagnetism and ferromagnetism can also be probed by metal NMR. NMR has also been used to investigate the structures of adsorbed organic

molecules (including passivating molecules and polymers), for which the most useful nuclei are ^{1}H, ^{13}C, and ^{31}P (Bradley, 1994).

- **Electrochemical NMR Spectroscopy (EC-NMR)**

EC-NMR was introduced in the late 1980s for the study of electrochemical surfaces, providing an electronic level description of electrochemical interfaces based on the local density of states at the Fermi level. ^{13}C and ^{195}Pt are particularly useful nuclei for investigating electrochemical interfaces and probing nanoparticle electrode surface modifications. In the field of nanoalloys, Babu and co-workers used EC-NMR extensively to study nanoalloy particles in fuel cell electrodes (Babu *et al*., 2003)

2.6.2.6 Ion Spectroscopy/Scattering (IS)

Ion spectroscopy is a technique, which involves accelerating ions onto a sample and detecting the energies and distribution of scattered ions. Ion energies are as follows: 1-10 keV for low-energy IS (LEIS), 20-200 keV for medium-energy IS, and 200-2000 keV for high-energy IS. The higher the incident ion energy, the smaller the target atoms appears, though the yields are smaller, so low energies are best for surface-specific information (Bradley, 1994).

The energy and angle of the scattered ions are analysed simultaneously, allowing measurement of atomic mass (and hence composition), depth (down to 1 atomic layer is possible), and surface structure. Depending on the incident ion energy, ion scattering may be accompanied by surface etching. Following the time evolution of the surface composition therefore allows depth profiling of the composition of bimetallic nanoparticles (Renouprez *et al*, 2001; Rousset *et al*, 2002).

2.6.2.7 Mass Spectrometry

Mass spectrometry is used to study the mass abundance of clusters in a cluster molecular beam by deflecting them (according to their mass) in an electric field after they have been ionized, generally by electron impact or laser ionization.

Mass abundances occasionally show peaks which are intense relative to their neighbours. These “magic numbers” can often be explained in terms of extra thermodynamic or kinetic stability at these particular sizes, which may be due to electronic or atomic packing effects (Brack, 1993; De Heer, 1993; Martin, 1996).

2.6.2.8 Inductively Coupled Plasma optimal emission spectroscopy

Inductively coupled plasma optical emission spectrometry (ICP-OES), which is also referred to as inductively coupled plasma atomic emission spectroscopy (ICP-AES) is an analytical technique used for the detection of trace metals. This technique is a type of emission spectroscopy that uses the inductively coupled plasma to produce excited atoms and ions that emit electromagnetic radiation at wavelengths characteristic of a particular element. The intensity of this emission is indicative of the concentration of the element within the sample. The ICP-AES is composed of two parts: the ICP and the optical spectrometer. The ICP torch consists of 3 concentric quartz glass tubes. The output or "work" coil of the radio frequency (RF) generator surrounds part of this quartz torch. Argon gas is typically used to create the plasma (Lide, 2000).

When the torch is turned on, an intense electromagnetic field is created within the coil by the high power radio frequency signal flowing in the coil. This RF signal is created by the RF generator which is, effectively, a high power radio transmitter driving the "work coil" the same way a typical radio transmitter drives a

transmitting antenna. The argon gas flowing through the torch is ignited with a Tesla unit that creates a brief discharge arc through the argon flow to initiate the ionization process. Once the plasma is ignited, the Tesla unit is turned off (Skoog, Holler, & West, 1996).

The argon gas is ionized in the intense electromagnetic field and flows in a particular rotationally symmetrical pattern towards the magnetic field of the RF coil. Stable, high temperature plasma of about 7000 K is then generated as the result of the inelastic collisions created between the neutral argon atoms and the charged particles (Skoog, Holler, & Crouch, 2007).

A peristaltic pump delivers an aqueous or organic sample into a nebulizer where it is changed into mist and introduced directly into the plasma flame. The sample immediately collides with the electrons and charged ions in the plasma and is itself broken down into charged ions. The various molecules break up into their respective atoms, which then lose electrons and recombine repeatedly in the plasma. Once the atoms or ions are in their excited states, they decay to lower stable states by releasing energy (Skoog, Holler, & Crouch, 2007).

In some designs, a shear gas, typically nitrogen or dry compressed air is used to 'cut' the plasma at a specific spot. One or two transfer lenses are then used to focus the emitted light on a diffraction grating where it is separated into its component wavelengths in the optical spectrometer. In other designs, the plasma impinges directly upon an optical interface, which consists of an orifice from which a constant flow of argon emerges, deflecting the plasma and providing cooling while allowing the emitted light from the plasma to enter the optical chamber. Still

other designs use optical fibres to convey some of the light to separate optical chambers (Skoog, Holler, & Crouch, 2007).

Within the optical chamber(s), after the light is separated into its different wavelengths (colours), the light intensity is measured with a photomultiplier tube or tubes physically positioned to "view" the specific wavelength(s) for each element line involved, or, in more modern units, the separated colours fall upon an array of semiconductor photodetectors such as charge coupled devices (CCDs). In units using these detector arrays, the intensities of all wavelengths (within the system's range) can be measured simultaneously, allowing the instrument to analyse for every element to which the unit is sensitive all at once. Thus, samples can be analysed very quickly (Skoog, Holler, & Crouch, 2007).

The intensity of each line is then compared to previously measured intensities of known concentrations of the elements, and their concentrations are then computed by interpolation along the calibration lines (Skoog, Holler, & West, 1996).

ICP-OES is especially important for the analysis of the platinum group metals (PGMs): platinum, palladium, rhodium, iridium and ruthenium, as well as base metals such as copper, zinc and nickel, being accurate to one part per million (ppm). The technique is destructive but it has accurately determined both major and trace elements (Lide, 2000).

The high precision of ICP methods is due to the stability of intensity quotients of emission lines, essentially of gold (267.6 nm), platinum (265.9 nm), and palladium (340.5 nm) and the internal standard element yttrium (371.02 nm). If the precious

metal and yttrium lines are measured simultaneously, reproducibility of the results of at least 0.01 % can be achieved. Special software generally corrects for interferences caused by the presence of different elements within a given sample matrix (Skoog, Holler, & Crouch, 2007).

2.6.3 Electrochemical properties

Varieties of electrochemical techniques have been applied to nanoalloys. These techniques range from cyclic voltammetry to scanning electrochemical microscopy. The measurements are particularly important for nanoparticles employed as electrode materials in electrocatalytic fuel cells. Russell and Rose (2004) reviewed research involving in-situ XAS measurements in electrochemical cells, whereby the variation of particle size, coordination number, and other structural parameters can be investigated.

Compared with UHV and electron-based spectroscopic techniques, electrochemical techniques for surface measurement allow direct investigation of the surfaces of real catalysts under ambient conditions, thereby bridging the so-called “pressure” and “materials” gap between surface science and heterogeneous catalysis (Attard *et al,* 2003).

Attard *et al.* (2003) reported the combination of CV (used as a measure of local structure) and STM to characterize the surface morphology of Pt particles (by comparison with bulk Pt surfaces) as well as the bimetallic surfaces formed by Bi adsorption on Pt nanoparticles (Attard *et al.*, 2003).

2.6.3.1 Linear Sweep Voltammetry (LSV)

Linear sweep voltammetric measures the electric response whilst sampling it at a constant scan rate from initial to final electric potential. The voltage scan rate (***v***) is calculated from the slope of the line. Clearly by changing the time taken to sweep the range the scan rate is altered. The characteristics of the linear sweep voltammogram recorded depend on a number of factors including:

- The rate of the electron transfer reaction(s).
- The chemical reactivity of the electroactive species.
- The voltage scan rate.

In LSV measurements the current response is plotted as a function of voltage rather than time, unlike potential step measurements (Bard & Faulkner, 2001).

2.6.3.2 Cyclic Voltammetry (CV)

Cyclic voltammetry entails cycling a potential applied to an electrode immersed in a quiescent electrolyte solution, containing an analyte species, through a defined potential range and measuring the resultant current. The measured current is a result of electron flow through the electrochemical circuit and is due to the diffusional mass transfer of electro-active species as migration and convection are minimised. The applied potential is swept back and forth between two designated potentials, at a constant rate, by a potentiostat (Bard & Faulkner, 2001).

CV provides information on the thermodynamics of redox processes and the kinetics of heterogeneous electron-transfer reactions. It plays an integral role in a comprehensive characterization of nanostructured electrocatalysts. CV can be used advantageously to probe surface reactions in-situ under well-controlled

conditions, giving insight into the catalytic mechanisms and the catalytic activity of the electrocatalysts such as:

- Stability in oxidized and reduced forms.
- Molecular adsorption in redox process.
- Measurements of kinetic rate constants.
- Study of reaction mechanism.
- Reversibility of electrochemical reaction.
- Standard redox potential, $E_o = (E_{pa}+E_{pc})/2$
- Electron transfer number, $\Delta E = E_{pa}-E_{pc} = 58/n$,

  *n: electron transfer number per mole (Beden, Leger, & Lamy, 1992)

Typically, a three-electrode system consisting of a working electrode, a reference electrode, and counter electrode is used. The working electrode is the electrode of interest at which potential is applied. The reference electrode experiences zero current and has a known standard potential against which all other potentials are measured. The counter electrode completes the circuit and is usually Pt or gold wire, graphite, or glassy carbon. The output signal, called a voltammogram, represents a plot of current in amperes, versus potential in volts (Bard & Faulkner, 2001; Vielstsich, Lamm, & Gasteiger, 2003).

2.6.3.3 Chronoamperometry

Chronoamperometry is an electrochemical technique in which the potential of the working electrode is stepped and the resulting current from Faradic processes occurring at the electrode (caused by the potential step) is monitored as a function of time. Limited information about the identity of the electrolyzed species can be obtained from the ratio of the peak oxidation current versus the peak reduction

current. However, as with all pulsed techniques, chronoamperometry generates high charging currents, which decay exponentially with time as any RC circuit. The Faradaic current, which is due to electron transfer events and is most often the current component of interest, decays as described in the Cottrell equation. In most electrochemical cells, this decay is much slower than the charging decay-cells with no supporting electrolyte are notable exceptions. This method is most commonly investigated with a three electrode system. Since the current is integrated over relatively longer time intervals, chronoamperometry gives a better signal-to-noise ratio in comparison to other amperometric techniques (Bard & Faulkner, 2001).

2.7 Methanol Oxidation Reaction (MOR)

The oxidation of methanol and water molecules is the principal reaction occurring at the anode of DMFCs. Platinum is the best material for the adsorption and dehydrogenation of methanol. The formation of intermediate species such as CO (Hamnett, 1999; Bockris & Srinivasan, 1969), formic acid and formaldehyde poisons the anode, which impedes the catalytic performance for methanol oxidation. Poisoning from CO species is severe on a Pt electrode surface during the electro oxidation of methanol (Briggs & Seth, 1990).

Beden *et al*. (1992) have proposed the detailed mechanism for the oxidation of methanol at the Pt electrodes. The methanol is adsorbed on the Pt surface (equation 2.6) and then undergoes a sequence of dehydration steps to yield linearly bonded CO species (equation 2.7 to 2.10), as denoted below:

$$Pt + CH_3OH \rightarrow Pt\,(CH_3OH)_{ads} \qquad (2.6)$$

$$Pt\,(CH_3OH)_{ads} \rightarrow Pt\,(CH_3O)_{ads} + H^+ + e^- \quad (2.7)$$

$$Pt\,(CH_3O)_{ads} \rightarrow Pt\,(CH_2O)_{ads} + H^+ + e^- \quad (2.8)$$

$$Pt\,(CH_2O)_{ads} \rightarrow Pt\,(CHO)_{ads} + H^+ + e^- \quad (2.9)$$

$$Pt\,(CHO)_{ads} \rightarrow Pt\,(CO)_{ads} + H^+ + e^- \quad (2.10)$$

(Beden, Leger, & Lamy, 1992)

On the pure Pt surface water dissociation will occur only at higher anodic overpotentials to form Pt-$(OH)_{ads}$ species with Pt-adsorbed CO to give carbon dioxide (Equation 2.9):

$$Pt + H_2O \rightarrow Pt\,(OH)_{ads} + H^+ + e^- \quad (2.11)$$

The last step is the reaction of Pt adsorbed OH with Pt-CO species to give carbon dioxide (Equation 3.10):

$$Pt\,(CO)_{ads} + Pt\,(OH)_{ads} \rightarrow Pt + M + CO_2 + H^+ + e^- \quad (2.12)$$

At potentials of technical interest for DMFCs (<0.6V vs. RHE), the dissociation of water on the Pt surface is the rate determining step (Chandrasekaran, Wass, & Bockris, 1990).

Water dissociation will, however, occur at less positive potentials on the promoter metal, M, like Ru (0.2 V vs. RHE) and Ru^0 transfers oxygen more effectively than Pt^0 (equations 2.11 to 2.13) (Ticianelli *et al*., 1988).

$$M + H_2O \rightarrow M\text{-}(H_2O)_{ads} \quad (2.11)$$

$$M\text{-}(H_2O)_{ads} \rightarrow M\text{-}(OH)_{ads} + H^+ + e^- \quad (2.12)$$

$$Pt\,(CO)_{ads} + M\text{-}(OH)_{ads} \rightarrow Pt + M + CO_2 + H^+ + e^- \quad (2.13)$$

An efficient catalyst must allow complete oxidation to CO_2 during methanol oxidation. Carbon supported Pt/Ru catalyst has been shown to be promising among the candidates available for the electrochemical oxidation of methanol at anodes of DMFCs. A Pt/Ru atomic ratio of 1:1 was reported as the preferred atomic composition (Iannielo *et al.,* 1994; Gasteiger *et al.*, 1994).

The enhanced electrocatalytic activities enabled by oxophilic metals such as Ru, Sn, Mo, Ni, Ti, Co and Au combined with Pt catalysts have been explained by the bifunctional mechanism: contraction of Pt–Pt bonding distance leading to a favourable condition for the ORR (Watanabe & Motoo, 1975) and the ligand (electronic) mechanism (Pt d-band vacancy modification) (Rodriquez & Goodman, 1992). Lu and Masel (2001) have noticed that the bifunctional effect has a larger effect on CO removal than the ligand effect when they used 0.25 monolayer of Ru deposited on Pt (110) surface in ultra-high vacuum (UHV) conditions. They found out that of the 4-6 kcal/mol (170-260 meV) reduction in the potential for CO removal, only about 1 kcal/mol (40 meV) is associated with the ligand effect, whereas 3-5 kcal/mol (130-220 meV) is associated with the bifunctional mechanism.

Another key factor used to better understand the relationship between the surface composition and the catalytic activity is surface segregation. The segregation phenomenon is the tendency of one metal to segregate to the surface of another metal and basically controls the alloy surface composition. So it is very important

to determine if surface segregation occurs for the bimetallic alloys. In regards to this phenomenon, it is also known that, for similar atomic sizes, the metal of the alloy having the lower heat of sublimation tends to segregate (Kiejna, 1990). For similar heats of sublimation, it is the metal with the smallest atomic radius that tends to segregate (Fain & McDavid, 1976). Moreover, the metal having the larger Wigner-Seitz radius segregates (Yamauchi, 1976). The Wigner-Seitz radius is defined as the radius of a sphere of the same volume as the volume per particle. In fact, the driving force for the surface segregation is the reduction in the surface energy of the segregated alloy (Kiejna, 1990).

It is virtually undisputed that Pt/Ru is better than Pt and there is a consensus about the fact that, for the methanol oxidation, Pt/Ru is the best material among the Pt-based bimetallic electrocatalysts (Wasmus, 1999; Antolini, Salgado, & Gonzalez, 2006; Sundmacher *et al*., 2001; Liu *et al.,* 2006; Markovic & Ross, 2002). These two metals, i.e. Pt and Ru, have close electronegativities and similar bulk Wigner-Seitz radii. Pt, when alloyed with Ru, strongly segregates while Ru strongly antisegregates. Therefore, a Ru site should be surrounded by some Pt sites, which is in agreement with the three to five Pt atoms as seen in reactions 2.6-2.13 necessary to activate the adsorption of methanol and the single Ru atom necessary to activate water (Greeley & Norkov, 2005). Moreover, the Pt electronic structure should be changed by the presence of neighbouring Ru. According to Lima, et al.(2006), Demirci (2007), Ruban *et al*.(1997), Hammer & Norskov (2000) and Greeley & Norkov (2005), the Pt d-band centre shifts down when Pt is alloyed with Ru, which suggests weaker Pt-adsorbate bonds, while the Ru d-band centre slightly shifts up. In other words, when Pt and Ru are alloyed, the adsorption of adsorbates is weaker on the Pt sites and stronger on the Ru sites. These

tendencies may explain the enhanced activity of Pt/Ru, which is attributed to both the bifunctional mechanism and electronic effect, where the bifunctional mechanism involves the adsorption of OH^- species on Ru atoms thereby promoting the oxidation of CO to CO_2 (Watanabe & Motoo, 1975). In this way, the Pt poisoning by the CO-like species would be decreased because these species would more weakly adsorb on Pt and Ru would provide the necessary OH^- species, which would be available permanently on the Ru surface sites, more strongly adsorbing the OH^- species.

Another fundamental insight into the oxidation mechanism can be obtained with the advent of computational methods. Ishikawa *et al*. (2000) have studied the adsorption functional self-consistent field X_α method. It was found from their results that the presence of M atoms weakens the Pt-C bond, and generally slightly lowers the CO stretching frequency of adsorbed CO. Ru and Sn electronic substation for platinum is found to alter the dissociation energy of H_2O. The results indicate that the promoting effect of alloying atoms involves both modification of Pt-CO binding and water activation.

The inclusion of Ni in Pt, Pt/Ru or Pt/Sn can greatly be of benefit to the enhancement of the catalytic activity and stability toward MOR in acidic media. This is because of the combined effect of the oxygen donation from Ni-oxide/hydroxide and the change of electronic structure of Pt by electron transfer from Ni to Pt (Choi *et al.*, 2003; Poh *et al*., 2012; Ribareneira & Hoyos, 2010).

XPS data collected by Park *et al.* (2002) confirmed that Ni and Ru additives to Pt exist as mixed metal/oxide phases, whereas Pt is entirely metallic. In the Pt/Ni alloy nanoparticles, the Ni species include metallic Ni, NiO, $Ni(OH)_2$, and NiOOH,

and the ratio between the three oxides is similar for the different Pt/Ni alloys. The existences of these oxides in the catalyst were found to provide an oxygen source for CO oxidation at lower potentials by this group (Park, *et al.,* 2002).

Furthermore, in the potential range, at which the alcohol electrooxidation proceeds, Ni from the Pt/Ni alloy would not dissolve in electrolyte, while Ru would dissolve out of the Pt/Ru alloy. Resistance to dissolution has been attributed to a nickel hydroxide passivated surface which enhances the stability of Ni in the Pt lattice (Rodriquez & Goodman, 1992). The Pt/Ni alloy also presents improved activity for oxygen reduction than Pt alone by reducing the cell voltage when used as a cathode (Mukerjee & Srinivasan, 1993).

Since the bonding energy of Ru-O is similar to that of Pt-C, Ru in the Pt/Ru easily oxidizes the CO intermediate CO_2 by the bifunctional mechanism. Subsequently, the energy of the Ni-O bond is 200 kJ/mol lower than that of Pt/C. Some essential characteristics of Pt/Ni may not be explained by the bifunctional mechanism alone but could be explained by the segregation phenomenon (Lide, 2000; Ley, *et al*., 1997; Gura, *et al.*, 1998).

Pt, when alloyed with Ni, moderately segregates, as already reported by Park, *et al.* (2002) and its Pt d-band centre shifts down. The d-band centre of Ni shifts up when they are alloyed with Pt. This analysis of the surface modifications suggests the following remarks: compared with Pt/Ru, (i) the adsorption of OH^- species on the Ni sites should be weaker; (ii) the lower segregation of Pt in Pt/Ni is an indication of a higher dilution of Pt and so a decrease in the number of Pt surface sites. Therefore, Pt/Ru should be a better catalyst than Pt/Ni as has been mentioned in statements leading up to this point.

Ti, on the other hand, strongly segregates when alloyed with Pt but its Pt d-band centre shifts up (Ringer *et al.,* 2000). Due to this phenomenon, Ti has also been studied as a promoter of Pt catalyst activity because it was identified as a promising candidate for improving both the MOR (Abe *et al*., 2008; Janssen & Moolhuysen, 1976; Hamnett, Weeks and Kennedy, 1988), and ORR activity (Ding, More, & He, 2008; Shimm *et al*., 2001).

As early as 1976, Janssen and Moolhuysen (1976) reported a Pt/Ti alloy as a promising catalyst for the MOR. Hamnett *et al.* (2003) reported that TiO_2 acts as a promoter for the MOR at low current densities while it acts as an inhibitor at high current densities. A Pt/Ti catalyst investigated by Abe *et al.* (2008) exhibited higher MOR activity than Pt/Ru and Pt catalysts. In addition, they claimed that the ordered Pt/Ti phase exhibited higher MOR activity than disordered Pt/Ti.

For the ORR, Ding *et al.* (2008) reported that they could achieve a two-fold improvement over the ORR activity of pure Pt with a $Pt_{75}Ti_{25}$ catalyst. They observed the Pt/Ti phase in their Pt_{75}/Ti_{25} catalyst, but the role of the Pt/Ti phase was not clear, as they could not obtain 100% ordered Pt/Ti phase even after 950°C annealing. A $Pt/TiO_2/C$ catalyst was also reported to exhibit higher ORR activity than pure Pt/C catalyst (Shimm, Lee, Cairns & Lee, 2001). Xiong and Manthiram (2004) reported that a $Pt/TiO_x/C$ catalyst showed higher ORR activity than Pt in the presence of methanol. These reports suggest that Pt/Ti alloys merit further investigation for application as MOR and ORR catalysts.

CHAPTER 3

METHODOLOGY

3.1 Experimental Overview

Platinum nanoparticles were electrodeposited on carbon paper; nickel foam and titanium mesh as reported by (Ticianelli *et al*, 1988, Abson, 2006 and Bidault *et al*., 2009, Freitas *et al.*, 2006 and Lim *et al.*, 2004) following the methods used by Mkwizu *et al. (*2011*).* These substrates were chosen because of their high surface areas, porosity, high conductivity and their proven ability to function as catalyst substrates, current collectors and mechanical support materials. The substrates were placed in a specially designed flow cell. The flow diagram below (Figure 3.1) illustrates the sequence of events during deposition and characterization methods.

The deposited Pt nanoparticles were characterized using scanning electron microscopy coupled to energy dispersive X-ray spectroscopy (SEM/EDX). SEM helped with the determination of the morphology and EDX was used to verify the presence of platinum after the deposition. Inductively coupled plasma was used to determine the change in weight of Pt with each layer deposited. The sizes of the deposited agglomerated Pt nanoparticles were determined using atomic force microscopy (AFM). The activity of the prepared catalyst towards methanol oxidation was studied using electrochemical methods (i.e. cyclic voltammetry (CV), CO stripping and chronoamperometry (CA)).

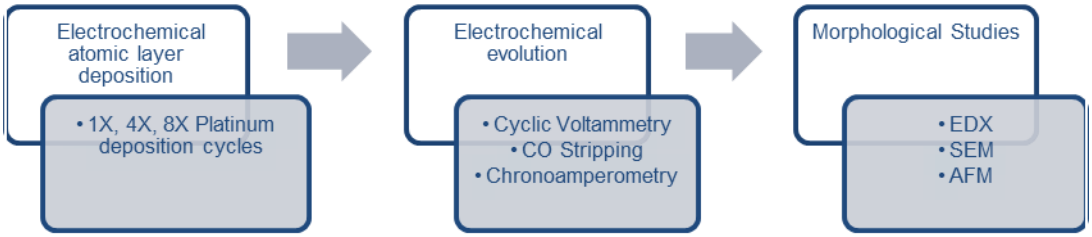

Figure 3.1: Flow chart summarizing the experimental process/approach

3.2. Experimental Details

3.2.1 Reagents and Material

The following Table 3.1 is a summary of all materials used, their suppliers and the countries from which they are sourced.

Table 3.1: Material used and their suppliers**.**

Reagent	Supplier
99.9 % Methanol (CH_3OH)	Merck, South Africa
99.9% Isopropanol (C_3H_8O)	Merck, South Africa
15% wt Nafion	Ion Power Inc., USA
Vulcan XC-72 carbon black	Cabot Corporation, USA
TGPH060 Carbon Paper	Toray Inc., Japan
Nickel foam	Celmet, Japan
Titanium mesh	DEXMET Corporation, USA
Copper Sulphate pentahydrate ($CuSO_4.5H_2O$)	Merck, South Africa
Hydrogen hexachlorohydroxyplatinate ($H_2PtCl_6.6H_2O$)	SA Precious Metal, South Africa
70 % Perchloric acid ($HClO_4$)	GFS Chemicals, USA
Oxalic Acid ($H_2C_2O_4$).	Sigma-Aldrich, South Africa
99 % Acetone (C_3H_6O)	Sigma-Aldrich, South Africa
32% Hydrochloric acid (HCl)	Merck, South Africa
65% Nitric Acid (HNO_3)	Merck, South Africa

Gases (N_2, compressed air, CO) were supplied by Air Liquid with at least 99.99 % purity. The chemicals were used as received without any further purification. All

solutions were prepared with deionised water of resistivity not less than 18.2 MΩ cm.

3.2.2 Pre-treatment of substrates

- **Pre-treatment of titanium mesh**

Ti mesh was washed with distilled water, in a sonicator for 10 min, followed by etching with 10 % oxalic acid for 1 hr at 80 ºC, thoroughly rinsed in warm distilled water and then sonicated, first in acetone for 30 min and then in isopropanol for another 30 min. It was stored in distilled water.

- **Pre-treatment of Ni foam**

Ni foam was cleaned in acetone for 30 min, etched with HCl for 10 min and sonicated in isopropanol for 30 min followed by a sonication in distilled water for 30 min. Compressed air was used to dry the substrate.

- **Modification of carbon paper and Ni foam with a microporous carbon layer**

Prior to Pt electrodeposition, the Ni foam and carbon paper substrates were modified with 0.4 g of carbon black mixed with 7 mL of isopropanol and 5 wt% Nafion solution to prepare an ink. The ink (0.0342 g) was applied on the substrates using the brush method forming a microporous carbon layer.

3.2.3. Instrumental descriptions

- **Electrochemical atomic layer deposition (ECALD)**

The automated experiments for the formation of Pt nanostructures were performed using custom-developed Lab-VIEW (National Instruments, TX) programs (virtual instruments). The pumps, the five-way valve, and the potentiostat were all computer-controlled via standard RS-232 and USB interfaces. Four solutions

could be independently delivered to the flow-cell via the outlet channel of the five-way valve. Figure 3.2 (a and b) shows the actual ECALD instrumental setup used at the CSIR Energy Material fuel cell lab. Below that (Figure 3.3) is an illustration of the ECALD system. A vacuum pump was used to deoxygenate sample solutions prior to saturation with nitrogen. Nitrogen gas (99.99 %) was purged through the cell for 120 min before the measurements and this atmosphere was maintained throughout the experiments.

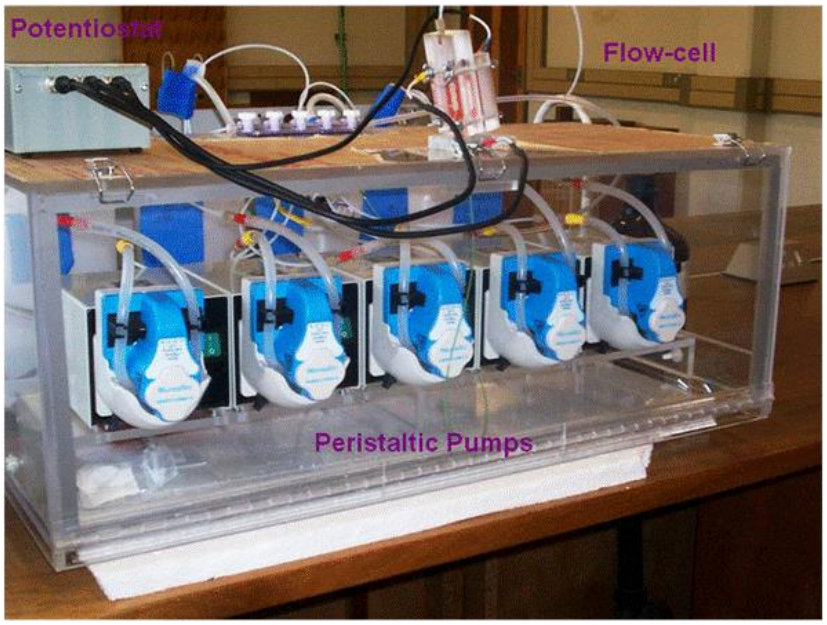

Figure 3.2a: The photograph showing the instrumental set-up – pumping system, potentiostat and flow-cell connectivity (Mkwizu, Modibedi, & Mathe, 2011)

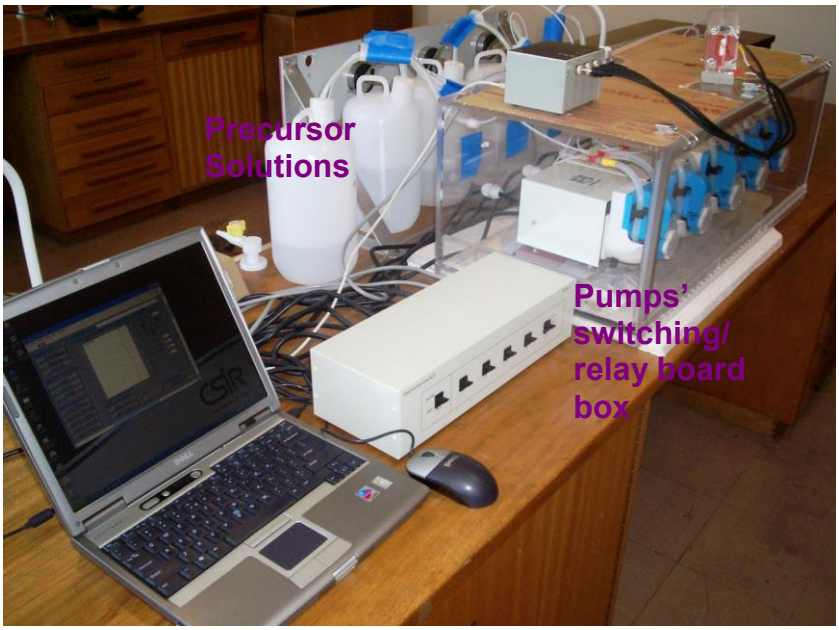

Figure 3.2b: The photograph showing the instrumental set-up – computer-control, relay/switch box, solution reservoirs (Mkwizu, Modibedi, & Mathe, 2011)

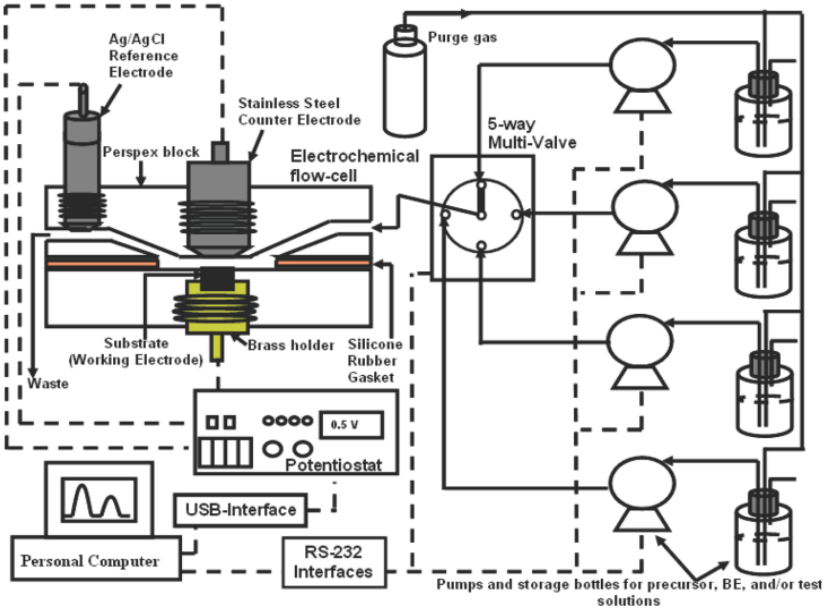

Figure 3.3: Schematic diagram of the instrumental set up developed for automated electrodeposition using the flow cell (Mkwizu, Mathe, & Cukrowski, 2010)

The three-electrode flow cell (Figure 3.4) was used at 25°C for the electrochemical depositions. The flow cell was made up of two Perspex blocks for housing the 0.84 cm thick Au wire and Ag/AgCl(3 M KCl) (BASF) as counter and reference

electrodes respectively. The reference electrode was placed at the outlet channel of the cell. The substrate was used as the working electrode. The exposed area for deposition was 4.35 cm^2. Silicone rubber gaskets were used for sealing purposes. After assembling the cell, electrochemical cleaning was done in 0.1 M $HClO_4$ by applying a one volt potential for 5 min.

Figure 3.4: Photograph of the electrochemical flow-cell used for Pt deposition (Mkwizu, Modibedi, & Mathe, 2011)

The solutions (pH ±1) were delivered by a sequenced cycle which involved: (i) rinsing the cell with the background electrolyte (BE, 0.1M $HClO_4$), followed by filling the cell with 0.1 mM Cu^{2+} solution at selected applied potential E_{appl}, (ii) Cu deposition at E_{dep}, followed by rinsing the cell with the BE at E_{dep}, (iii) filling the cell with the 0.1 mM Pt^{4+} solution at open-circuit (OC), followed by the OC galvanic displacement reaction of Cu adlayers by Pt adlayers, followed by rinsing the cell with the BE at Edep (Mkwizu, Mathe, & Cukrowski, 2010). This process can be followed on Figures 3.5 (a-c) for the unmodified substrates. The numbers 1 through 8 represents the number of cycles. The procedure was repeated for 4 and

8x cycles, so that their electrochemical activities for hydrogen oxidation could be compared.

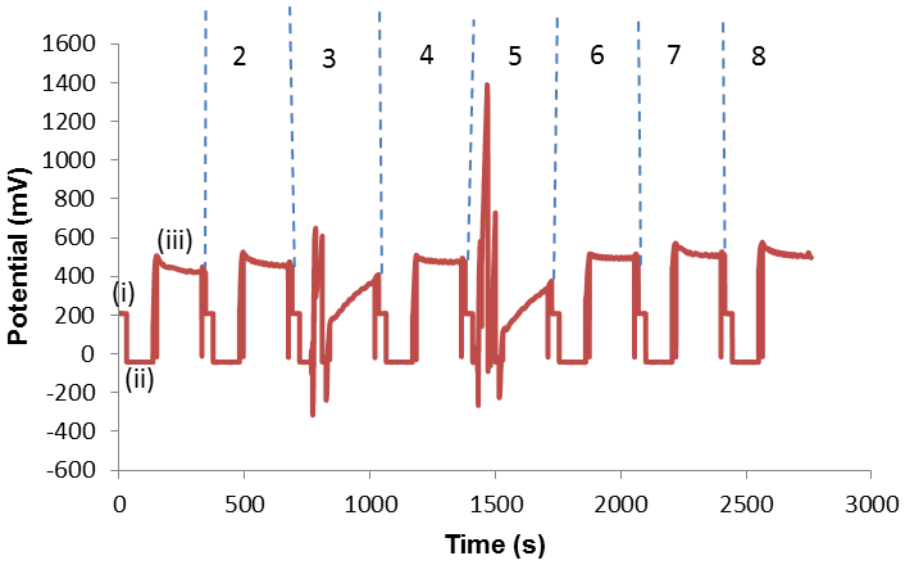

Figure 3.5a: Time-potential curve recorded during Pt depositions on carbon paper

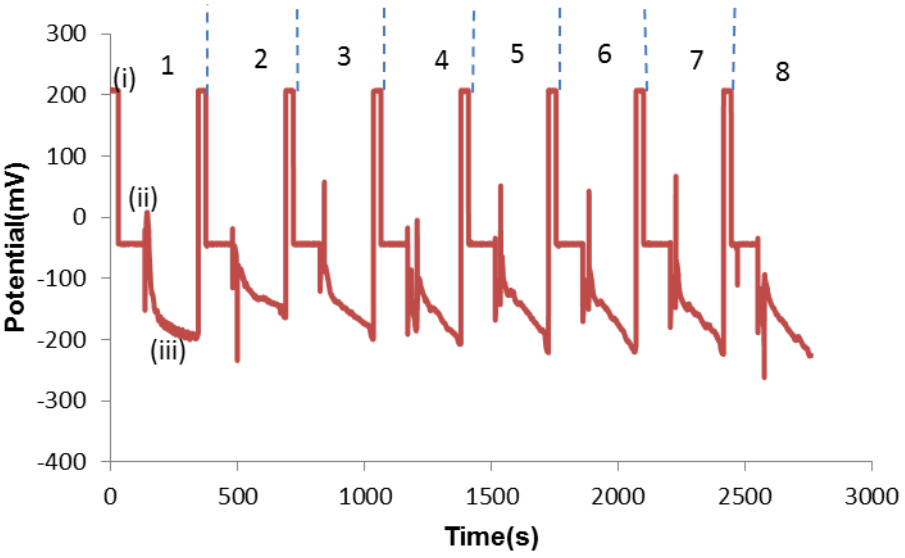

Figure 3.5b: Time-potential curve recorded during Pt depositions on Ni foam

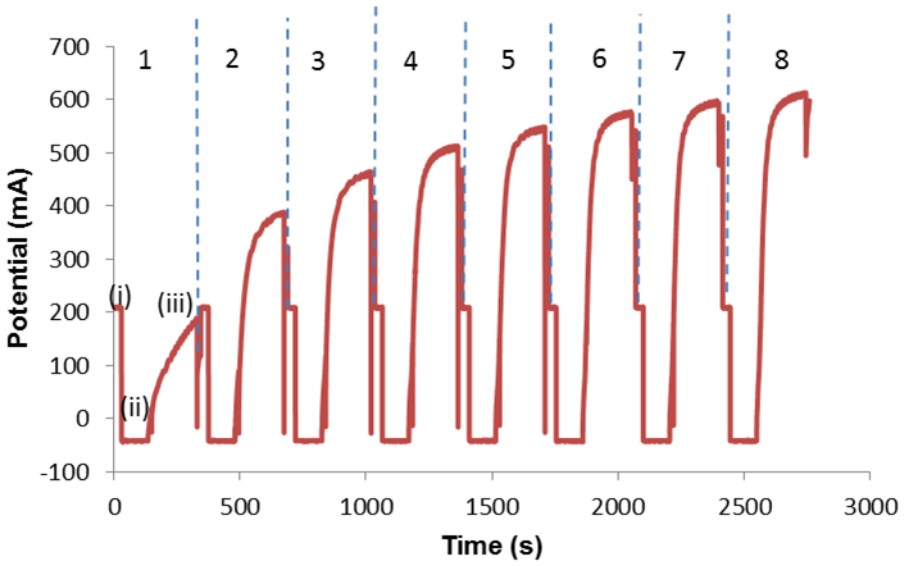

Figure 3.5c: Time-potential curve recorded during Pt depositions on Ti mesh

The ideal step-by-step procedure for Pt deposition is summarized in Figure 3.6. Prior to this experiment, the optimum deposition time and optimum small OPD potential of the sacrificial Cu was determined on the substrates.

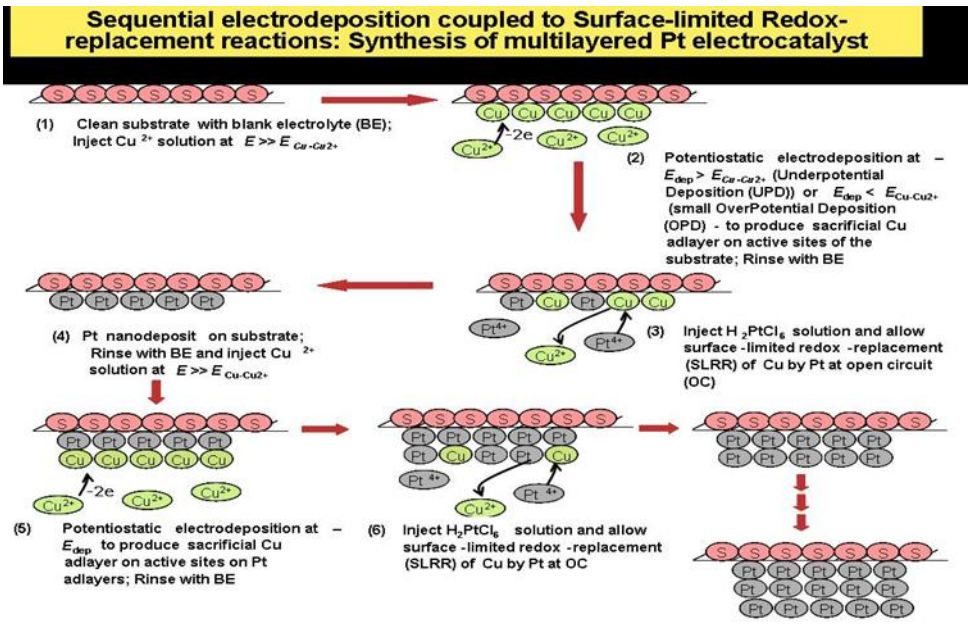

Figure 3.6: Schematic representation of the Sequential deposition of Pt using Cu as a sacrificial metal on various substrates (Mkwizu, Modibedi, & Mathe, 2011)

3.2.4 Electrochemical Characterization

Cyclic voltammetry (CV) and chronoamperometry were used in the study of electrode surface reactions, the behaviour of electrochemically active species and to investigate the quality of electrocatalysts as demonstrated by Larmine (2003) and Pletcher (2009).

These studies were carried out with the three-electrode ECALD flow cell. An AutoLab PGSTAT101 was used for the CA and CV studies. An AutoLab PGSTAT302 potentiostat was used for the CO stripping studies. Au wire and Ag/AgCl/3M KCl (BASF) were used as counter and reference electrodes respectively. The Pt electrodeposited on the substrates (4.35 cm^2) was used as the working electrode. CO stripping voltammograms were measured by the oxidation of pre-adsorbed CO (CO_{ads}) in 0.1 M $HClO_4$ solution at a scan rate of 50 mV/s. CO was introduced into the 0.1 M $HClO_4$ solution for 1 hr. The solution was purged for another 30 min at 0.1 V vs. Ag/AgCl electrode to allow the complete adsorption of CO. The excess CO in the electrolyte was purged out with N_2 for 50 min.

3.2.5 Physical Characterisation

The scanning electron microscope (SEM) coupled with an energy dispersive X-ray spectroscopy was used to observe the morphological structure. The EDX was used for estimating the bulk composition of the nanocatalysts. Atomic force microscopy was used to measure the particle size of the catalysts and ICP-OES was used to calculate the weight of the deposited Pt.

- **Scanning electron microscopy (SEM)**

SEM was used in this study to extract qualitative information pertaining to surface appearance of supported. SEM combined with Energy Dispersive X-ray (EDX) spectroscopy also makes it possible to find out the elemental analysis or chemical characterization of the sample electrocatalysts (Goldstien *et al.*, 1981; Briggs & Seth, 1990).

SEM/EDS measurements were carried out in a vacuum chamber with a commercial Joel JSM-7500F SEM-EDS (Joel Ltd, USA) which had an accelerating voltage of 15 KeV. The samples were supported on double-sided conductive carbon tape and mounted on an aluminium sample stub. No sputter coating was required as all the samples in the study were electron-conductive

- **Inductively coupled plasma-optimal emission spectroscopy (ICP-OES)**

To observe a trend in Pt weight, depositions (1x, 4x, 8x repetitions) were completed for all three substrates. These electrodes were digested in aqua regia and run on the Spectro Ciros ICP-OES (SPECTRO Analytical Instruments, GmbH) to determine the Pt content with every repetition cycle. The wavelength 265.9 nm was chosen in this work, because the best-known Pt wavelength, 214.1 nm, (Skoog, Holler, & Crouch, 2007) had numerous interferences. The working parameters used for Pt determination were as follows:

Forward power - 1500 W

Coolant gas flow rate - 15 L/min

Auxiliary gas flow rate - 0.5 L/min

Nebulizer gas flow rate - 0.8 L/min

Pump speed - 2.0 mL/min

Horizontal viewing position (x) - 0.0 mm

Vertical viewing position (y) - +4.0 mm

Nebulizer - Bergener T2002

Spray chamber - Cyclonic

- **Atomic force microscopy (AFM)**

The AFM measurements in this work were carried out in air under ambient conditions with a commercial Agilent 5500 AFM (Agilent Technologies, USA). The Acoustic AC mode (tapping mode) was used for the morphological images with a scanning frequency of 1 Hz. Silicon cantilevers with a nominal resonant frequency of 190 kHz and a nominal force constant of 48 N/m was used. The current sensing images were obtained in the contact mode (CSAFM) with their corresponding topography images at a scanning rate of 0.5 Hz. For these images, a platinum-coated (to allow conductivity) silicon probe with a force constant of 0.35 N/m was used. The bias voltage between the samples and the tip, which creates the current that constructs a conductivity map, was set at 1 V. All the images were analysed by the imaging processing software by Agilent, Pico Image version 6.2.

CHAPTER 4

RESULTS AND DISCUSSION

4.1. Cu deposition on carbon paper, nickel foam and titanium mesh

The first step taken before Pt deposition was to determine the under potential deposition (UPD) of Cu on each substrate. The redox behaviour of Cu on carbon paper, nickel foam and titanium mesh electrode was investigated using cyclic voltammetry (CV) (Figure. 4.1) in 0.1 M $HClO_4$ and 1mM $CuSO_4.5H_2O$.

All voltammagram cycles commenced at 0.5 V, reversed at -0.2 V and terminated at 0.5 V. Figure 4.1a shows that, initially, there was no current produced until a potential around -0.14 V was reached. At this voltage, the cathodic current had started to increase and formed a curve at a potential ca. -0.019 V. The UPD for Cu on carbon paper was not expected since the substrate is less noble than the Cu adlayer. For the most part, metal substrates such as Ag and Au have been proven to work as their electrochemistry is well understood and they are all relatively noble i.e. they do not oxidize at potentials used for electrochemical atomic layer deposition (EC-ALD) (Stickney *et al.*, 2006). Since one of the objectives of these experiments was to produce cost effective fuel cells, the use of the above-mentioned materials is counterproductive.

The reaction responsible for the curve in Figures 4.1 is reaction 4.1:

$$Cu^{2+} + 2e^{-} \rightarrow Cu \qquad (4.1)$$

The decaying cathodic current past this curve represents reaction 4.1 in diffusion-controlled regime (Cazay *et al*., 2006)

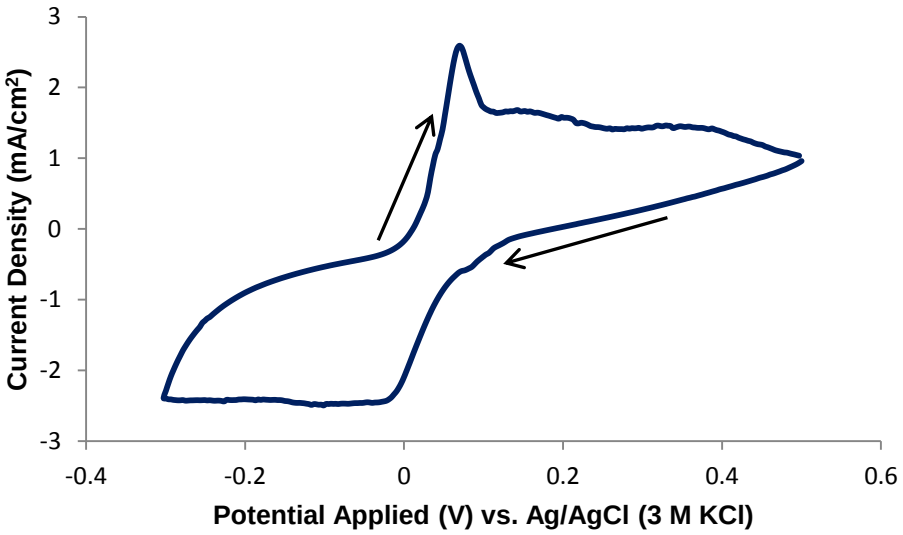

Figure 4.1a: Cyclic voltammogram of Cu deposition on carbon paper at 50 mV/s in 0.1 M $HClO_4$ and 1 mM $CuSO_4.5H_2O$

Upon the sweep reversal, the cathodic current density gradually decreases, until it turns into anodic current. Further sweep in the positive direction results in the anodic peak, which corresponds to reaction 4.1 in the reverse direction.

The current density past the peak is supposed to be zero, indicating the completion of the oxidative dissolution of metallic copper at the electrode surface (Gotterfeld & Zawodzinski, 1997). Figure 4.1a shows that the oxidation reaction is incomplete as indicated by the current density past the peak being ca. 1.44 mA/cm^2.

Many factors could be responsible for this uncharacteristic behaviour, such as pH of the solution in respect to the carbon paper, the temperature at the time of the experiment and the concentration of Cu^{2+} (Kolbe, Przasynski, & Gerischer, 1974). These factors were not dwelled on since the main interest in this work was to obtain the current needed for Cu UPD. Since the UPD peak was not recorded as it was expected in this figure, a small overpotential in relation to potential Cu^{2+}/Cu was used to deposit the sacrificial Cu adlayer.

An overpotential of -0.05 V vs Ag/AgCl was chosen as the potential needed to deposit the sacrificial Cu adlayer on the substrates. The use of this overpotential was prescribed by Mkwizu *et al. (*2011*)* the reason being that deposition of copper on the foreign substrates commences at potentials that are more negative compared with the redox potential of Cu/Cu^{2+} (Martin, 1996) and since bulk Cu deposition theoretically starts at E < 0.05 V, the negative value of this potential was used. This is because the deposition potential of metallic ions on a foreign substrate is usually higher than deposition potential on the electrode made of the same metal due to crystallographic substrate-metal misfit.

Deposition of Cu(s) will likely occur through kinetically controlled 3D nucleation and progressive growth of nanoclusters when the potential mentioned above is set (Gotterfeld & Zawodzinski, 1997). This overpotential was also used to deposit Cu on both Ni foam (Figure 4.1b) and Ti mesh (figure 4.1c) since no Cu UPD peaks were observed in these voltammograms.

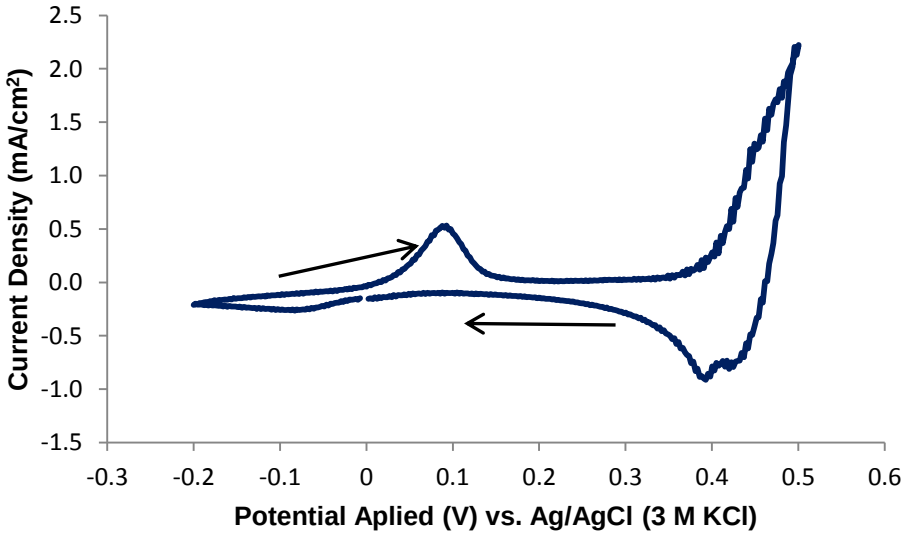

Figure 4.1b: Cyclic voltammogram of Cu deposition on Ni foam paper at 50 mV/s in 0.1 M $HClO_4$ and 1 mM $CuSO_4.5H_2O$

Apart from the lack of the Cu UPD, the shapes of the curves in Figure 4.1a and Figure 4.1b are similar to each other. The major difference between the figures is that the Ni foam voltammogram represents archetypal Cu deposition characteristics in that the current density at the onset and past the anodic peak is zero (Gotterfeld & Zawodzinski, 1997). This indicates the completion of oxidative dissolution of metallic copper at the electrode surface. The other difference is the onset potential for Cu^{2+} reduction for the foam at 0 V.

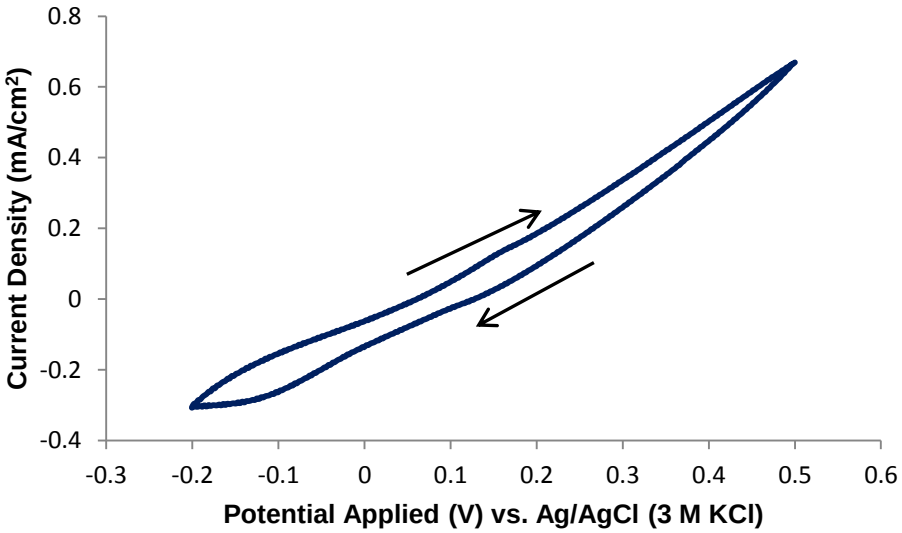

Figure 4.1c: Cyclic voltammogram of Cu deposition on Ti mesh at 50mV/s in 0.1 M $HClO_4$ and 1 mM $CuSO_4.5H_2O$

The shape of the curves in Figure 4.1c is dissimilar to the figures 4.1a and b. The shape on this graph is not characteristic depositing/stripping peaks, but small peaks around 0.15 V in the anodic cathodic scans are observed. These peaks could be interpreted as the cathodic depositing and anodic stripping peaks, but not with certainty, since their shape does not resemble archetypical depositing and stripping peaks. This inclusive result could possibly be explained by surface segregation. According to Demirci (2007), Cu experiences no segregation when alloyed with Ti, but the latter has been shown to experience strong segregation.

This could be confirmed by the many cases where Ti has been alloyed with Cu (Cocke, 1990; Ohkubo & Shimura, 2003; Egorov, Volkov, & Golstcev, 2012).

Deposition time is another important parameter that affects the amount of Cu deposited (Kim *et al.,* 2006). The effect of this parameter was investigated by carrying out the deposition at an applied potential of -0.05 V for different times (60s, 90s and 120s). After each deposition, the corresponding voltammograms were recorded by sweeping the potential from -0.05 to 0.7 V. This experiment was performed on the carbon paper only and then the time obtained from the results was used for the other substrates. Figure 4.1d shows the effect of deposition time on the Cu oxidation at -0.05 V. It can be seen that the stripping current reaches a plateau after 90s, indicating that the deposition process is saturated, and there is no further increase in the oxidation charge with time. Therefore, an applied potential of -0.05 V and deposition time of 90 s was chosen as the optimal values for the Cu deposition process in the present work.

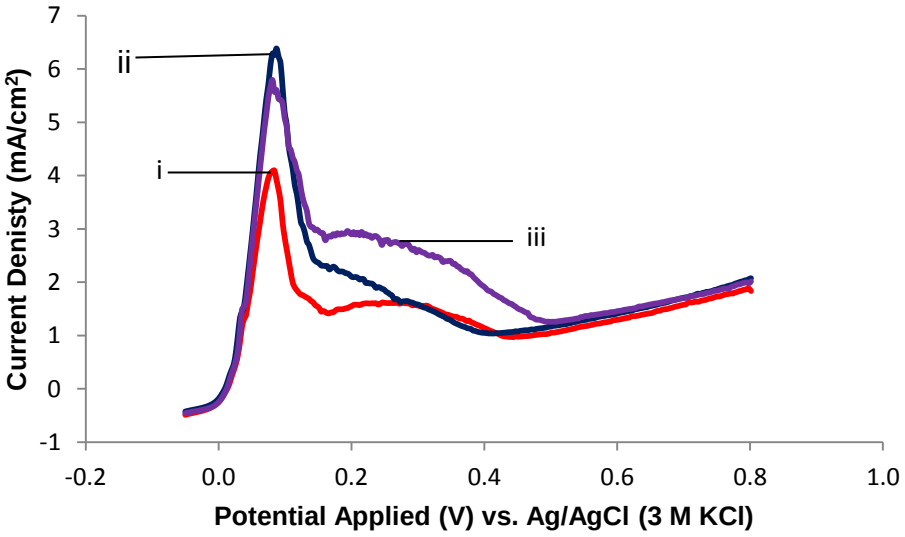

Figure 4.1d: Cyclic voltammagram of Cu deposition on Carbon paper at 60s **(i),** 90s **(ii)** and 120s **(iii)** at 50mV/s in 0.1 M $HClO_4$ and 1 mM $CuSO_4.5H_2O$

4.2 Voltammetric behaviour of Pt/Substrates electrodes

To achieve Pt deposition, the substrate electrodes were inserted into a custom-made flow cell and Cu^{2+} and Pt^{4+} solutions were alternated through the cell to allow monatomic surface Cu atoms to react with Pt (IV) ions. The redox replacement of Cu with Pt should have ideally resulted in the formation of a sub-monolayer of Pt (Brankovic, Wang, & Adzic, 2005), but this was not likely to occur in this experiment since UPD was not used. This replacement cycle was repeated up to eight layers with Pt successfully fabricated onto the substrates.

Cyclic voltammetry tests for the prepared catalysts were performed in a deaerated 0.1 M $HClO_4$ electrolyte at a 50 mV/s scan rate between -0.19 and 1.25 V (vs. Ag/AgCl) to characterize the interactions of the metal surface with hydrogen and to probe the potential range for electrochemical stability of these Pt materials. The results are shown in Figure 4.2. For comparison, the CVs of the blank carbon paper, Nickel foam and Ti mesh electrodes were acquired immediately prior to Pt deposition.

Voltammetric measurements were used since they provide sufficient evidence of the formation of a Pt overlayer on the substrate because the measurements can be regarded as surface sensitive techniques that only detect the electrochemical properties of surface atoms rather than bulk atoms (Barbir, 2005). The identification of peaks in hydrogen, methanol and CO oxidation voltammograms is cited from (Barbir, 2005; Bard & Faulkner, 2001; Gasteiger, Markovic, Ross, & Cairns, 1994; Larmine, 2003; Wasmus, 1999)

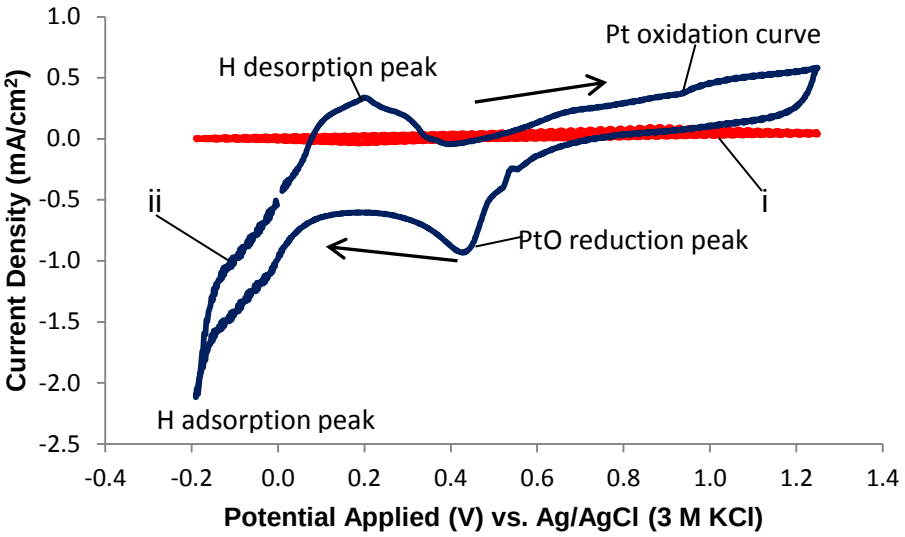

Figure 4.2a: Cyclic voltammograms of blank carbon paper **(i)** and Pt/Carbon paper **(ii)** at 50 mV/s in 0.1M $HClO_4$ (5^{th} scan)

It can be seen in Figure 4.2a that a couple of oxidation-reduction hydrogen peaks appeared between 0.35 V and -0.2 V which arise from the deposition and stripping (adsorption/desorption) of hydrogen on Pt, followed by sharp cathodic and anodic peaks indicative of massive hydrogen evolution and oxidation. The broadness of adsorption/desorption peaks can be caused by the participation of different Pt crystallographic orientations in hydrogen (Kolbe, Przasynski, & Gerischer, 1974). The charge consumed for the electrooxidation of adsorbed and desorption hydrogen (Q_H) on the Pt surface can be used to estimate the Pt electroactive surface area of the electrodes, assuming that 210 mC/cm^2 is the charge on polycrystalline Pt. The calculated Pt surface areas are presented in Table 4.3 and will be discussed in Section 4.9.

A slight curve can be observed in the anodic direction around 0.92 V for Pt/Carbon paper. This curve is due to the formation of OH^- and oxide on the surface of the catalyst, respectively. The oxidized Pt layer is then reduced around 0.57 V for the carbon paper in the cathodic sweep (Bockris & Srinivasan, 1969).

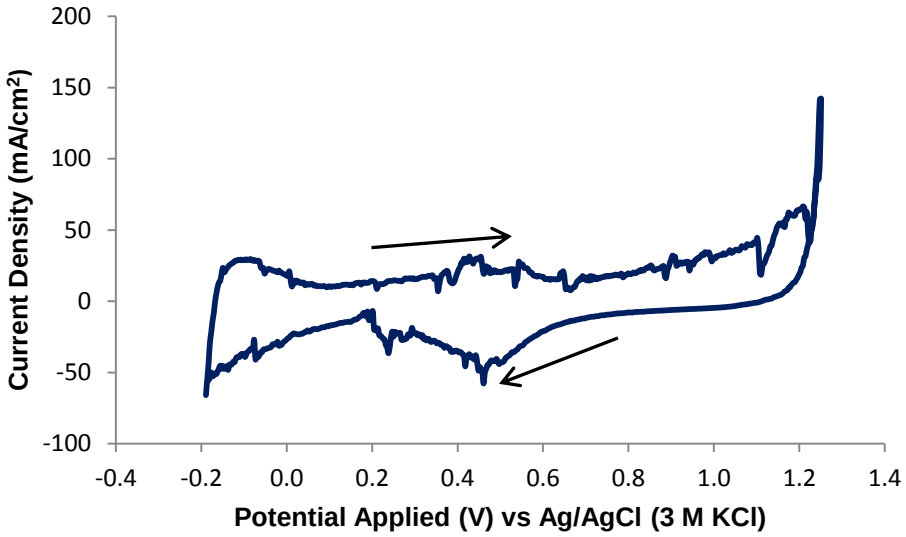

Figure 4.2b: Cyclic voltammograms of Pt/C/Carbon paper at 50 mV/s in 0.1 M $HClO_4$. (5^{th} scan)

The hydrogen peak for the modified Pt/Carbon paper shows an increased current density. The hydrogen desorption peak in Figure 4.2b is more cathodic than its unmodified version. The oxidation curve is not visible here due the noise, but a PtO reduction peak is recorded around 0.48 V.

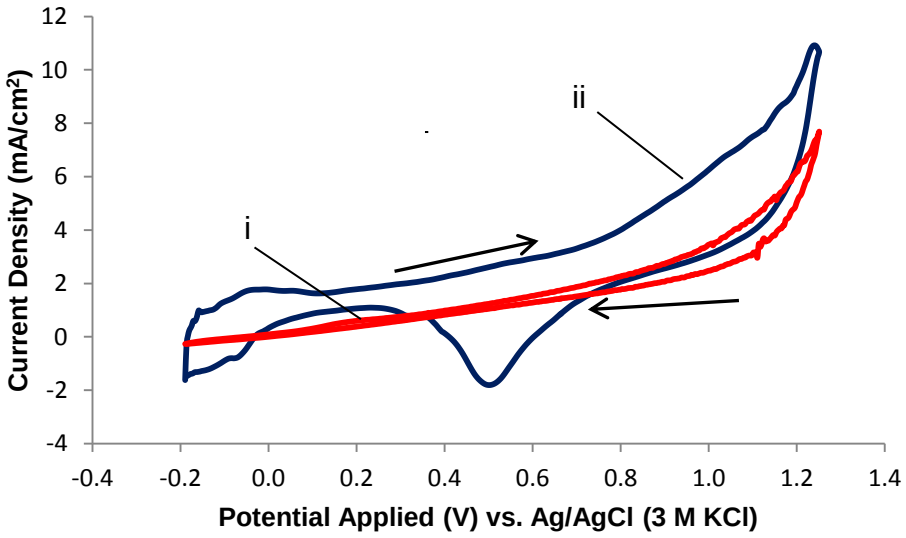

Figure 4.2c: Cyclic voltammograms of blank Ni foam **(i)** and Pt/Ni foam **(ii)** at 50 mV/s in 0.1 M $HClO_4$. (5^{th} scan)

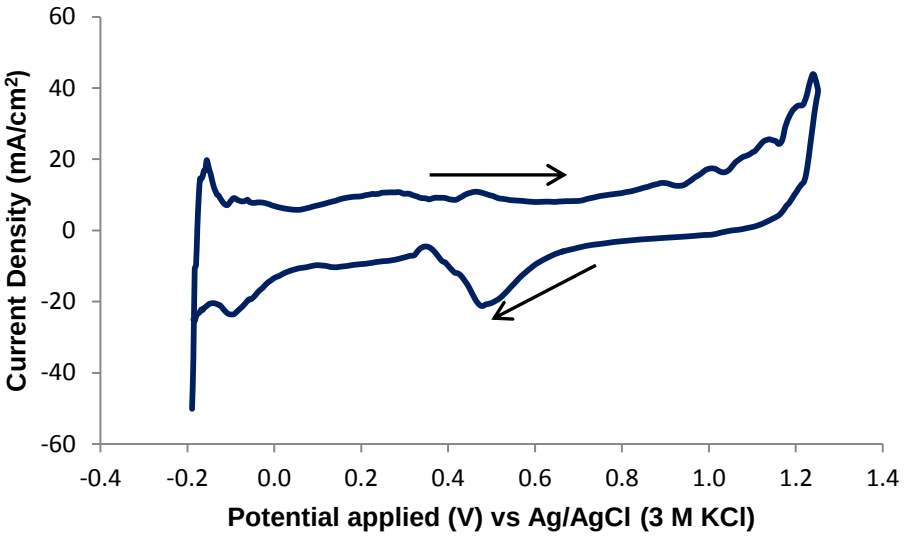

Figure 4.2d: Cyclic voltammograms of Pt/C/Ni foam (ii) at 50 mV/s in 0.1 M $HClO_4$ (5^{th} scan)

The hydrogen desorption peak in Figure 4.2c for the Pt/Ni foam substrate is rather small and broad. This might be due to the structural modifications of Pt caused by the Pt–Ni interaction (Bidault *et al*, 2009). The hydrogen peak is followed by a typical Pt oxidation curve at ca. 1.12 V and its corresponding PtO reduction peak can be seen around 0.77 V.

The modified version of Pt/Ni foam (Figure 4.2c) possesses a more cathodic hydrogen peak as opposed to its unmodified version. The current densities of these peaks are also higher than that of the unmodified version. The Pt oxidation curve and its corresponding PtO reduction peak appear at around the same potential as in its unmodified versions, but with possess higher current densities.

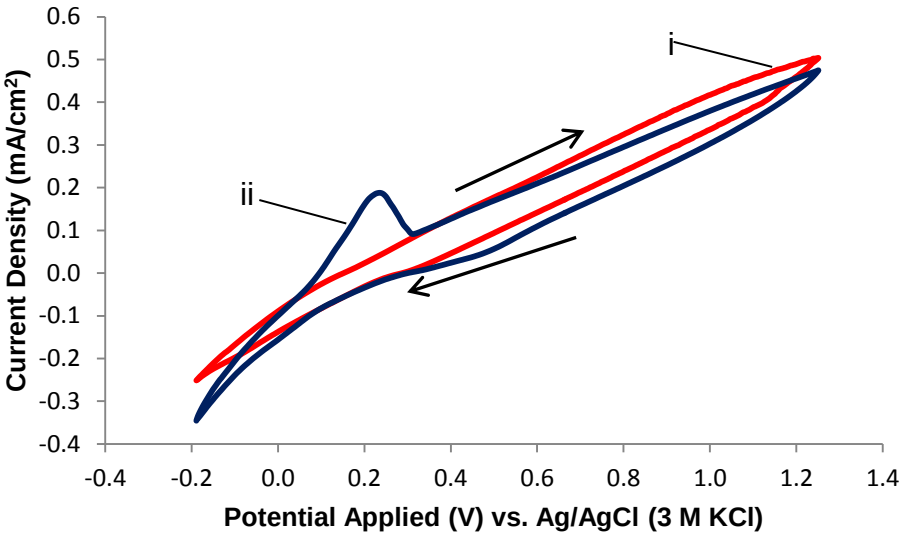

Figure 4.2e: Cyclic voltammograms of blank Ti mesh (i) and Pt/Ti mesh (ii) at 50 mV/s in 0.1 M $HClO_4$. (5^{th} scans)

The Ti mesh voltammagram in Figure 4.2e shows a defined hydrogen peak around 0.2 V, but the expected Pt oxidation curve was not recorded. There is coincidently a corresponding Pt reduction curve is observed around 0.6 V though, suggesting that Pt could have been oxidised. This discrepancy could be due to Ti inability to conduct electricity very well.

The thinking behind this could be that the anodisation of Ti in moderately acidic aqueous media (in this case pH1 solutions) could result in the formation of a thermodynamically stable titanium oxide film (TiO_2). The oxide film (TiO_2) formed on the metal surface is known to be compact and poorly conducting (Rahin & Hassan, 2009). This also explains the small current density in the cyclic voltammogram for hydrogen oxidation (Figure 4.2e) and its inability to show notable Cu reduction and oxidation peaks in Figure 4.1c.

4.3. Electrooxidation of methanol

The electrocatalytic activity of the electrodes for methanol oxidation reaction (MOR) was investigated by recording CVs of the substrate electrodes in 0.1 M

$HClO_4$ solution in the presence and absence of methanol. The current densities were generated through experiments repeated five times. Figure 4.3 shows voltammograms for methanol electrooxidation on Pt/Substrate electrodes in a solution containing 0.1 M CH_3OH and 0.1 M $HClO_4$ at 50 mV/s in the range of -0.19 to 1.25 V (vs. Ag/AgCl). For comparisons, the activity of the blank substrates were tested and included in these figures.

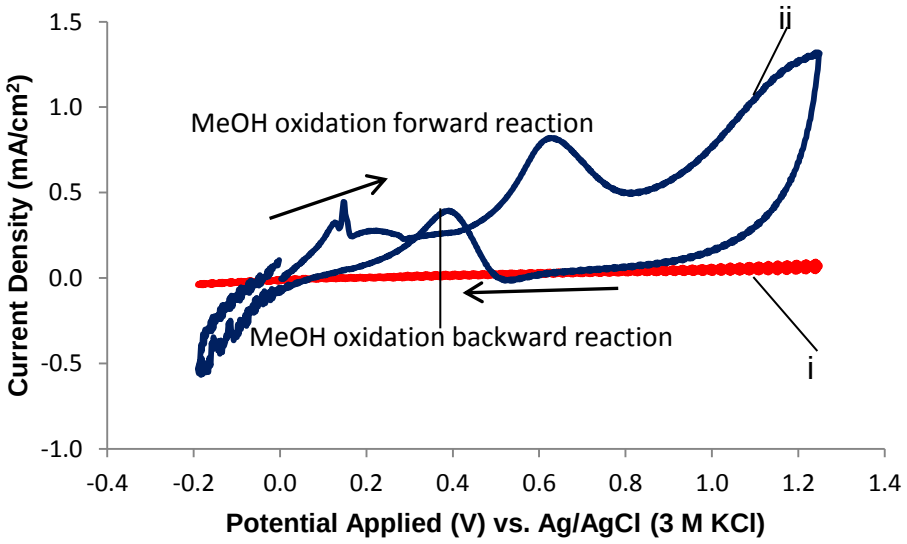

Figure 4.3a: Cyclic voltammograms of blank carbon paper (i) and Pt/Carbon paper (ii) at 50 mV/s in 0.1 M $HClO_4$ and 0.1 M MeOH (5^{th} scan)

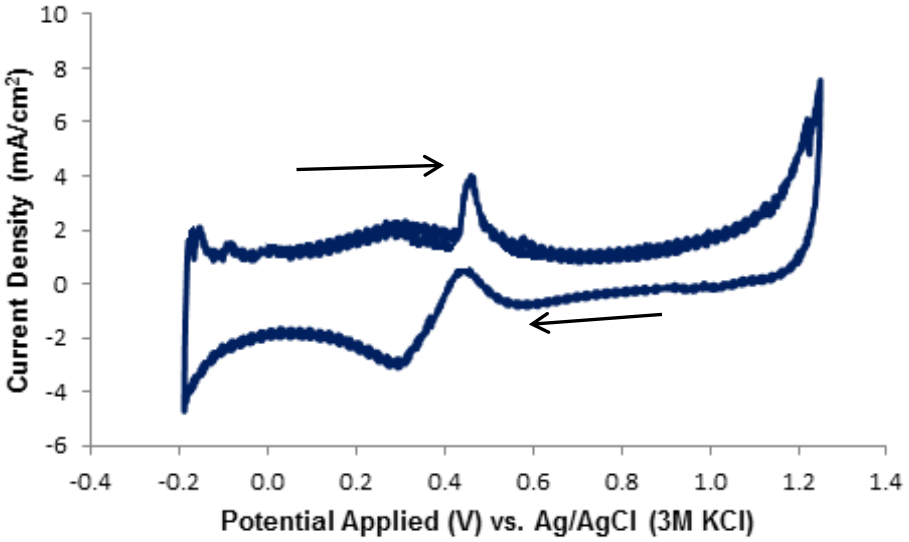

Figure 4.3b: Cyclic voltammogram of Pt/C/Carbon paper at 50 mV/s in 0.1 M $HClO_4$ and 0.1 M MeOH (5^{th} scan)

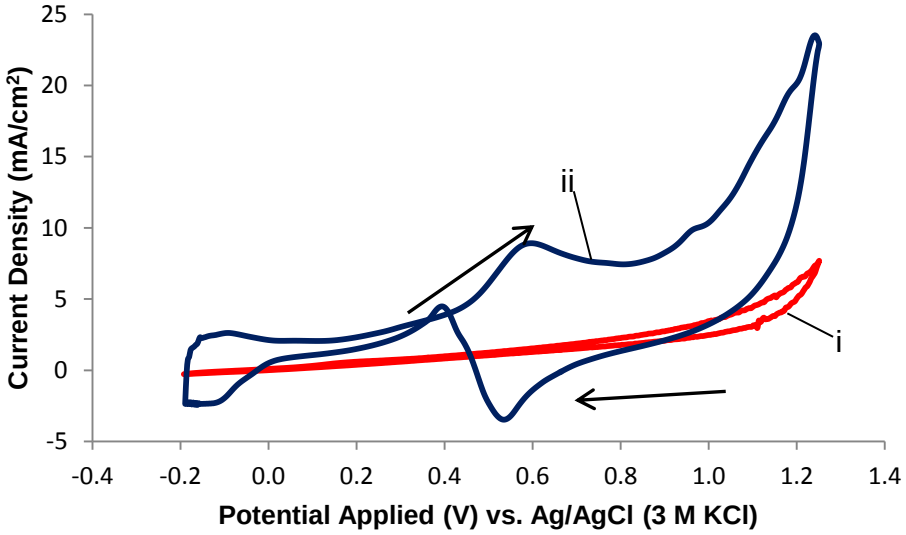

Figure 4.3c: Cyclic voltammograms of blank Ni foam (i) and Pt/Ni foam (ii) at 50 mV/s in 0.1 M $HClO_4$ and 0.1 M MeOH (5^{th} scan)

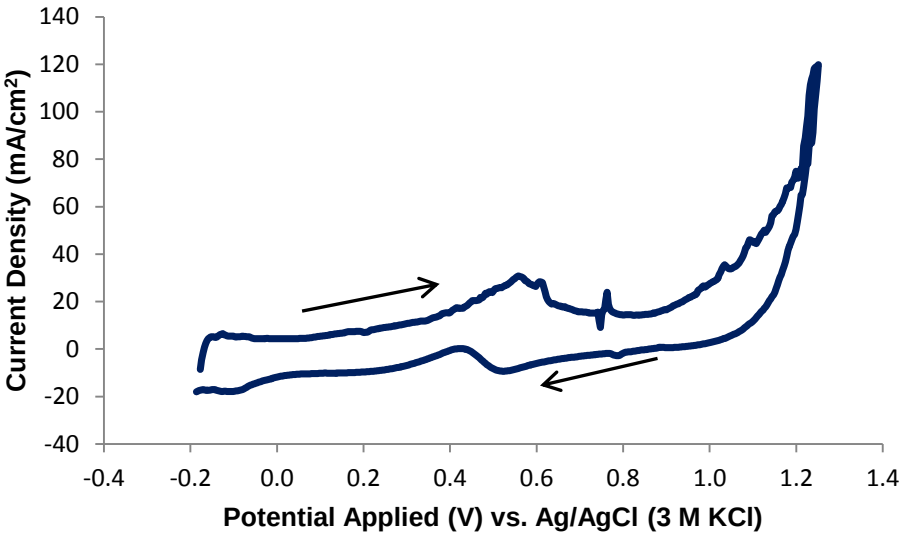

Figure 4.3d: Cyclic voltammograms of Pt/C/Ni foam at 50 mV/s in 0.1 M $HClO_4$ and 0.1 M MeOH (5^{th} scan)

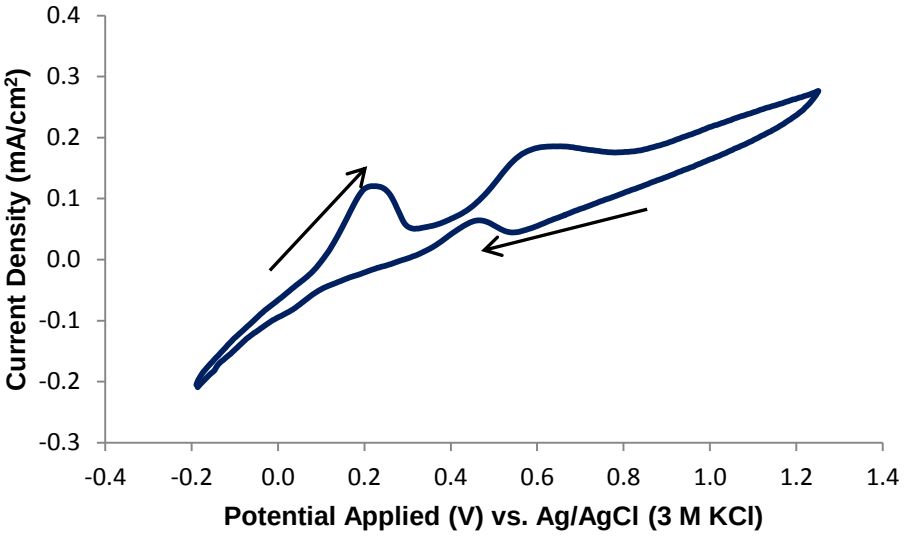

Figure 4.3e: Cyclic voltammograms of Pt/Ti mesh at 50 mV/s in 0.1 M $HClO_4$ and 0.1 M MeOH (5^{th} scan)

The shapes in Figure 4.3 represent typical CV curves for alcohol electrooxidation reactions. Two anodic current peaks in the positive and negative sweeps are observed. The forward anodic peak current density (I_f) is attributed to the methanol oxidation reactions during the positive sweep. The reverse anodic peak current density (I_r) is due to the oxidation of the incompletely oxidized carbonaceous

residues on the catalyst surface in the negative sweep (Bockris & Srinivasan, 1969). It is likely that the latter intermediates are strongly adsorbed on the Pt surface, which blocks the active catalyst sites for the next turnover, thus rendering the anodic reactions slower (Bockris & Srinivasan, 1969).

The values for the anodic current density peak are summarized in Figure 4.1. Furthermore, the I_f /I_r ratio seen in Table 4.1, indicates the catalysts tolerance to carbonaceous species accumulation during the methanol electrooxidation processes. A higher value of I_f/I_r indicates better oxidation of methanol to carbon dioxide during the anodic scan and less accumulation of carbonaceous residues on the catalyst surface (Brankovic, Wang, & Adzic, 2005).

Table 4.1: Summary of the important activity indicator of methanol oxidation reaction, CO anodic stripping and chronoamperometic studies

Catalyst	**Maximum current density (mA/cm^2)**	**Onset Potential (V) for MOR**	**I_f/I_r**	**Current Density (mA/cm^2) after 100s**	**Onset Potential (V) for CO stripping**
Pt/Carbon paper	0.85	0.40	4.30	0.30	0.66
Pt/C/Carbon paper	3.67	0.39	8.00	0.86	0.59
Pt/Ni foam	5.94	0.37	2.81	1.90	0.37
Pt/C/Ni foam	27.21	0.26	19.16	1.93	0.34
Pt/Ti mesh	0.22	0.48	2.32	0.12	0.50

The surface layer of Pt/Ni catalysts has been proven to contain Ni hydroxides, Ni $(OH)_2$ and NiOOH, which are relatively stable in acidic media and are protected from corrosion through alcohol electrooxidation (Bidault *et al.*, 2009). This helps in providing oxygen in the removal of adsorbed CO on the Pt catalyst surface. The same can be said about Ti since it forms TiO_2 that can donate its oxygen to the

adsorbed CO (Rahin & Hassan, 2009). So, theoretically, this would mean that the I_f/I_r ratio for the Ni foam and the Ti mesh electrodes would be superior, but this is not the case as seen in Table 4.1. There are many factors that could be responsible for this but these were not explored since the aim of this work was to examine the feasibility of the ECALD method in the deposition of Pt on selected substrates. The existence of the typical methanol I_f and I_r peaks suggests that Pt was deposited and therefore that the deposition method is feasible.

The I_f/I_r ratio of the modified Pt electrodes however conformed to the theory that modification of the substrates with carbon black improves its performance since the ratios proved to be better than the unmodified versions. It cannot be ignored though that Pt/C/Ni foam electrode is far superior when compared to the other examined electrodes terms of the methanol oxidation onset potential. This can be said because the onset potential for these electrodes is seen around 0.4 V and that of the modified Pt/Ni foam shows much earlier at 0.28 V. Since the onset potential can be related to the rate of the reaction (Appleby & Foulkes, 1989), it could be implied that methanol oxidation reaction on Pt/C/Ni foam is faster than on the other sampled electrodes. The conclusion is that the addition of 40 % ionomer/carbon black on Ni foam can greatly enhance the electrode performance when the I_f/I_r ratio and onset potential is taken into consideration.

4.4. Chronoamperometry

Chronoamperometry was employed in a solution of 0.1 M $HClO_4$ and 0.1 M methanol to evaluate the stability of the Pt/Carbon paper, Pt/Ni foam and Pt/Ti mesh catalysts and their modified versions. The results are shown in Figure 4.4 (a-e). As it has been noted in the previous section, the methanol

oxidation onset potential for most of the electrodes (Table 4.1) is around 0.4 V, so this value was chosen as the fixed potential for chronoamperometry measurements.

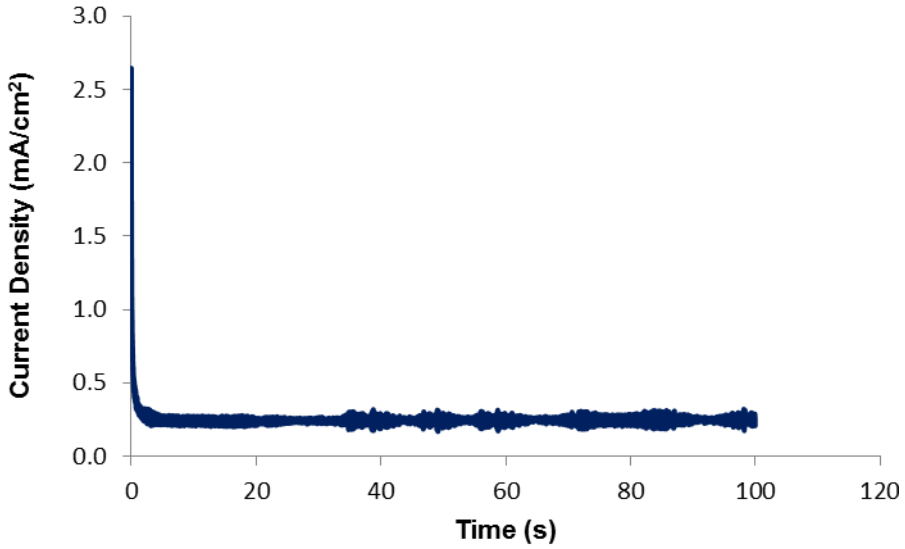

Figure 4.4a: Chronoamperometry measurements of Pt/Carbon paper at 0.4 V in 0.1 M $HClO_4$ and 0.1 M MeOH

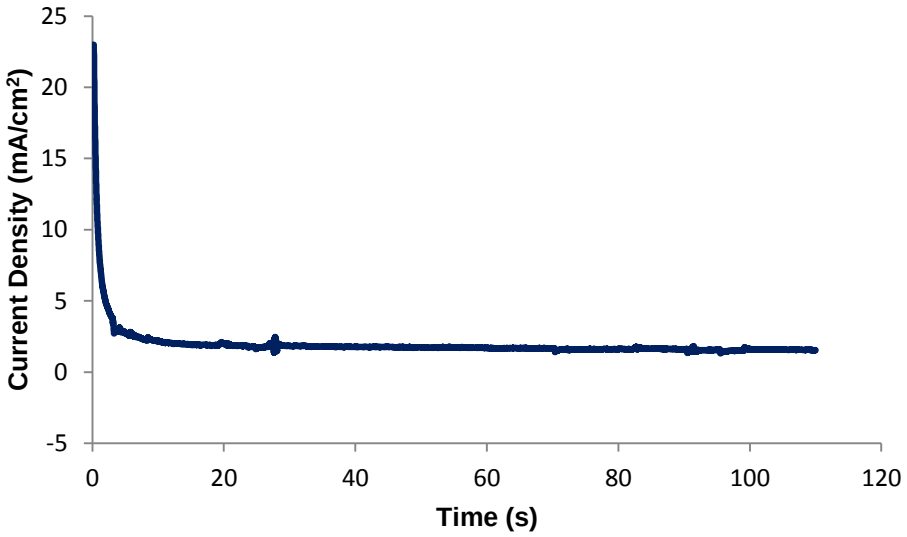

Figure 4.4b: Chronoamperometry measurements of Pt/C/Carbon paper at 0.4 V in 0.1 M $HClO_4$ and 0.1 M MeOH

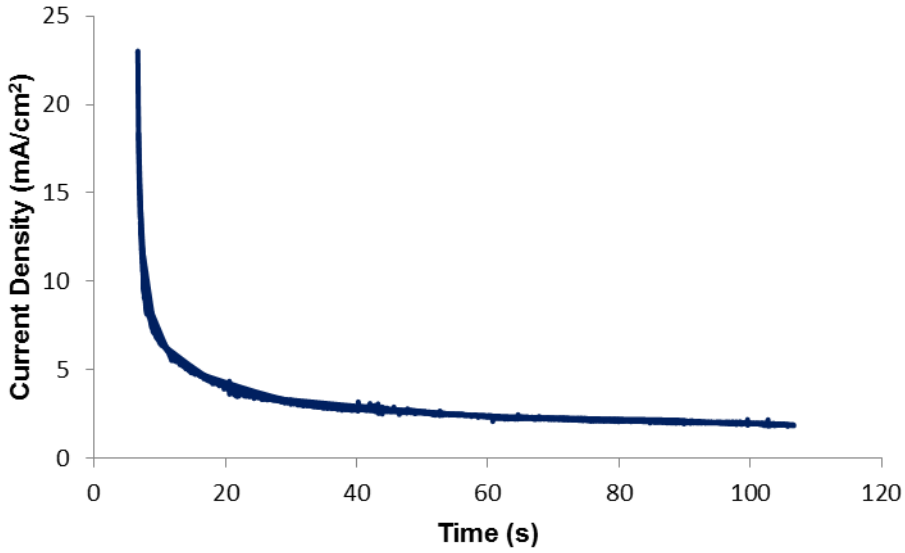

Figure 4.4c: Chronoamperometry measurements of Pt/Ni foam at 0.4 V in 0.1 M $HClO_4$ and 0.1 M MeOH

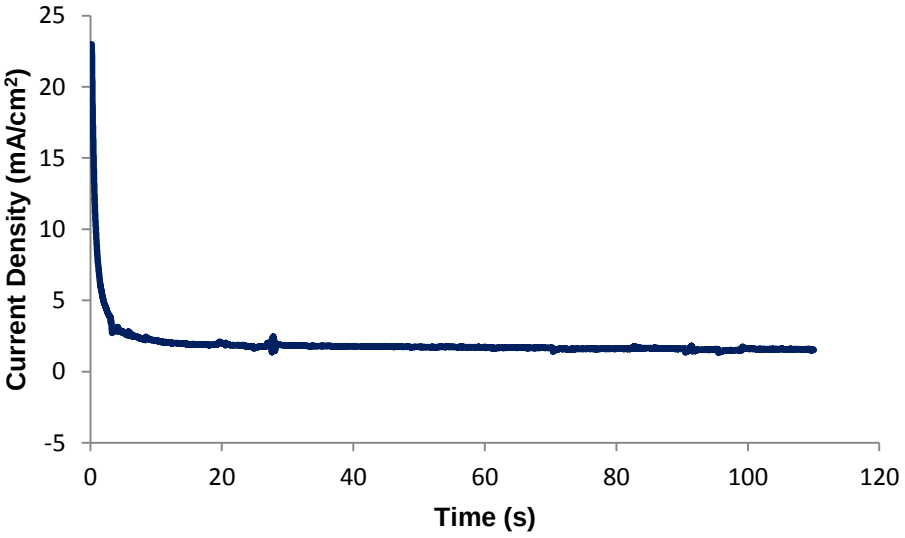

Figure 4.4d: Chronoamperometry measurements of Pt/C/Ni foam at 0.4 V in 0.1 M $HClO_4$ and 0.1 M MeOH

As displayed in Figure 4.4 (a-e), initial rapid decreases in current density were observed for all of the catalysts. Subsequently, the current decreased and reached a pseudosteady state. At the fixed potential, methanol is continuously oxidized on the catalyst surface and tenacious reaction intermediates such as adsorbed CO begin to accumulate if the kinetics of the removal reaction does not keep pace with that of methanol oxidation. A more gradual decay of current density with time is

nevertheless an indication of improved CO resistance (Delmon *et al*., 1979). This steady decay is more evident in Figure 4.4c, suggesting that Pt/Ni foam is more resistant to CO compared to its modified version and the other electrodes. The improved CO-tolerance of the Pt/Ni foam catalyst can be conclusively explained by a bifunctional mechanism (Briggs & Seth, 1990) in which the reaction between strongly bound Pt_3CO species and adsorbed OH^- on neighbouring Ni sites constitutes the major removal mechanism (Zhang, Wang, & Zhang, 2008).

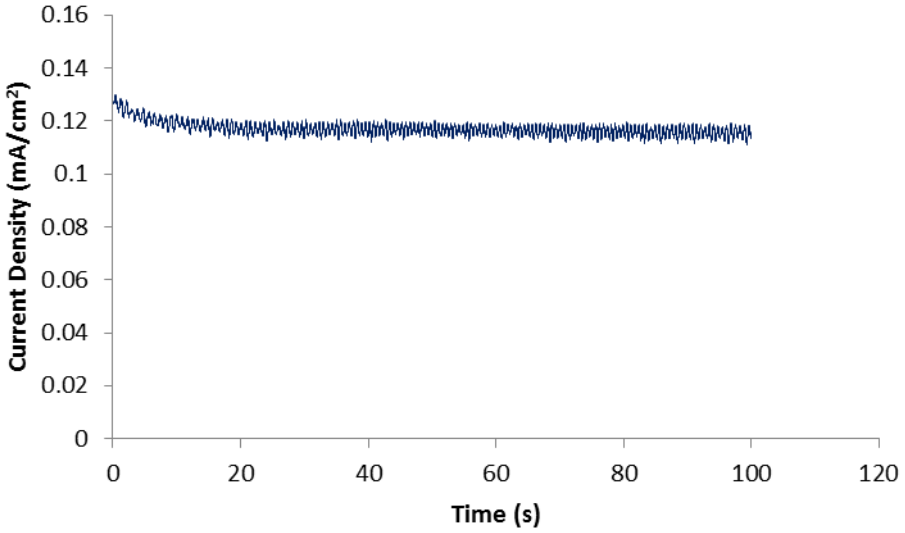

Figure 4.4e: Chronoamperometry measurements of Pt/Ti mesh at 0.4 V in 0.1 M $HClO_4$ and 0.1 M MeOH

When comparing the unmodified to the modified electrodes in Figures 4.4 (a and c), it can be concluded that the activity order of MOR in terms of the current density is Pt/Ni foam ~ Pt/C/Ni foam and Pt/C/Carbon paper > Pt/Carbon paper. The inclusion of 40% ionomer/C on Ni foam did not have a significant impact on the Pt/Ni foams current density, but there was a ~34 % increase when Pt/Carbon paper was modified. These chronoamperometric measurements conclude that Pt/Ni foam has optimal methanol oxidation reaction activity and CO resistance

(Appleby & Foulkes, 1989) when compared to the other electrodes that are being studied.

4.5 CO anodic Stripping

The electrocatalytic activity of the catalysts for CO oxidation was investigated using CO anodic stripping voltammetry. The CO stripping voltammograms for the Pt/Carbon paper, Pt/C/Carbon paper, Pt/Ni foam, Pt/C/Ni foam and Pt/Ti mesh catalysts are shown in Figure 4.5 (a-e). The onset potential of CO oxidation for both Pt/Ni foam and Pt/Ti mesh are observed in the Figure 4.5(c and e) to be lower by 0.29 V and 0.16 V when compared to Pt/Carbon paper, respectively. This indicates that the electrocatalytic activities of these electrodes are superior to that of Pt/Carbon paper when oxidising CO. This deduction can be explained by the bifunctional mechanism for CO oxidation (Chem *et al*., 2005), which implies that the removal of adsorbed CO proceeds via adsorbed OH^- on Ni and Ti sites formed by dissociative water adsorption (Bard & Faulkner, 2001). The actual data can be seen in Table 4.1.

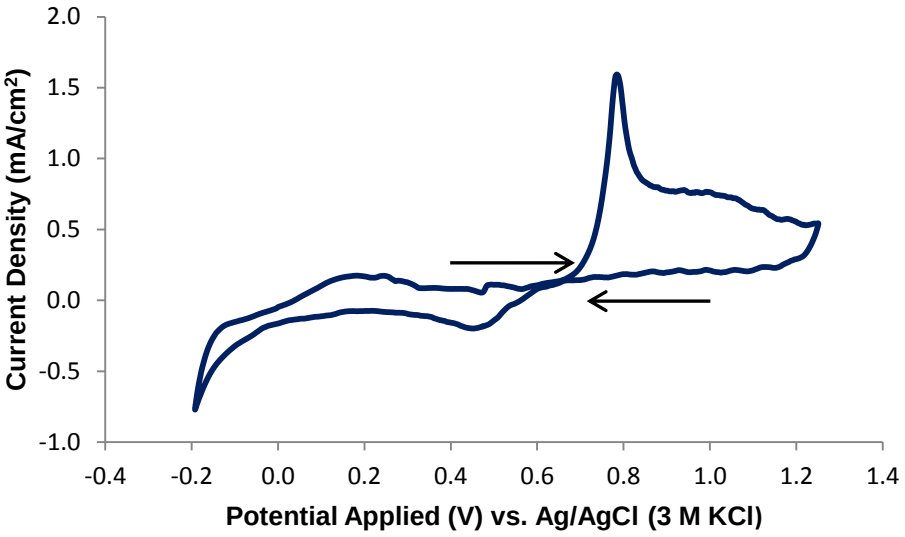

Figure 4.5a: Cyclic voltammograms of Pt/Carbon paper at 50 mV/s in 0.1 M $HClO_4$ and CO (5^{th} scan)

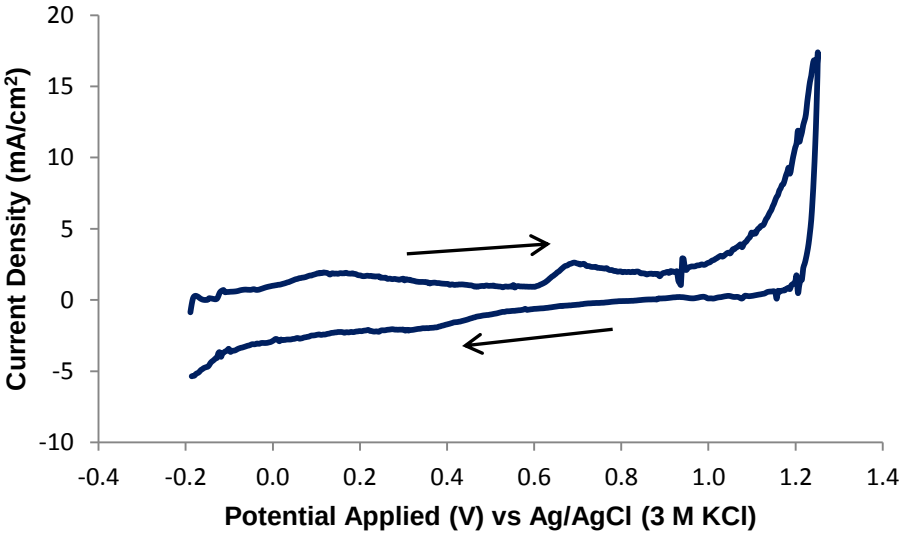

Figure 4.5b: Cyclic voltammograms of Pt/C/Carbon paper at 50 mV/s in 0.1 M $HClO_4$ and CO (5^{th} scan)

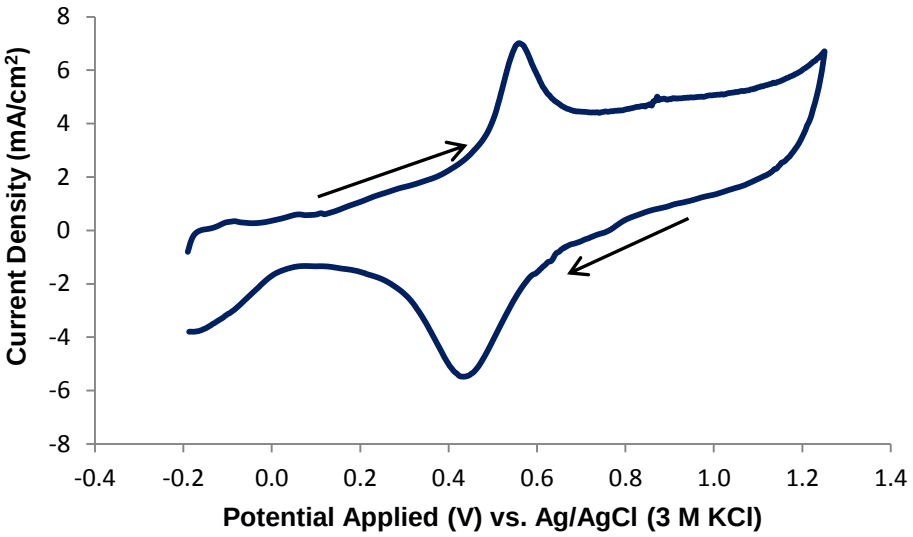

Figure 4.5c: Cyclic voltammograms Pt/Ni foam at 50 mV/s in 0.1 M $HClO_4$ and CO (5th scan)

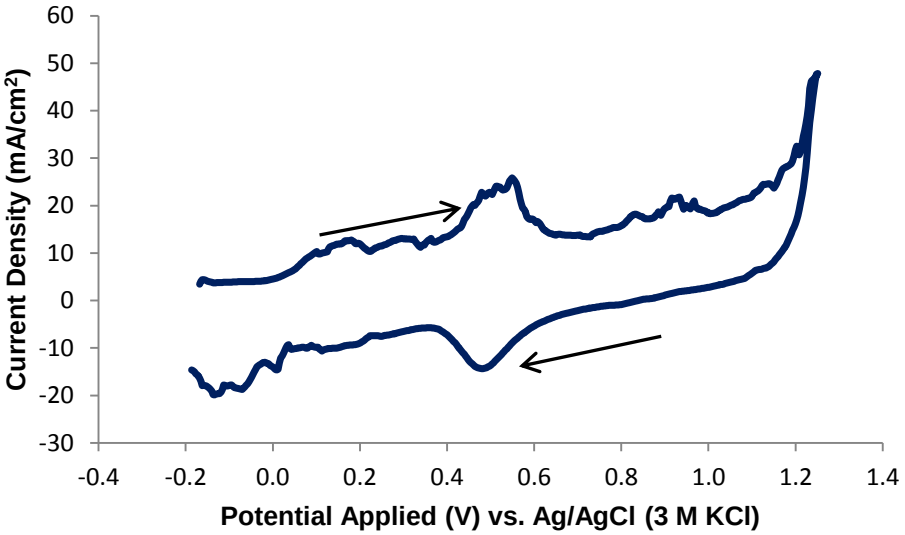

Figure 4.5d: Cyclic voltammograms Pt/C/Ni foam at 50 mV/s in 0.1M $HClO_4$ and CO (5th scan)

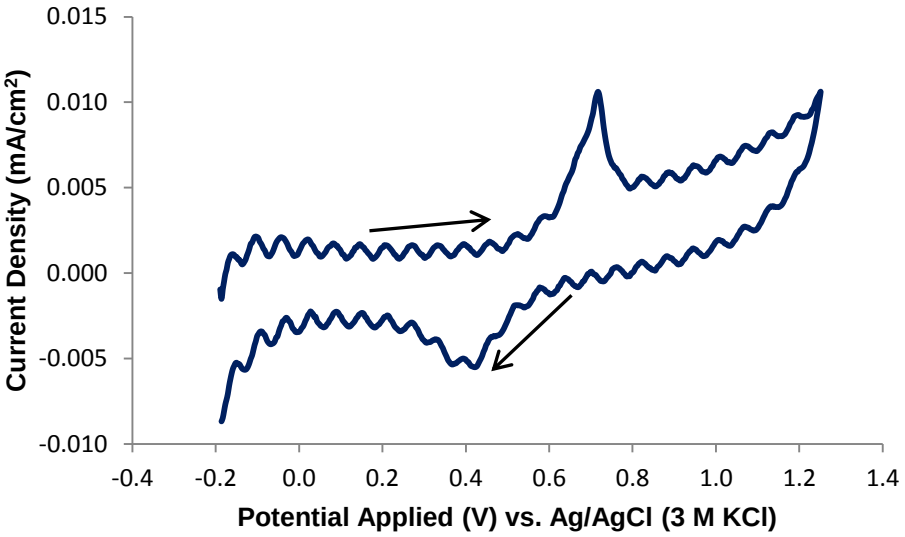

Figure 4.5e: Cyclic Voltammograms Pt/Ti mesh at 50 mV/s in 0.1 M $HClO_4$ and CO (5^{th} scan)

The onset potential for the modified Pt/Substrates was slightly lower than that of the unmodified versions. The differences were not large, but there was a consistency in the change which demonstrated that modification improved the electrodes performance.

4.6 SEM/EDX

To examine the structural differences and composition of the catalyst-coated substrates, SEM and EDX were employed. SEM micrograms and EDX profiles of the pre-treated blank substrates along with Pt/Substrate electrodes are shown in Figure 4.6 to compare results obtained before and after deposition. Figure 4.6(a-c) shows SEM micrographs of the substrates structure (i), substrates without (ii), with the catalyst (iii) and modified substrates with Pt (iii). The carbon paper structure seen in figure 4.6a (i) is composed of inter woven carbon fibres. A closer magnification of the images shows a clear picture of the differences in the surface morphology. There are white particles present (Figure 4.6a (iii)) that are clearly not seen in Figure 4.6a (iv) due to its higher magnification. These particles confirm a

change in the surface morphology when compared to before deposition images. So it could be safe to assume that these changes are due to the deposited Pt.

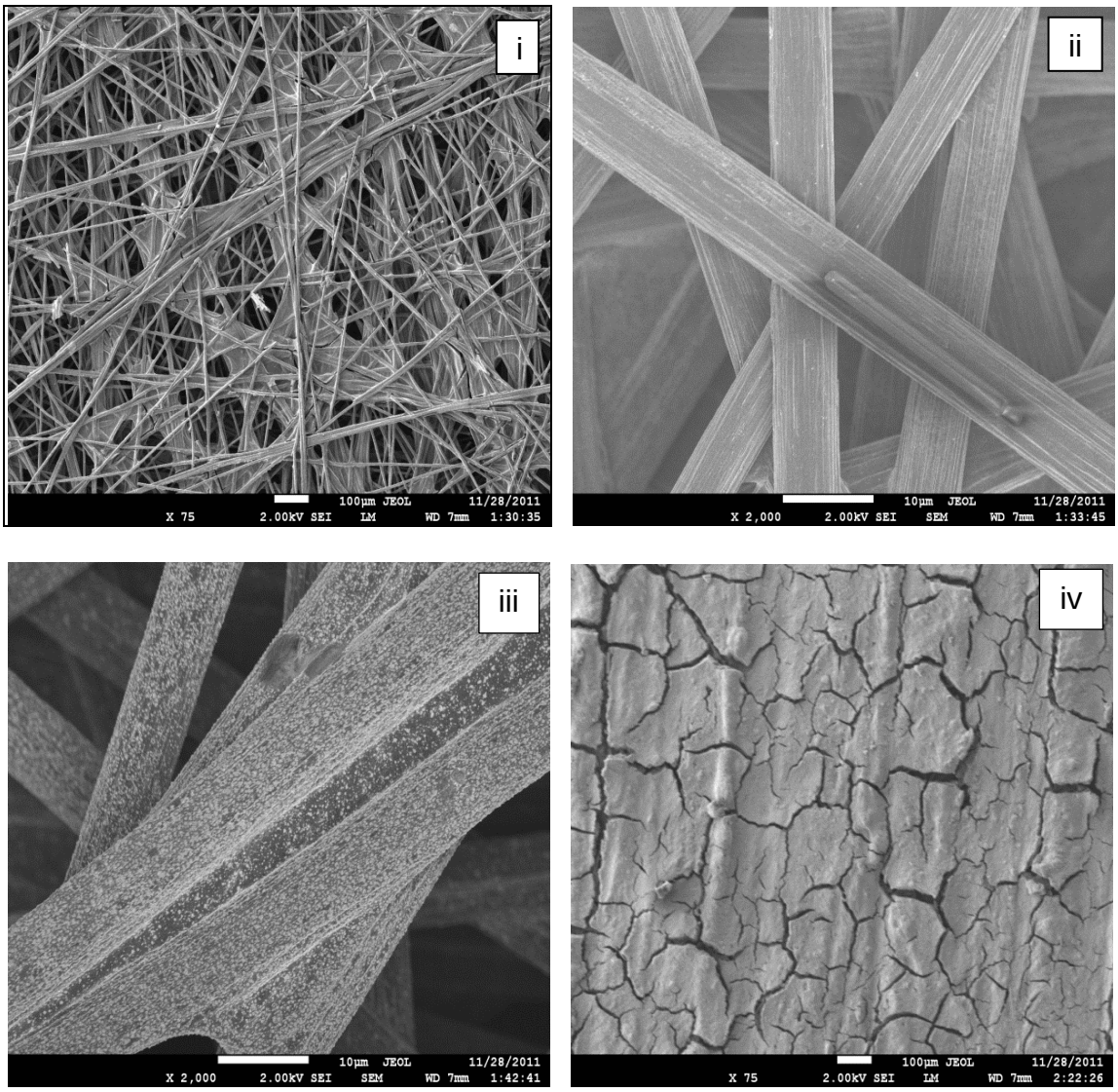

Figure 4.6a: SEM micrographs of Carbon paper structure **(i)**, Carbon paper before deposition **(ii)**, after **(iii)** Pt deposition and Carbon paper/C after deposition **(iv)**

Figure 4.6b shows SEM micrographs for nickel foam with the same conditions as the carbon paper. The image in Figure 4.6b (i) represent the nickel foam skeleton. This structure is composed of holed cells linked to each other. The arch ribs of these cells with sharp edges are non-porous. Figures 4.6b (ii and iii) are easily differentiable from each other due to the chipped paint appearance seen on the

Pt/Ni foam image. These flaky chips images could indicate agglomerated Pt particles on the surface of the Ni foam.

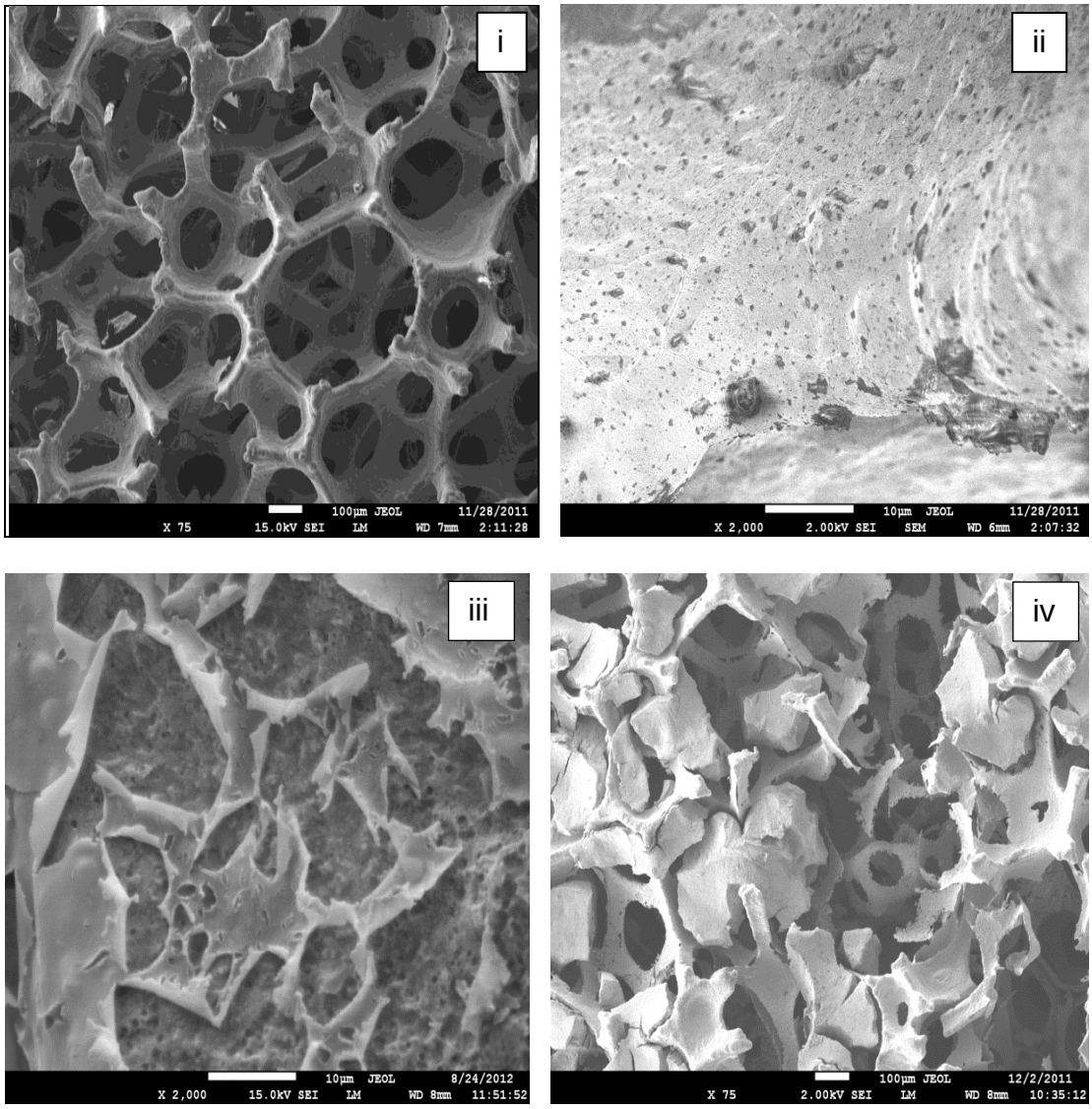

Figure 4.6b: SEM micrographs of Ni foam structure **(i)**, Ni foam before **(ii)** deposition, after **(iii)** Pt deposition and Ni foam/C after deposition **(iv)**

The SEM images for Pt/C/Carbon paper and Pt/C/Ni foam in Figure 4.6 for Pt/Carbon paper and Pt/Ni foam show a more pale and matt image of the deposited Pt, which is clearly seen. There is absolutely no carbon paper weave design visible on the Pt/C/Carbon paper SEM image, but the arch rib design for Ni foam is still visible. This could indicate that the high surface area with the high

conductivity of the 40 % ionomer/carbon black on Ni foam could improve its performance.

Figure 4.6c shows SEM micrographs for titanium mesh. The Ti mesh is composed of criss-crossed metal linked to each other. The presence of Pt could not be visibly noted (even after several tries) in the Ti mesh images, so mapping (see Figure 4.6d) had to be performed to prove that deposition occurred. An element map is an image showing the spatial distribution of elements in a sample. Because it is acquired from a polished section, it is a 2D section through the unknown sample. Element maps are extremely useful for displaying element distributions in textural context, particularly for showing compositional zonation (Briggs & Seth, 1990).

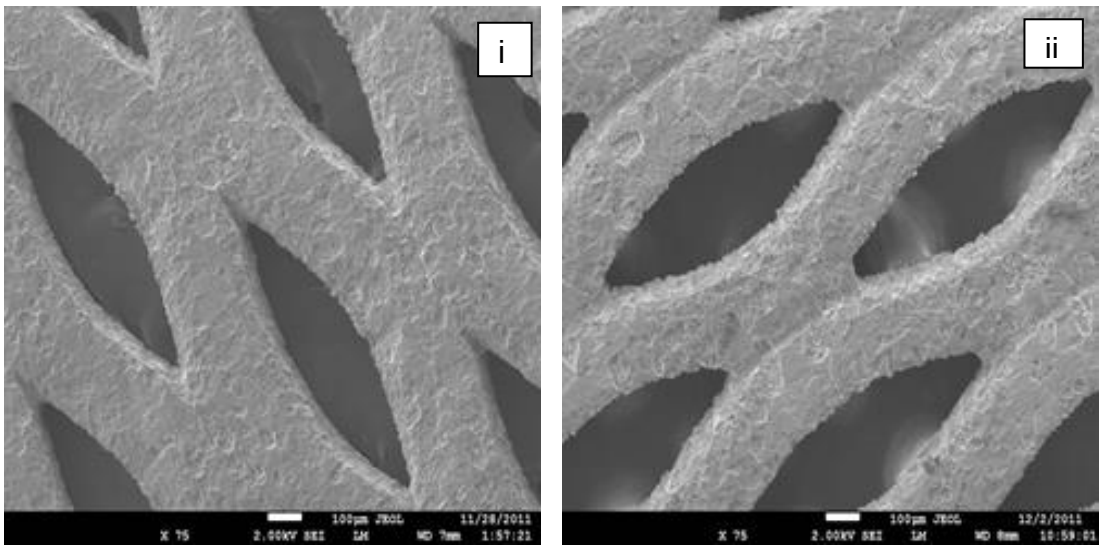

Figure 4.6c: SEM micrographs of Ti mesh before **(i)** and after **(ii)** deposition

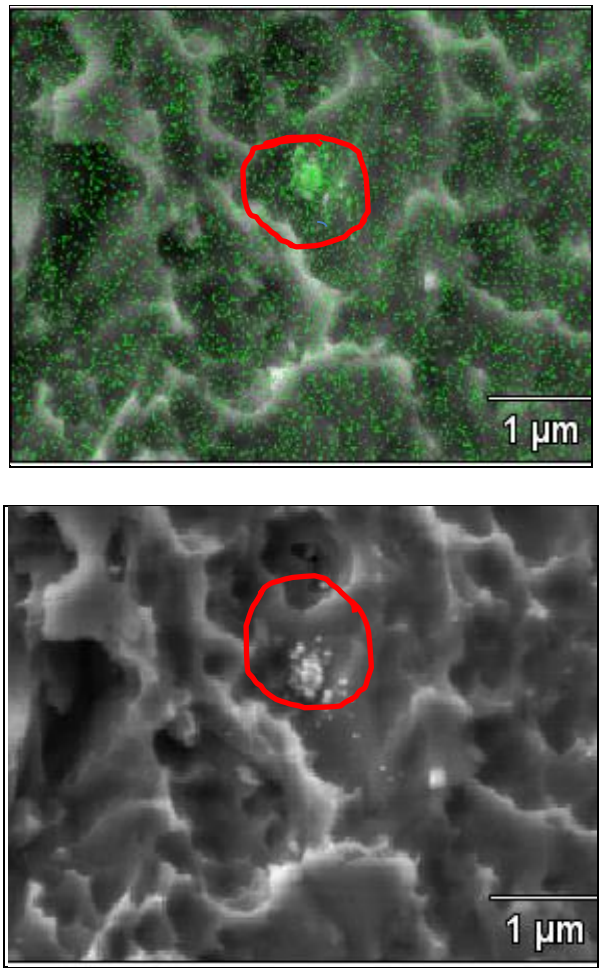

Figure 4.6d: Image mapping of Pt/Ti mesh electrode

The green dots in Figure 4.6d represent the deposited Pt. These particles indicate the presence of platinum even though minimal deposition may have occurred. Agglomeration of Pt is shown (circled in red) to indicate the validity of the mapping. EDX analysis (Figure 4.6(e-i)) showed the presence of Pt on the substrates when comparing the before and after profiles to each other. The Pt content on the Pt/Ti mesh EDX profile however was not recorded in Figure 4.6i. This does not mean that no Pt deposition took place because the EDX composition portfolio revealed a 0.33 % Pt content. This only implies that the Pt peak is too diminutive to be visible when compared to that of Ti.

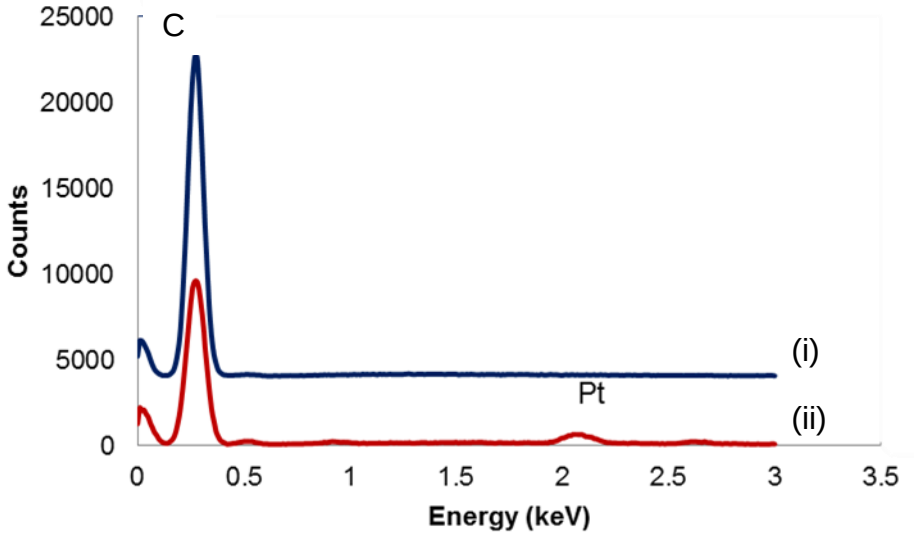

Figure 4.6e: EDX profiles of Carbon paper before (i) and after (ii) Pt deposition

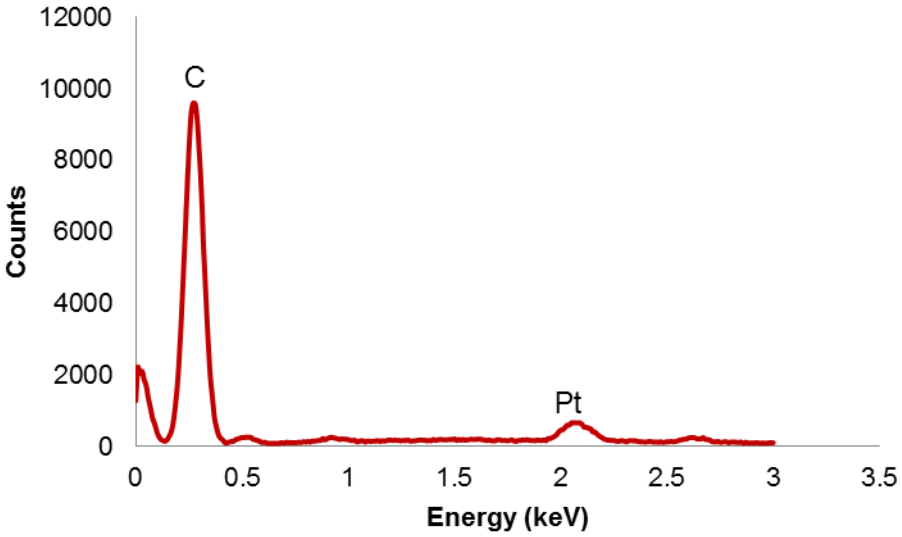

Figure 4.6f: EDX profiles of Carbon paper/C after Pt deposition

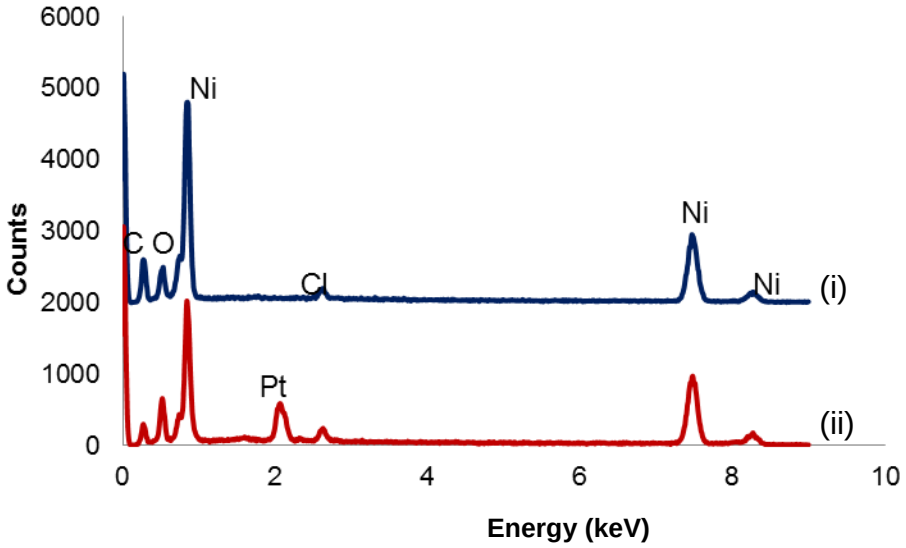

Figure 4.6g: EDX profiles of Ni foam before (i) and after (ii) Pt deposition

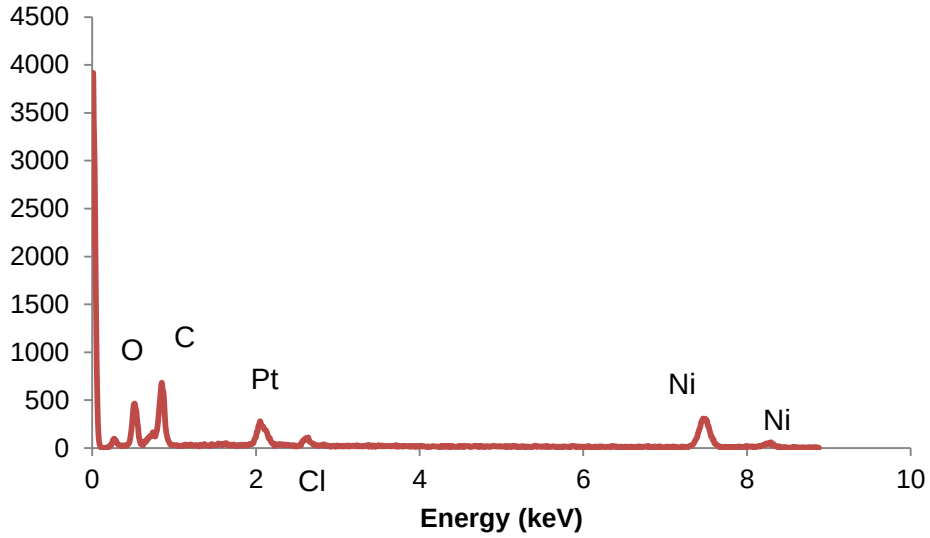

Figure 4.6h: EDX profiles of Ni foam/C after deposition Pt deposition

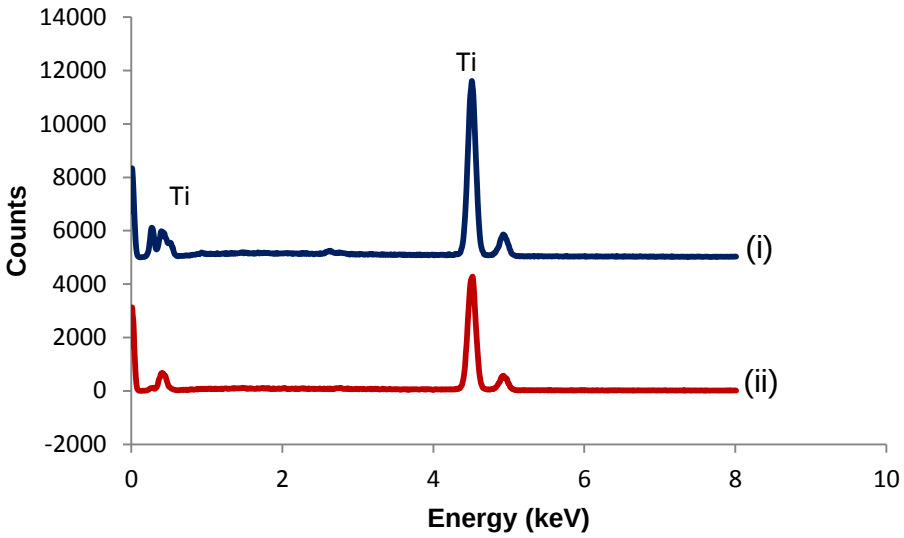

Figure 4.6i: EDX profiles of Ti mesh before (i) and after (ii) Pt deposition

4.7 AFM

The 3-D AFM images obtained before and after Pt deposition on carbon paper are shown in Figure 4.7(a and b). Root mean square (RMS) surface roughness of the catalyst was calculated to be 105 nm after deducting 19 nm from the blank surface height. The difference in the surface roughness value in the two cases can be correlated to the particle size of the deposited film (Briggs & Seth, 1990). The average Pt size was estimated to range between 24 and 99.2 nm from the AFM histogram shown in Figure 4.7c.

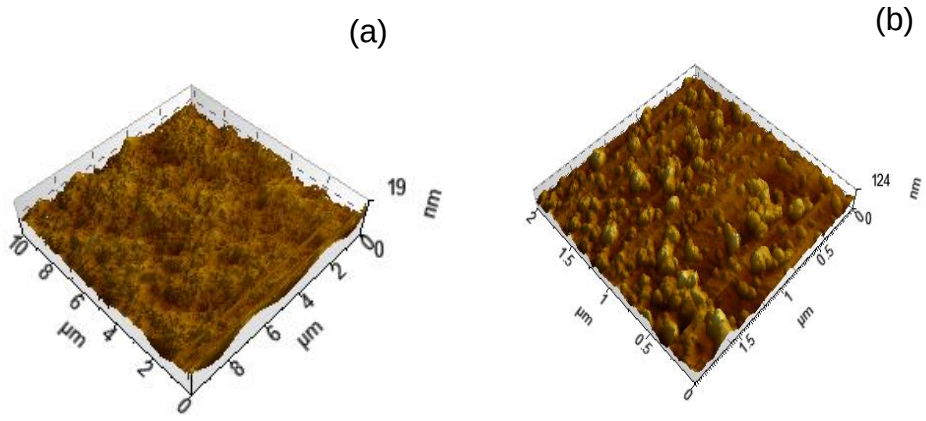

Figure 4.7: AFM micrographs of carbon paper before **(a)** and after Pt deposition **(b)**

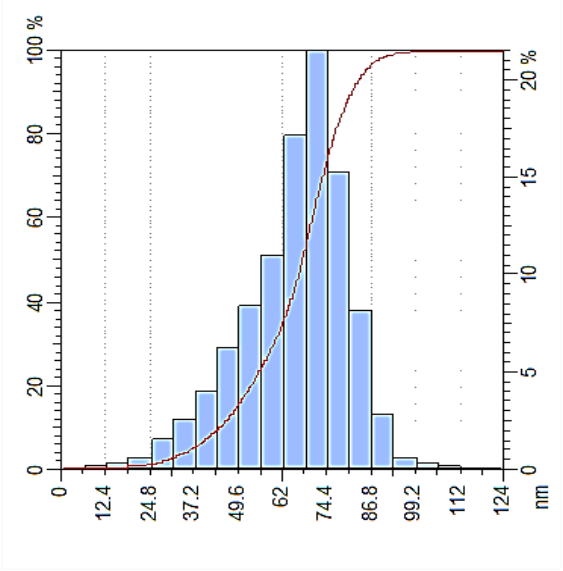

Figure 4.7c: Particle size histogram

Ideally, after the eight repetitions, one should obtain an atomic radius of around 1.11 nm (Briggs & Seth, 1990), but in this case the radius in the experimental work was 3 times bigger than the theoretical work. This result was expected, since a small overpotential was used to deposit the sacrificial Cu instead of the endorsed underpotential deposition. This could have yielded results closer to the ideal number.

AFM could not be performed on Ni foam and Ti mesh, because AFM probes are generally not used in measuring steep walls or overhangs since their surface is too rough to raster. There are specially made cantilevers and AFMs that can be used to modulate the probe sideways as well as up and down to measure sidewalls but these come at the cost of more expensive cantilevers, lower lateral resolution and additional artefacts.

4.8 ICP-OES

Deposition of Pt at different repetitions (1x, 4x, 8x) for all three substrates was completed to observe the trend in weight. These electrodes were digested and run on the ICP-OES to determine the Pt content with every repeated cycle. The results are plotted in Figure 4.8 (a-c). There is an upward rise in these linear curves, which proves that with each repetition, there is an increase in Pt mass. Table 4.2, below, illustrates the increasing Pt mass with the number of deposition repetitions.

Table 4.2: Summary of weight vs. deposition repetitions

Substrate	**Amount of Pt(µg) (1x cycles)**	**Amount of Pt(µg) (4x cycles)**	**Amount of Pt(µg) (8x cycles)**
Carbon paper	101.40	125.38	196.27
Ni foam	92.50	793.92	3545.30
Ti mesh	16.81	74.58	174.13

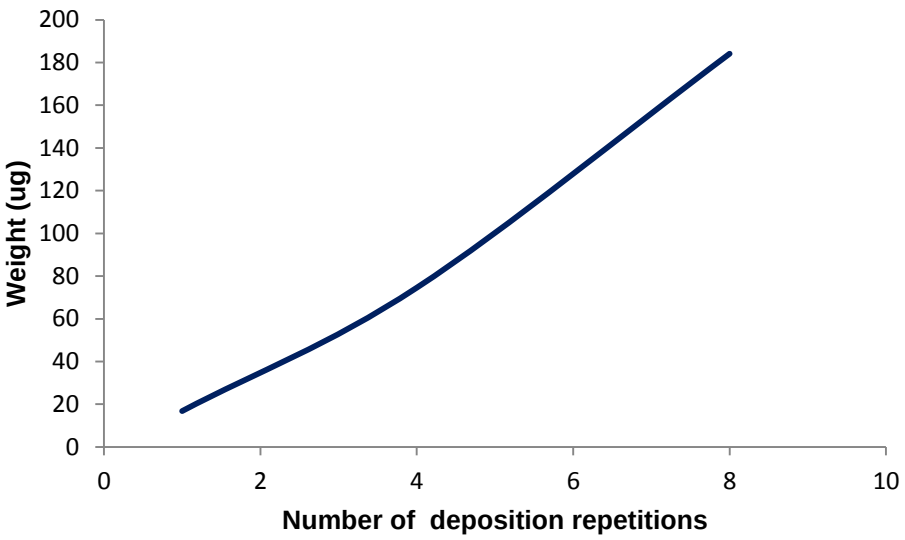

Figure 4.8a: Weight vs. number of deposition repetitions for Carbon paper

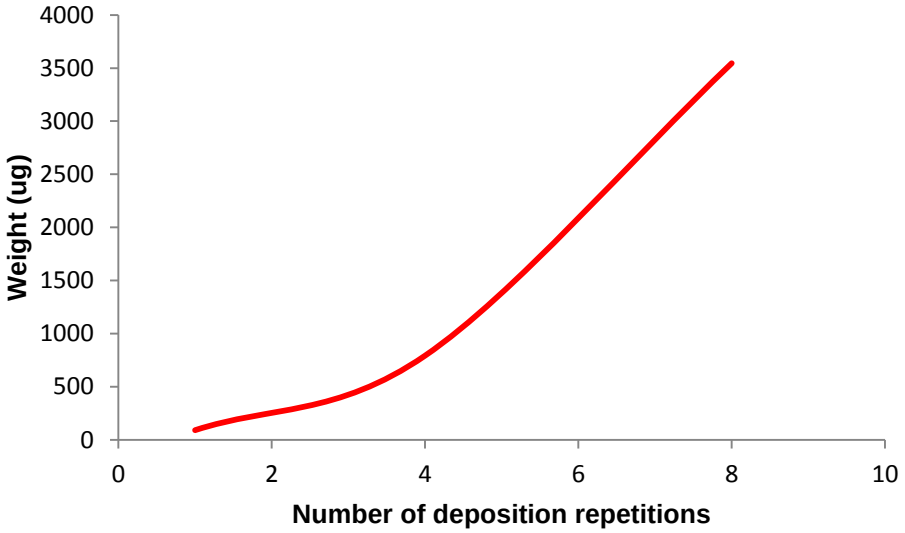

Figure 4.8b: Weight vs. number of deposition repetitions plot for Ni foam

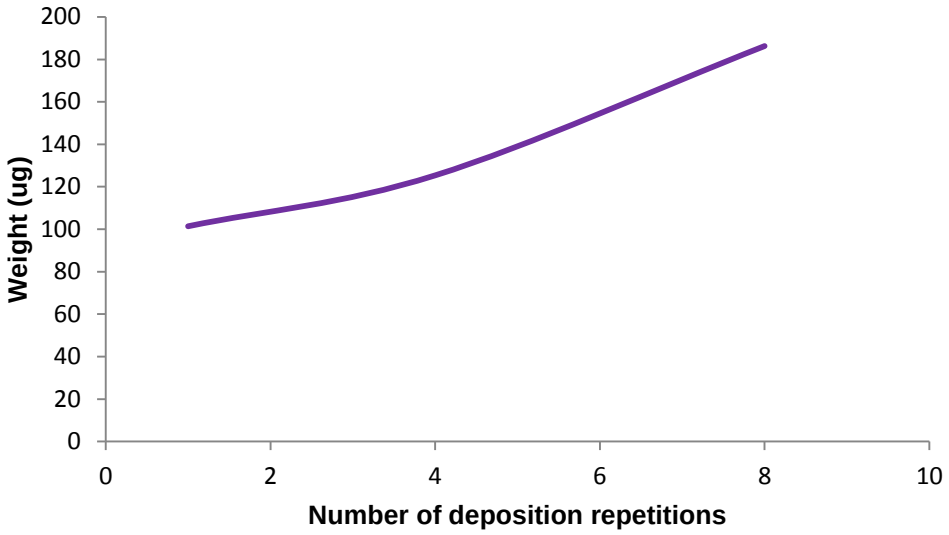

Figure 4.8c: Weight vs. number of deposition repetitions for Ti mesh

It can be seen on the table that when comparing the electrodes with respect to their mass, the Pt content on Ni foam after eight cycles exceeds the Pt masses on carbon paper and Ti mesh. The high mass of Pt on the substrate could be attributed to the foam's high surface area (Abson, 2006) caused by the inter-linked holed cells.

4.9 Electrochemical Surface Area (EAS)

There are two electrochemical methods used to estimate the EAS. The first method relies on the hydrogen adsorption/desorption ($H_{ads/des}$) charges (Kolbe, Przasynski, & Gerischer, 1974; Briggs & Seth, 1990). The hydrogen desorption peak areas from Figures 4.2 were employed to estimate this value. The amount of Pt used within the catalyst layer [Pt] (see Table 4.2) results is known, so the EAS was calculated by using Equation 4.1 (Appleby & Foulkes, 1989):

$$\mathrm{EAS} = \frac{Q_{\mathrm{H}}}{[\mathrm{Pt}] \times 0.21}$$

(Eqn. 4.1)

A discrepancy was discovered after calculating the EAS from Figure 4.2. These EAS results have been given in Table 4.3. The calculated value for the Pt/Ni foam electrode was the smallest from the three electrodes, yet it had produced the best results in terms of current density in methanol oxidation and only showed a small difference in a real surface area with that of the carbon paper electrode. The Pt mass and real surface of the Ti mesh electrode was the lowest, yet it surpassed the Ni foam electrode's EAS (see Table 4.3 for these values). This prompted further investigation into the use of desorbed hydrogen in calculating EAS.

Table 4.3: Comparisons in EAS methods

Catalyst	**Real surface area H_{dep} (cm^2)**	**EAS H_{dep} (m^2/g)**	**Real surface area CO stripping (cm^2)**	**EAS CO stripping (m^2/g)**
Pt/Carbon paper	44.66	22.75	479.08	244.09
Pt/C/Carbon paper	230	N/A	49.92	N/A
Pt/Ni foam	34.28	0.97	1615.59	45.57
Pt/C/Ni foam	500.79	N/A	397.71	N/A
Pt/Ti mesh	10.19	5.85	0.72	0.41

It is clear that from Equation 4.1, one may charge a wide range of loading to obtain EAS. This is only true if all the platinum loading on the electrode was very active (Beden, Leger, & Lamy, 1992). However, the fact is that as the loading increases, the electrode thickness grows. Consequently, some platinum particles are blocked

on the substrate and not exposed to the electrolyte solution (Bockris & Srinivasan, 1969). The occurrence does not apply in this case since the morphology of deposits does not change significantly from cycle to cycle but the surface area of the nanostructures increases because recorded currents were progressively larger. This was proven when cyclic voltammagrams of the number deposition repetitions (4x and 8x) were performed in 0.1 M $HClO_4$ at 50 mV/s as shown in Figure 4.9. This leads to the conclusion that the equation above does not entirely reflect the true electrochemical surface area in this work.

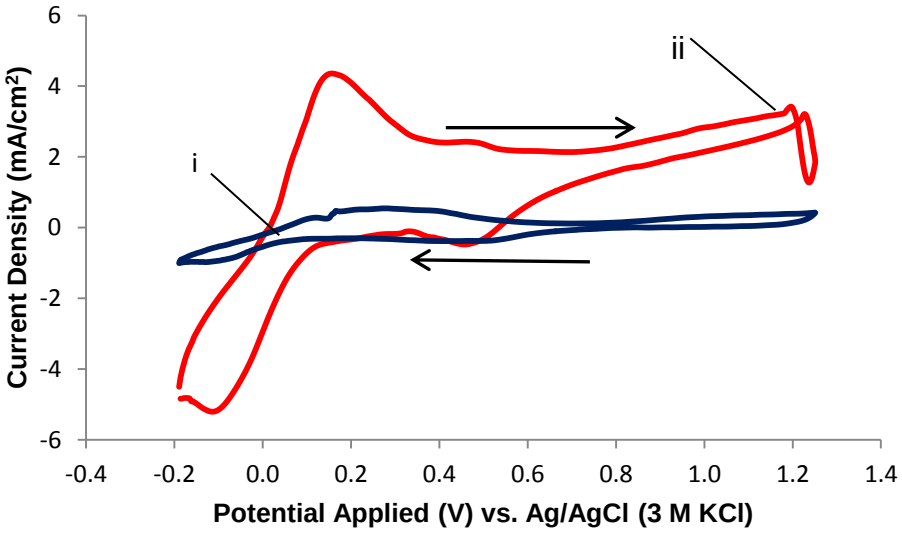

Figure 4.9a: Cyclic Voltammograms of Pt_4/Carbon paper **(i)** and Pt_8/Carbon paper **(ii)** at 50 mV/s in 0.1M $HClO_4$. (5^{th} scan)

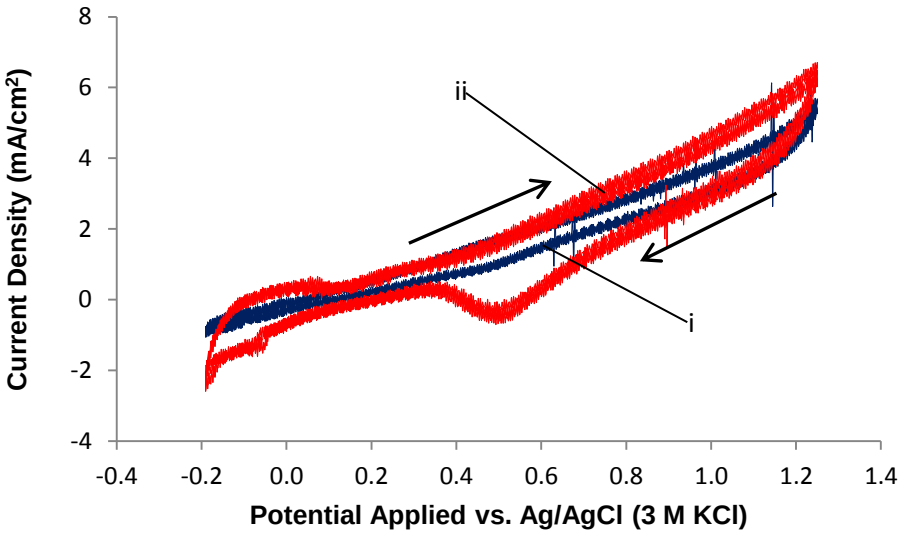

Figure 4.9b: Cyclic Voltammograms of Pt_4/Ni foam (i) and Pt_8/Ni foam (ii) at 50 mV/s in 0.1M $HClO_4$. (5^{th} scan)

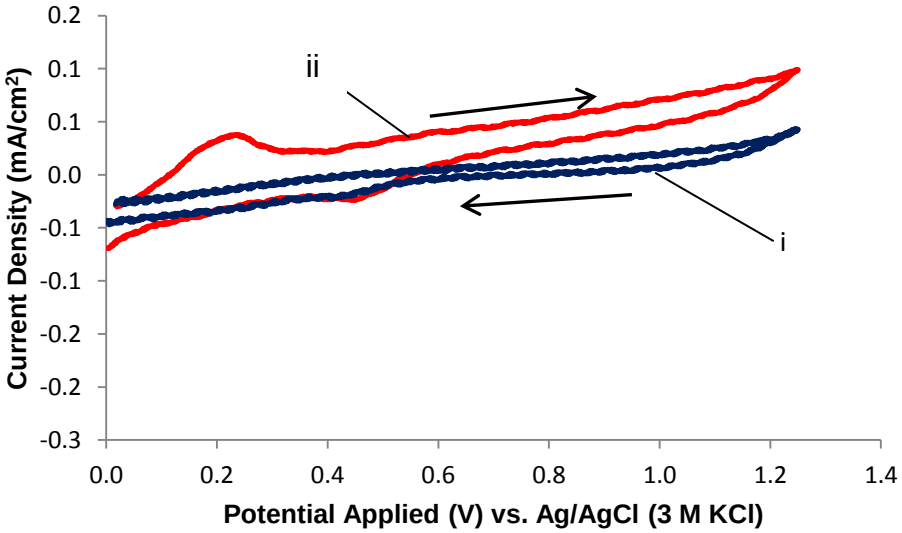

Figure 4.9c: Cyclic Voltammograms of Pt_4/Ti mesh **(i)** and Pt_8/Ti mesh **(ii)** at 50 mV/s in 0.1M $HClO_4$. (5^{th} scan)

The EAS obtained from $H_{ads/des}$ may not be suitable for implementation in the particular bimetallic catalyst such as Pt/Ru, Pt/Ni, and Pt/Fe and so forth (Kolbe, 2008). These catalysts showed an unclear double layer region and overlapping of hydrogen and oxygen adsorption region. This condition may prevent any straightforward application of $H_{ads/des}$ charges and thus hinder the determination of the exact value of its EAS and other parameters (Beden, Leger, & Lamy, 1992).

Because of this ambiguity, another method for the calculation of the EAS was also explored.

The second electrochemical method for the estimation of EAS is CO stripping voltammetry. CO can be strongly adsorbed onto the surface of Pt to form a monolayer. This monolayer is subsequently stripped anodically. The area underneath the peak formed is employed to estimate the EAS by utilizing Equation 4.2 (Brankovic, Wang, & Adzic, 2005; Bard & Faulkner, 2001).

$$\mathrm{EAS_{CO}} = \frac{Q_{\mathrm{CO}}}{[\mathrm{Pt}] \times 0.484}$$

(Eqn. 4.2)

Kolbe (2006) *et al.* has suggested that EAS calculated by means of CO adsorption seems to be independent on the Pt loading. It may be due to the stripping mechanism dominated by the electronic conduction of the oxidation reaction with the hydroxyl group from water (Chem et al., 2005). In this particular study of bimetallic Pt/Ni foam, the CO stripping method gives a higher value for EAS (seen in Table 4.3) compared to the $H_{ads/des}$ method, but the carbon paper electrode is still in the lead as a consequence of the high mass of Pt on the Ni foam electrode (Table 4.2).

The real surface area of the modified electrodes behaved predictably when employing the $H_{ads/des}$ method. There was an increase in surface area when compared to the unmodified electrodes. On the other hand, the CO stripping method showed the opposite trend. There was a decrease in surface area when compared to the unmodified electrodes. This could imply that not all the surface area of these electrodes was covered with CO or there was difficulty in converting

CO to CO_2. The Ni foam/C electrodes real surface area was approximately eight times higher than that of carbon paper/C. These results were expected due to the Ni foams high surface area. EAS could not be calculated for the modified electrodes since their weights were not known.

CHAPTER 5

CONCLUSION AND RECOMMENDATION

Platinum was deposited on carbon paper, carbon paper modified with carbon microporous layer, Ni foam; Ni foam modified with carbon microporous layer and Ti mesh using ECALD technique.

The UPD was not recorded on the CVs used to determine the potential, so an overpotential of -0.05 V was chosen as prescribed by Mkwizu *et al (*2011*)*. The deposition time for Cu was determined as 90s.

The platinum deposited on the substrates showed activity towards hydrogen and methanol oxidation. The methanol oxidation CV results for the modified Pt/Ni foam electrode indicated a more negative onset potential and a higher I_f/I_r value when compared to the other electrodes.

For the anodic CO stripping voltammagram, the onset potentials for the modified Pt/Substrates were more anodic than their unmodified versions. The differences were not substantial, but there was a consistency in the change which demonstrated that modification improved these electrodes performances.

Chronoamperometry measurements concluded that Pt/Ni foam and Pt/C/Ni foam has the optimal methanol oxidation activity compared to the other Pt/Substrates, but Pt/Ni foam showed a more gradual decay with time, which indicated an improved CO resistance.

SEM images showed a homogenous distribution of Pt particles on the substrates. EDX confirmed the presence of Pt on the substrates. ICP results also confirmed the presence of Pt and showed an increase in weight with every repetition. Pt/Ni

foam had higher Pt mass accumulation than Pt/Carbon paper and Pt/Ti mesh due to its superior surface area. The average particle size obtained from AFM ranged from 24-99.2 nm.

The findings discussed in Chapter 4 validated the feasibility of ECALD on the tested substrates. The electrochemical performance of Pt/C/Ni foams was better than the other substrates. This electrode proved to be the best in terms of its application in hydrogen oxidation, methanol oxidation activity, CO tolerance and its improved real surface area.

The following views are recommendations prescribed in order to improve and apply this work in fuel cell development.

- Perform oxygen reduction using the same substrates and this project is ongoing in collaboration with (UWC-CSIR)
- These anode materials are planned to be used in the fabrication of membrane electrode assemblies (MEAs) for fuel cell performance testing. These activities are ongoing in our laboratory for the direct alcohol fuel cell performance in alkaline media.
- Prepare bimetallic electrocatalysts using ECALD technique such as Pt/Ru to reduce poisoning based on bifunctional mechanism for methanol electro-oxidation.

APPENDIX

References

ABE, H., MATSUMOTO, F., ALDEN, L. R., WARREN, S. C., ABRUNA, H. D., & DI SALVO, P. J. 2008. Electrocatalytic performance of fuel oxidation by Pt_3Ti nanoparticles. *Journal of the American Chemical Society, 130*, 5452-5458.

ABSON, N. M. 2006, November 22. *Patent No. 05010605.3.* Europe.

ADZIC, R., ZHANG, J., SASAKI, K., VUKMIROVIC, M., SHOA, M., NILEKAR, U. 2007. Platinum monolayer fuel cell electrocatalyst. *Topics in Catalysis, 46*, 249-262.

ANTOLINI, E., SALGADO, J., & GONZALEZ, E. 2006. Carbon supported $Pt_{75}M_{25}$ (M=Co, Ni) alloys as anode and cathode electrocatalyst for direct fuel cells. *Journal of Electroanalytical Chemistry, 580*, 145-154.

APPLEBY, A. J., & FOULKES, F. R. 1989. *Fuel Cell Handbook.* New York: Van Nostrand Reinhold.

ARICO, A., BAGLIO, V., & ANTONUCCI, V. 2009. *Direct Fuel Cells: History, Status and Perspectives.* Weiheim: Wiley VCH.

ATTARD, G. A., AHMADI, A., JENKINS, D. J., & HAZZAZI, O. A. 2003. The characterisation of supported platinum nanoparticles on carbon used for enatioseletive hydrogenation: A combined electrochemical STM approach. *Journal of the American Chemical Society, 4*, 123-130.

BABU, P. K., KIM, H. S., OLDFIELD, E., & WIECKOWSKI, A. 2003. Electronic alteration caused by ruthenium in Pt-Ru alloy nanoparticles revealed by electrochemical NMR. *Journal of Physical Chemistry B, 107-110*, 7595.

BAGKAR, N., CHEN, H., PARAB, H., & LUI, R. 2009. Nanostructured electrocatalyst synthesis: Fundamental and Methods. In H. Liu, & J. Zhang (Eds.), *Electrocatalysis of Direct Methanol Fuel Cells: Fundamentals to Application*. Weiheim: Wiley VCH.

BARBIR, F. 2005. *PEM fuel cells: Theory and Practice.* Burlington: Elsevier Academic Pres.

BARD, A. J., & FAULKNER, L. R. 2001. *Electrochemical Methods: Fundamentals and Applications.* 2nd ed). New York: John Wiley & Sons Ltd.

BEDEN, B., LEGER, J. M., & LAMY, C. 1992. *Modern Aspects of Electrochemistry.* (J. Bockris, B. Conway, & R. White, Eds.) New York: Plenum Press.

BIDAULT, F., BRETT, D., MIDDLETON, P., ABSON, N., & BRANDO, N. 2009. A new application for nickel foam in alkaline fuel cell. *International Journal of Hydrogen Energy, 34*, 6799-6808.

BOCKRIS, J., & SRINIVASAN, S. 1969. *Fuel Cell: Their Electrochemistry.* New York: McGraw-Hill Book Company.

BOUTONNET, M., KIZLING, J., STENIUS, P., & MAIRE, G. 1982. The preparation of monodisperse metal particles from microemulsions. *Colloid Surface, 5*, 209-225.

BRACK, M. 1993. The physics of simple clusters: self-consistent jellium model and semi-classical approaches. *Reviews of Modern Physics, 65*, 677-732.

BRADLEY, J. 1994. *Colloids: From Theory to Applications.* (G. Schmid, Ed.) Wienheim VCH.

BRAGG, A. E., VERLET, J. R., KAMMRATH, A., & CHESHNOVSKY, O. 2005. Time-resolved intraband electronic relaxation dynamics of Hgn- clusters (n=7-13,15,18) excited at 1.0eV. *Journal of Physical Chemistry A, 122*, 54314-54320.

BRANKOVIC, S. R., WANG, J. X., & ADZIC, R. R. 2005. Pt submonolayer on Ru nanoparticles: A novel low Pt loading, high CO tolerance fuel cell electrocatalysts. *Electrochemical Solid State Letter, 4*, A217-A220.

BRANKOVIC, S., WANG, J., & ADZIC, R. 2001. Metal monolayer deposition by replacement of metal adlayers on electrode surfaces. *Surface Science, 474*, L173-L180.

BRIGGS, D., & SETH, M. P. 1990. *Practical Surface Analysis*. New York: John Wiley & Sons Inc.

BUGBEE, E. 1940. *Textbook of Fire Assaying.* New York: Chapman and Hall.

CAZAYOUS, M., LANGLOIS, C., OIKAWA, T., RICOLLEAU, C., & SACUTO, A. 2006. Cu-Ag core shell nanoparticles: A direct correlation between micro-Raman and electron microscopy. *Physics Review B, 73*, 113402-113412.

CHANDRASEKARAN, K., WASS, J., & BOCKRIS, J. 1990. The potential dependence of intermediates in methanol oxidation observed in the steady state by FTIR spectroscopy. *Journal of Electrochemical Society, 137*, 518-526.

CHEM, Z., QUI, X., LU, B., ZHANG, S., ZHU, W., & CHEN, L. 2005. Synthesis of hydrous ruthenium oxide supported platinum catalysts for direct methanol fuel cells. *Electrochemistry Communications, 7*, 593-596.

CHOI, J., PARK, K., KWON, B., & SUNG, Y. 2003. Methanol oxidation on Pt/Ru, Pt/Ni and Pt/Ru/Ni. *Journal of Electrochemical Society, 150*, A973-A978.

COCKE, D. 1990. The surface reactivity of Ti-Cu and Ti-Al alloy and the ion chemistry of their oxide overlayers. *Solid State Ionic, 43*, 119-131.

DE HEER, W. A. 1993. The physics of simple metal clusters: experimental aspects and simple models. *Reviews of Modern Physics, 65*, 611-676.

DELMON, B., GRANGE, P., JACOBS, P., & PONCELET, G. 1979. *Preparation of Catalyst II*. Amsterdam: Elsevier.

DEMIRCI, U. 2007. Theoretical means for searching bimetallic alloys as anode electrocatalysts for direct liquid-feed fuel cells. *Journal of Power Sources, 173*, 11-18.

DICKINSON, A., CARRETTE, L., COLLINS, J., FRIENDRICH, K., & STIMMING, U. 2002. Preparation of a Pt-Ru/C catalyst from carbonyl complexes for fuel cell application. *Electrochimica Acta, 47*, 3733-3739.

DING, E., MORE, K. L., & HE, T. 2008. Preparation and characterisation of carbon-supported Pt-Ti alloy electrocatalysts. *Journal of Power Sources, 175*, 794-799.

EGOROV, G., VOLKOV, A., & GOLSTCEV, V. 2012. Delamination of Cu and Ti thin films deposited by magnetron sputtering on Cu substrate: Analysis of reason. *Material Science Forum, 706*, 2863-2868.

FAIN, S. C., & MCDAVID, J. M. 1976. Work-function variation with alloy composition: Cu-Au. *Physical Review B, 9*, 5099-6003.

FEDKIV, P., & HER, W. 1989. An impregnation-reduction method to prepare electrodes on Nafion SPE. *Journal of Electrochemical Society, 136*, 899-910.

FREITAS, R. G., OLIVEIRA, R. T., SANTOS, M. C., BULHOES, L. O., & PEREIRA, E. C. 2006. Preparation of Pt thin film electrodes using Pechini method. *Material letters,* 60, 1906-1910.

GASTEIGER, H., MARKOVIC, N., ROSS, P. J., & CAIRNS, E.(1994. CO Electrooxidation on well-characterized Pt-Ru alloys. *Journal of Physical Chemistry, 98*, 617-625.

GOLDSTIEN, J. I., NEWBURY, D. E., ECHLIN, P., JOY, D. C., FIORI, C., & LIFSHIN, E. 1981. *Scanning Electron Microscopy: A text for Biologist, Materials Scientist, and Geologist.* New York: Plenum Press.

GOTTERFELD, S., & ZAWODZINSKI, T. 1997. *Advances in Electrochemical Sciences and Engineering.* New York: Wiley-VCH.

GREELEY, J., & NORKOV, J. 2005. A general scheme for the estimation of oxygen binding energies on binary transition metal surface alloys. *Surface Science, 592*, 104-111.

GROVE, W. R. 1839. Voltaic Series and Combination of Gas by Platinum. *Philosophical Magazine and Journal of Sciences, XIV*, 127-130.

GULLA, A., SAHA, M., & MUKERJEE, S. 2005. Dual ion- beam- assisted deposition as a method to obtain low loading high performance electrodes for PEMFCs. *Electrochemical Society, 8*, A504-A508.

GURA, B., VISWANTHAN, R., LUI, R., LAFRENZ, T., LEY, K., SMOTKIN, E. 1998. Structural and electrochemical characteristics of binary, tertiary and quaternary platinum alloy catalyst for methanol electrooxidatioin. *Journal of Physical Chemistry B, 102*, 9997-10002.

HAMMER, B., & NORSKOV, J. 1995. Electronic factors determining the reactivity of metal surfaces. *Surface Science, 343*, 211-220.

HAMMER, B., & NORSKOV, J. K. 2000. *Advances in Catalysis.* San Diego: Academic Press Inc.

HAMNETT, A. 1999. *Interfacial Electrochemistry, Theory and Applications.* (A. Wieckowski, Ed.) New York: Mercel Dekker.

HAMNETT, A. 2003. The Components of a Fuel Cell. In W. Vielstich, A. Lamm, & H. Gastieger (Eds.), *Handbook of Fuel Cells: Fuel Cell Technology and Application* (3rd ed.). New York: John Wiley and Sons Ltd.

HAMNETT, A., KENNEDY, B. J., & WEEKS, S. A. 1988. Base metal oxides as promoters for the electrochemical oxidation of metal. *Journal of Electroanalytical Chemistry, 240*, 349-353.

HIERSO, J., FEUNER, R., & KALCK, P. 2000. Platinum and palladium film obtained by low-temperature MOCVD for the formation of small particles on divided supports as catalytic materials. *Chemical Materials, 12*, 390-399.

HIRANO, S., KIM, J., & SRINIVASAN, S. 1997. High performance proton exchange membrane fuel cells with sputter-deposited Pt-layer electrodes. *Electrochimica Acta, 42*, 1587-1593.

HOSHINO, K., NAGANUMA, T., WATANABE, K., & KONISHI, Y. 1995. Ionization energies of cobalt-vanadium bimetallic clusters. *Chemical Physics Letters, 239*, 359-364.

IANNIELO, R., SCHMIDT, V., STIMMING, V., STUMPER, U., & WALLAM, A. 1994. CO adsorption oxidation on Pt and PtRu alloys: Dependence on substrate composition. *Electrochimica Acta, 39*, 1863-1870.

ISHIKAWA, Y., CABRERA, C., & LIAO, M. 2000. Theoretical study of CO adsorption on Pt, Ru and Pt-M (M= Ru, Sn, Ge). *Surface Science,* 445, 267-282.

JANSSEN, M., & MOOLHUYSEN, J. 1976. Binary systems of platinum and a second metal as oxidation catalysts for methanol fuel cells. *Electrochimica Acta, 21*, 869-878.

JOHNSON MATTHEY. 2012, March 1. Retrieved March 1, 2012, from http://www.platinum.matthey.com/pgm_prices

KAWATS, S. 1998. Advanced PEFC development for fuel cell powered vehicles. *Journal of Power Sources, 71*, 150-155.

KIEJNA, A. 1990. Comment on surface segregation in alkali-metal alloys. *Journal of Physics: Condensed Matter, 2*, 6331-6333.

KIM, J. Y.(2008. *Ultrahigh surface analysis studies electrochemical atomic layer deposition of metals and semiconductors.* Georgia, Athens, United States of America.

KIM, Y., KIM, J., VAIRAVAPANDIA, D., & STICKNEY, J. 2006. Platinum nanofilm formation by UDP copper: Studies using in-situ scanning tunneling microscopy. *Journal of Physical Chemistry B, 110*, 17998-18006.

KOLBE, D., PRZASYNSKI, M., & GERISCHER, H.1974. Underpotential deposition of metals and work function differences. *Journal of Electroanalytical Chemistry, 54*, 25-31.

KOLBE, G. 2008. *Fuel Processing for Fuel Cells.* Weiheim: Wiley VCH.

Kordesch, G., & Simadar, G. 1996. *Fuel cell and their Applications.* Weinheim: VCH.

KORETSKY, G. M., KERNS, K. P., NIEMAN, G. C., & KNICKELBEIN, M. B. 1999. Reactivity and photoionization: Studies of bimetallic cobalt-manganese clusters. *The Journal of Physical Chemistry A, 103*, 1997-2003.

KOYASU, K., MITSUI, M., NAKAJIMA, A., & KAYA, K. 2002. Photoelectron spectroscopy of palladium-doped gold cluster anion. *Chemical Physics Letters, 358*, 224-230.

LARMINE, J. 2003. *Fuel cell system explained* 2nd ed. SAE International.

LEY, K., LIU, R., PU, C., FAN, Q., LEYAROVSKA, N., SEGRE, C. 1997. Methanol oxidation on single phase Pt-Ru-Os ternary alloys. *Journal of Electrochemical Society, 144*, 1543-159.

LIDE, D. (2000). *Handbook of Chemistry and Physics* (81st ed. Florida: CRC Press.

LIM, C., SCOTT , K., ALLAN, R. G., & ROY, S. 2004. Direct methanol fuel cells using thermally catalyzed Ti mesh. *Applied Electrochemistry, 34*, 929-933.

LIMA, F., ZHANG, J., SHAO, M., SASAKI, K., VUKMIROVIC, M., TICIANELLI, E. 2006. Catalytic Activity-d-band center correlation for the O_2 reduction reaction on platinum in alkaline solutions. *Journal of Physical Chemistry, 111*, 404-410.

LISTER, L., & STICKNEY, J. 1996. Formation of the first monolayer of CdSe on Au(111) by electrochemical ALE. *Surface Science, 107*, 153-159.

LIU, H., SONG, C., ZHANG, L., ZHANG, J., WANG, H., & WILKINSON, D. 2006. A review of anode catalysis in the direct methanol fuel cell. *Journal of Power Sources, 155*, 95-110.

LU, C., & MASEL, R. 2001. The effect of ruthenium on the binding of CO, H_2 and H_2O on Pt(110). *Journal of Physical Chemistry B , 105*, 9793-9797.

LUO, J., WANG, L., MOTT, D., NJOKI, P., KARIUKI, N., ZHONG, C., 2006. Ternary alloy nanoparticles with controllable sizes and composition and electrocatalytic activity. *Journal of Materials Chemistry, 16*, 1665-1673.

MAIER-BORST, M., CAMERON, D. B., ROKNI, M., & PARKS, J. H. 1999. Electron diffraction of trapped cluster ions. *Physics Review A, 59*, R3162-R3165.

MARKOVIC, N., & ROSS, P. 2002. Surface science studies of model fuel cell electrocatalysts. *Science Report, 45*, 117-123.

MARTIN, T. P. 1996. Shells of atoms. *Physics Reports, 273*, 199-241.

MAYRHOFER, K., BLIZANAC, B., ARENZ, M., STAMERIKOVIC, V., ROSS, P., & MARKOVIC, N. 2005. The impact of geometric and surface electronic properties of Pt-catalysts on the particle size effect in electrocatalysis. *Journal of Physical Chemistry B, 109*, 14433-14440.

MEHTA, V., & COPPER, J. 2003. Review and analysis of PEM fuel cell design and manufacturing. *Journal of Power Sources, 114*, 32-53.

MENEZES, W. J., & KNICKELBEIN, M. B. 1991. Bimetallic clusters of cobalt and aluminium ionization potentials versus reactivity and the importance of geometric structures. *Chemical Physics Letters, 183*, 357-363.

MKWIZU, T. S., MODIBEDI, M., & MATHE, M. 2011. Multistage electrodepostion of supported platinum-based nanostructured systems for electrocatalytic applications . *219th ECS Meeting*. Montreal, Canada: Journal of the Electrochemical Society.

MKWIZU, T., MATHE, M., & CUKROWSKI, I. 2010. Electrodeposition of multideposition of bimetallic nanoclusters of ruthenium and platinum via surface limited redox-replacement reactions for electrocatalytic applications. *Langmuir, 26*, 570-580.

MROZEK, M., XIE, Y., & WEAVER, M. J. 2001. Surface-enhanced Raman scattering on uniform platinum-group overlays: Preparation by redox replacement underpotential-deposited metal on gold. *Journal of Analytical Chemistry, 73*, 5953-5960.

MUKERJEE, S., & SRINIVASAN, S. 1993. Enhanced electrocatalysis of oxygen reduction on platinum alloys in proton membrane fuel cell. *Journal of Electroananalystical Chemistry, 357*, 201-224.

MUKERJEE, S., SRINIVASAN, S., & APPLEBY, A. 1993. Effect of sputtered film of platinum on low platinum loading electrodes on electrode kinetics of oxygen reduction in proton exchange membrane fuel cells. *Electrochimica Acta, 38*, 1661-1669.

NONOSE, S., SONE, Y., & KAYA, K. Z. 1991. Reactivity and stability of bimetallic clusters. *Zeitschrift fur Physik D: Atoms, Molecules and Clusters, 19*, 357-364.

OHKUBO, C., & SHIMURA, I. 2003. Wear resistance of experimental Ti-Cu alloys. *Biomaterials, 24*, 3377-3381.

PADDISON, S. 2003. First principles and modeling of sulfonic acid based ionomers. In W. Vielstich, A. Hamm, & H. Gasteiger (Eds.), *Handbook of Fuel Cells: Fuel Cell Technology and Applications* 3rd ed.. New York: John Wiley & Sons Ltd.

PARK, K., CHOI, J., KWON, B., LEE, A., SUNG, Y., HA, Y.2002. Chemical and electronic effect of Ni in Pt/Ni and Pt/RuNi alloy nanoparticles in methanol electrooxidation. *Journal of Physical Chemistry, 106*, 1869-1877.

PAUWELS, B., VAN TENDELOO, G., ZHURKIN, E., HOU, M., & VERSCHOREN, Y. 2001. Transmission electron microscopy and Monto Carlo simulations of order in Au-Cu clusters produced in a laser vaporization source. *Physics Review B, 63*, 16506-16512.

PIELA, P., EICKS, C., BROSHA, E., GARZON, F., & ZELENAY, P. 2004. Ruthenium crossover in DMFC with PtRu black anode. *Journal of Electrochemical Society, 151*, A2059-A2068.

PLETCHER, D. 2009. *A First Course in Electrode Process* 2nd ed. Cambridge: Royal Society of Chemistry.

POH, C., TIAN, Z., GAO, J., LUI, Z., LIN, J., & FENG, Y. 2012. Nanostructured trimetallic Pt/FeRuC, Pt/NiRuC and Pt/CoRuC. *Journal of Material Science, 1*, 1-10.

RAHIN, M., & HASSAN, H. 2009. Titanium and platinum modified titanium electrodes and catalysts for methanol electrooxidation. *Thin Solid Films, 517*, 3362-3369.

RAJALAKSHMI, N., & DHATHATHREYAN, K. 2007. Catalyst layer in PEMFC electrode fabrication, Characterisation and analysis. *Chemical Engineering Journal, 129*, 31-40.

RENOUPREZ, A. J., LEBAS, K., BERGERET, G., & ROUSSET, J. L. 1996. Supported Pd-Cu catalysts prepared from bimetallic complexes: relation between surface composition measured by ion scattering and reactivity. *Studies in Surface Science and Catalysis, 101*, 1105-1114.

RENOUPREZ, A. J., ROUSSET, J. L., CADROT, A. M., SOLDO, Y., & STIEVANO, M. 2001. Structure and catalytic activity of palladium-platinum aggregates obtained by laser vaporisation of bulk alloys. *Journal of Alloys and Compounds, 328*, 50-56.

RIBARENEIRA, R., & HOYOS, B. 2010. CO-Catalytic effect of Ni in Pt-Ru/C and Pt-Sn electrocatalysts for ethanol electrooxidation. *Latin American Applied Research, 40*, 113-118.

RINGER, S., JANIN, E., BOUTONNET-KIZLING, M., & GOTHELID, M. 2000. Pt_3Ti alloy formation on the Pt(III) surface. *Applied Science, 163*, 190-191.

RODRIQUEZ, J., & GOODMAN, D. 1992. The nature of the metal-metal bond in bimettalic surfaces. *Science, 252*, 897-905.

RONGZHONG, J., & CHU, D. 2009. Combinatorial and high throughput screening of DMFC electrocatalysts. In H. Liu, & J. Zhang (Eds.), *Electrocatalysis of Direct Methanol Fuel Cells*. Weinheim: Wiley-VCH.

ROUSSET, J. L., STIEVANO, L., CADETE SANTOS AIRES, F. J., & GEANTET, C. (2002). Hydrogenation of Tetralin in sulphur over y-Al_2O_3 supported on Pt, Pd, and Pd-Pt model catalysts. *Journal of Catalysis, 202*, 163-171.

RUBAN, A., HAMMER, B., STOLTZE, P., SKRIVER, H., & NORSKOV, J. 1997. Surface electronics structure and reactivity of transition and noble metals. *Journal of Molecular Catalysis A: Chemical, 115*, 421-429.

RUSSELL, A. E., & ROSE, A. 2004. X-ray absorption spectroscopy of low temperature fuel cell catalysts. *Chemical Reviews A, 104*, 4613-4619.

SAKELLAROPOULOS, G. P., ELEY, D. D., & PINES, H. 1981. *Advances in Catalysis.* (P. Weisz, Ed.) New York: Academic Press.

SAMOR, P. 2004. Scanning probe microscopy beyond imaging. *Journal of Material Chemistry, 14*, 1353-1360.

SASKI, K., WANG, J., BALASUBRAMANIAN, M., MCBREEN, J., URIBE, F., & ADZIC, R. 2004. Ultra low platinum content fuel cell anode electrocatalyst for a long-term stability performance . *Electrochimica Acta, 49*, 3873-3877.

SHIMM, J., LEE, H. K., CAIRNS , E. J., & LEE, J. S. 2001. Electrochemical characteristics of Pt-WO_3/C and Pt-TiO_2/C electrocatalysts in polymer fuel cell electrolysis. *Journal of Power Sources, 102*, 172-177.

SHOA, Z.G., LIN, W.-F., ZHU, F., & CHRISTENSEN, P. A. 2006. A tubular direct methanol fuel cell with Ti mesh anode. *Journal of Power Sources, 160*, 1003-1008.

SKOOG, D. A., HOLLER, F. J., & CROUCH, S. R. 2007. *Principles of Instrumental Analysis* 6th ed.. Belmont: Thomson Brooks/Cole.

SKOOG, D. A., HOLLER, F. J., & WEST, D. M. 1996. *Fundamentals of Analytical Chemistry* 7th ed.. Florida: Saunders College Publishers.

STICKNEY, J. 2002. *Advances in Electrochemical Science and Engineering.* (R. Alkire, & D. Kolbe, Eds.) Weiheim: Wiley-VCH.

STICKNEY, J. L., KIM, Y.G., KIM, J. Y., & VAIRAVAPANDIAN, D. 2006. Platinum nanofilm formation by EC-ALE via redox replacement of UDP copper: Studies using in-situ scanning tunneling microscopy. *Journal of Physical Chemistry. B, 110*, 17998-18006.

SUNDMACHER, K., SCHULTZ, T., ZHOU, S., SCHOTT, K., GINKEL, M., & GILLES, E. 2001. Dynamics of the direct methanol fuel cell (DMFC): Experiments and model-based analysis. *Chemical Engineering Science, 56*, 333-341.

TAYLOR, E., ANDERSON, E., & VILAMBI, N. 1992. Preparation of high platinum utilization gas diffusion electrodes for proton-exchange-membrane fuel cells. *Journal of Electrochemical Society, 139*, L45-L46.

THAMBIDURAI, C., KIM, Y.G., & STICKNEY, J. L. 2008. Electrodeposition of Ru by atomic layer deposition (ALD). *Electrochimica Acta, 53*, 6157-6164.

TICIANELLI, E. A., DEROUIN, C. R., & SCINIVASAN, S. 1988. Localization of platinum in low catalyst electrode to attain power densities in SPE fuel cells. *Electroanalytical Chemistry, 251*, 275-295.

TICIANELLI, E., BEERY, J., PAFFETT, M., & GOTTESFELD, S. 1989. An electrochemical, ellipsometric and surface science investigation of the PtRu bulk alloy surface. *Journal of Electroanalytical Chemistry and Interfacial Electrochemistry, 258*, 61-77.

TOSHIMA, N., & YONEZAWA, T. 1998. Bimetallic nanoparticles-Novel materials for chemical and physical applications. *New Journal of Chemistry, 22*, 1179-1201.

U.S DEPARTMENT OF ENERGY. 2011, September 5. *Fuel Cell comparison chart pdf*. Retrieved December 15, 2011, from US Department of Energy Web site: http://www.eere.energy.gov/hydrogenandfuelcells/fuelcells/fc_types.html

U.S DEPARTMENT OF ENERGY. 2011, September 5. *Hydrogen Program " Record 11012: Fuel Cell system cost-2011"*. Retrieved December 15, 2011, from US Department of Energy Web site: http://www.hydrogen.energy.gov/program_record.html.

VAIDYANATHAN, J., STICKNEY, J., & HAPPEK, U. 2004. Quantum confinement in PbSe thin films electrodeposited by electrochemical atomic layer epitaxy (EC-ALE). *Electrochimica Acta, 49*, 1321-1329.

VAIDYANATHAN, R., COX, S., HAPPEK, U., BANGA, D., MATHE, M., & STICKNEY, J. 2006. Preliminary studies in the electrodeposition of PbSe/PbTe superlattice thin via electrochemical atomic layer deposition (ALD). *Langmuir, 22*, 10590-10597.

VENKATASAMY, V., JAYARAJU, N., COX, S., THAMBIDURAI, C., & STICKNEY, J. 2007. Ultrathin vacuum surface studies of the electrochemical atomic layer deposition of indium telluride on n-type GaAs(100). *Journal of Electrochemical Society, 154*, H720-H730.

VIELSTSICH , W., LAMM, A., & GASTEIGER, H. A. 2003. Fuel Cell principles, systems and Applications. In *Handbook of fuel cells: Fundamental Technology and Applications* (4 Ed. West Sussex: John Wiley & Sons Ltd.

VILLEGAS, I., & STICKNEY, J. 1992. Preliminary studies of Gaas deposition on Au(111),(110) and (100) surfaces by electrochemical atomic layer epitaxy. *Journal of Electrochemical Society, 139*, 686-692.

VOYLES, P. M., MULLER, D. A., GRAZUL, J. L., & CITRIN, P. H. 2006. Atomic-scale imaging of individual dopant atoms and clusters in highly n-type bulk Si. *Letters to Physics, 73*, 113402-113409.

VUKMIROVIC, M. B., BLIZNAKOV, S. T., SASAKI, K., WANG, J., & ADZIC, R. R. 2011. Electrodeposition of metals in catalyst synthesis: The case of Platinum monolayer electrocatalysis. *The Electrochemical Society Interface*, 11, 33-40.

WANG, G., VAN HOVE, M., ROSS , P., & BASKES, M. 2005. Quantitative prediction of surface segregation in bimetallic Pt-M alloy nanoparticles (M=Ni, Re, Mo). *Progress in Surface Science, 79*, 28-45.

WASMUS, S. 1999. Methanol oxidation and direct fuel cells. *Journal of Electrochemistry, 461*, 1431-1440.

WATANABE, M., & MOTOO, S. 1975. Electrocatalysis by ad-atoms part II: Enhancement of methanol oxidation on methanol by ruthenium ad-atoms. *Journal of Electroanalytical Chemistry, 60*, 263-273.

WEE, J. H., LEE, K. Y., & KIM, S. H. 2007. Fabrication method for Low-Pt-loading electrocatalysts in proton exchange membrane fuel cell system. *Power Sources, 165*, 667-677.

WEINER, S. 1998. Fuel cell stationary power business development. *Journal of Power Sources, 71*, 61-64.

XIONG, L., & MANTHIRAM, A. 2004. Synthesis and characterisation of methanol tolerant Ti/TiOx/C nanocomposites for oxygen reduction in direct methanol fuel cell. *Electrochimica Acta, 49*, 4163-4170.

XUE, X., LIU, C., XING, W., & LU, T. 2006. Physical and electrochemical characterizations of PtRu/C catalysts by spray pyrolysis for electrocatalytic oxidation of methanol. *Journal of Electrochemistry Society, 153*, E79-E84.

YAMAUCHI, H. 1976. Simple model for work-function changes due to adsorption by metals. *Physical Review B, 14*, 2687-2694.

ZHANG, H., WANG, X., & ZHANG, J. 2008. Conventional catalyst ink, catalyst layer and MEA preparation. In J. Zhang (Ed.), *PEM Fuel Cell Electrocatalysts and Catalyst Layers, Fundamentals and Applications.* London: Springer-Verlig Ltd.

ZHANG, J., LIMA, F., SHAO, M., SASKI, K., WANG, J., HANSO, J. 2005a. Platinum monolayer on non metals-noble metal core shell nanoparticle electrocatalyst for O_2 reduction. *Journal of Physical Chemistry B, 109*, 22701-22704.

ZHANG, J., VUKMIROVIC, M. V., SASKI, K., URIBE, F., & SERB, J. 2005b. Mixed-metal Pt monolayer electrocatalyst for enhanced oxygen reduction reaction kinetics. *Journal of the American Chemical Society, 70*, 513-525.

ZHONG, C., LUO, J., FANG, B., WANJALA, B., NJOLI, P., & LOUKRAKPAN, R. 2010. Ternary nanostructured catalysts in fuel cells. *Nanotechnology, 21*, 1-20.

ZOU, W., ROBINSON, K., & GONZALEZ, R. 1992. Improved mechanical stability of supported Ru catalysts: Preparation by the sol - gel method. *Journal of Catalysis, 136*, 621-625.

Conferences and Workshops

- Oral presentation: R. M. Modibedi, E. K. Louw, M. K. Mathe, and K. I. Ozoemena Electrodeposition of Pd on Carbon Paper and Ni Foam via Surface-Limited Redox-Replacement Reactions for Oxygen Reduction Reaction, 13th Topical Meeting, ISE, Pretoria, 7-10 April 2013
- Oral presentation: Eldah K. Louw, Mmalewane Modibedi, Leskey Cele, Mkhulu Mathe, Kenneth Ozoemena, Electrochemical Deposition and Characterization of Platinum on Carbon Paper and Ni Foam, 13th Topical Meeting, ISE, Pretoria, 7-10 April 2013
- Poster presentation: Eldah K. Louw, Mmalewane Modibedi, Leskey M. Cele, Kenneth Ozoemena and Mkhulu Mathe, Electrochemical Deposition of Platinum on Carbon Paper and Ni Foam for Methanol Electrooxidation, CATSA 2012 Langebaan, Cape Town, 11-14 November 2012
- Oral presentation: Remegia M. Modibedi, Eldah K. Louw, Kenneth I. Ozoemena, Mkhulu K. Mathe, The Electrochemical atomic layer deposition of Pt and Pd nanoparticles on Ni foam for the electro-oxidation of Alcohols, ECS Prime, Honolulu, Hawaii 7-12 October 2012
- Poster presentation: Eldah K. Louw, Mmalewane Modibedi, Kenneth Ozoemena and Mkhulu Mathe, *Electrochemical Atomic Layer Deposition of Pt nanostructures on Carbon Paper and Ni Foam*, SA-Korea Fuel Cell Workshop, Zebula Lodge, Bela Bela, 11-12 July 2012
- Oral presentation, *"Pt deposition on carbon paper and titanium mesh substrates using surface limited redox reaction",* Mmalewane Modibedi, Eldah Louw, Kenneth Ozoemena, Mkhulu Mathe, 6th International Conference of the Africa Materials Research Society (Africa MRS), 11-16 December 2011, Victoria Falls- Zimbabwe

Publications

- Remegia M. Modibedi, Eldah K. Louw, Kenneth I. Ozoemena, Mkhulu K. Mathe, *The Electrochemical atomic layer deposition of Pt and Pd nanoparticles on Ni foam for the electro-oxidation of Alcohols,* ECS Transactions, 50(21) (2013) 9